Eur. Phys. J. C (2012) 72:1844
DOI 10.1140/epjc/s10052-011-1844-6

THE EUROPEAN PHYSICAL JOURNAL C

Regular Article - Experimental Physics

Performance of missing transverse momentum reconstruction in proton-proton collisions at $\sqrt{s} = 7$ TeV with ATLAS

The ATLAS Collaboration[*]

CERN, 1211 Geneva 23, Switzerland

Received: 29 August 2011 / Revised: 6 December 2011 / Published online: 3 January 2012
© CERN for the benefit of the ATLAS collaboration 2011. This article is published with open access at Springerlink.com

Abstract The measurement of missing transverse momentum in the ATLAS detector, described in this paper, makes use of the full event reconstruction and a calibration based on reconstructed physics objects. The performance of the missing transverse momentum reconstruction is evaluated using data collected in pp collisions at a centre-of-mass energy of 7 TeV in 2010. Minimum bias events and events with jets of hadrons are used from data samples corresponding to an integrated luminosity of about 0.3 nb^{-1} and 600 nb^{-1} respectively, together with events containing a Z boson decaying to two leptons (electrons or muons) or a W boson decaying to a lepton (electron or muon) and a neutrino, from a data sample corresponding to an integrated luminosity of about 36 pb^{-1}. An estimate of the systematic uncertainty on the missing transverse momentum scale is presented.

1 Introduction

In a collider event the missing transverse momentum is defined as the momentum imbalance in the plane transverse to the beam axis, where momentum conservation is expected. Such an imbalance may signal the presence of unseen particles, such as neutrinos or stable, weakly-interacting supersymmetric (SUSY) particles. The vector momentum imbalance in the transverse plane is obtained from the negative vector sum of the momenta of all particles detected in a pp collision and is denoted as missing transverse momentum, $\boldsymbol{E}_{\mathrm{T}}^{\mathrm{miss}}$. The symbol $E_{\mathrm{T}}^{\mathrm{miss}}$ is used for its magnitude.

A precise measurement of the missing transverse momentum, $\boldsymbol{E}_{\mathrm{T}}^{\mathrm{miss}}$, is essential for physics at the LHC. A large $E_{\mathrm{T}}^{\mathrm{miss}}$ is a key signature for searches for new physics processes such as SUSY and extra dimensions. The measurement of $\boldsymbol{E}_{\mathrm{T}}^{\mathrm{miss}}$ also has a direct impact on the quality of a number of measurements of Standard Model (SM) physics, such as the reconstruction of the top-quark mass in $t\bar{t}$ events. Furthermore, it is crucial in the search for the Higgs boson in the decay channels $H \to WW$ and $H \to \tau\tau$, where a good $\boldsymbol{E}_{\mathrm{T}}^{\mathrm{miss}}$ measurement improves the reconstruction of the Higgs boson mass [1].

This paper describes an optimized reconstruction and calibration of $\boldsymbol{E}_{\mathrm{T}}^{\mathrm{miss}}$ developed by the ATLAS Collaboration. The performance achieved represents a significant improvement compared to earlier results [2] presented by ATLAS. The optimal reconstruction of $\boldsymbol{E}_{\mathrm{T}}^{\mathrm{miss}}$ in the ATLAS detector is complex and validation with data, in terms of resolution, scale and tails, is essential. A number of data samples encompassing a variety of event topologies are used. Specifically, the event samples used to assess the quality of the $\boldsymbol{E}_{\mathrm{T}}^{\mathrm{miss}}$ reconstruction are: minimum bias events, events where jets at high transverse momentum are produced via strong interactions described by Quantum Chromodynamics (QCD) and events with leptonically decaying W and Z bosons. This allows the full exploitation of the detector capability in the reconstruction and calibration of different physics objects and optimization of the $\boldsymbol{E}_{\mathrm{T}}^{\mathrm{miss}}$ calculation. Moreover, in events with $W \to \ell\nu$, where ℓ is an electron or muon, the $\boldsymbol{E}_{\mathrm{T}}^{\mathrm{miss}}$ performance can be studied in events where genuine $E_{\mathrm{T}}^{\mathrm{miss}}$ is present due to the neutrino, thus allowing a validation of the $E_{\mathrm{T}}^{\mathrm{miss}}$ scale. In simulated events, the genuine $E_{\mathrm{T}}^{\mathrm{miss}}$, $E_{\mathrm{T}}^{\mathrm{miss,True}}$, is calculated from all generated non-interacting particles in the event and it is also referred to as true $E_{\mathrm{T}}^{\mathrm{miss}}$ in the following.

An important requirement on the measurement of $\boldsymbol{E}_{\mathrm{T}}^{\mathrm{miss}}$ is the minimization of the impact of limited detector coverage, finite detector resolution, the presence of dead regions and different sources of noise that can produce fake $E_{\mathrm{T}}^{\mathrm{miss}}$. The ATLAS calorimeter coverage extends to large pseudorapidities[1] to minimize the impact of high energy particles

[*] e-mail: atlas.publications@cern.ch

[1] ATLAS uses a right-handed coordinate system with its origin at the nominal interaction point (IP) in the centre of the detector and the z-axis coinciding with the axis of the beam pipe. The x-axis points from the IP to the centre of the LHC ring, and the y axis points upward.

escaping in the very forward direction. Even so, there are inactive transition regions between different calorimeters that produce fake $E_{\mathrm{T}}^{\mathrm{miss}}$. Dead and noisy readout channels in the detector, if present, as well as cosmic-ray and beam-halo muons crossing the detector, will produce fake $E_{\mathrm{T}}^{\mathrm{miss}}$. Such sources can significantly enhance the background from multi-jet events in SUSY searches with large $E_{\mathrm{T}}^{\mathrm{miss}}$ or the background from $Z \to \ell\ell$ events accompanied by jets of high transverse momentum (p_{T}) in Higgs boson searches in final states with two leptons and $E_{\mathrm{T}}^{\mathrm{miss}}$. Cuts are applied to clean the data against all these sources (see Sect. 3), and more severe cuts to suppress fake $E_{\mathrm{T}}^{\mathrm{miss}}$ are applied in analyses for SUSY searches, after which, for selected events with high-p_{T} jets, the tails of the $E_{\mathrm{T}}^{\mathrm{miss}}$ distributions are well described by MC simulation [3].

This paper is organised as follows. Section 2 gives a brief introduction to the ATLAS detector. Section 3 and Sect. 4 describe the data and Monte Carlo samples used and the event selections applied. Section 5 outlines how $\boldsymbol{E}_{\mathrm{T}}^{\mathrm{miss}}$ is reconstructed and calibrated. Section 6 presents the $\boldsymbol{E}_{\mathrm{T}}^{\mathrm{miss}}$ performance for data and Monte Carlo simulation, first in minimum bias and jet events and then in Z and W events. The systematic uncertainty on the $E_{\mathrm{T}}^{\mathrm{miss}}$ absolute scale is discussed in Sect. 7. Section 8 describes the determination of the $E_{\mathrm{T}}^{\mathrm{miss}}$ scale in-situ using $W \to \ell\nu$ events. Finally, the conclusions are given in Sect. 9.

2 The ATLAS detector

The ATLAS detector [1] is a multipurpose particle physics apparatus with a forward-backward symmetric cylindrical geometry and near 4π coverage in solid angle. The inner tracking detector (ID) covers the pseudorapidity range $|\eta| < 2.5$, and consists of a silicon pixel detector, a silicon microstrip detector (SCT), and, for $|\eta| < 2.0$, a transition radiation tracker (TRT). The ID is surrounded by a thin superconducting solenoid providing a 2 T magnetic field. A high-granularity lead/liquid-argon (LAr) sampling electromagnetic calorimeter covers the region $|\eta| < 3.2$. An iron/scintillator-tile calorimeter provides hadronic coverage in the range $|\eta| < 1.7$. LAr technology is also used for the hadronic calorimeters in the end-cap region $1.5 < |\eta| < 3.2$ and for both electromagnetic and hadronic measurements in the forward region up to $|\eta| < 4.9$. The muon spectrometer surrounds the calorimeters. It consists of three large air-core superconducting toroid systems, precision tracking chambers providing accurate muon tracking out to $|\eta| = 2.7$, and additional detectors for triggering in the region $|\eta| < 2.4$.

Cylindrical coordinates (r, ϕ) are used in the transverse plane, ϕ being the azimuthal angle around the beam pipe. The pseudorapidity is defined in terms of the polar angle θ as $\eta = -\ln\tan(\theta/2)$.

3 Data samples and event selection

During 2010 a large number of proton-proton collisions, at a centre-of-mass energy of 7 TeV, were recorded with stable proton beams as well as nominal magnetic field conditions. Only data with a fully functioning calorimeter, inner detector and muon spectrometer are analysed.

Cuts are applied to clean the data sample against instrumental noise and out-of-time energy deposits in the calorimeter (from cosmic-rays or beam-induced background). Topological clusters reconstructed in the calorimeters (see Sect. 5.1) at the electromagnetic energy (EM) scale[2] are used as the inputs to the jet finder [4]. In this paper the anti-k_t algorithm [5], with distance parameter $R = 0.6$, is used for jet reconstruction. The reconstructed jets are required to pass basic jet-quality selection criteria. In particular events are rejected if any jet in the event with transverse momentum $p_{\mathrm{T}} > 20$ GeV is caused by sporadic noise bursts in the end-cap region, coherent noise in the electromagnetic calorimeter or reconstructed from large out-of-time energy deposits in the calorimeter. These cuts largely suppress the residual sources of fake $E_{\mathrm{T}}^{\mathrm{miss}}$ due to those instrumental effects which remain after the data-quality requirements.

The 2010 data sets used in this paper correspond to a total integrated luminosity [6, 7] of approximately 600 nb^{-1} for jet events and to 0.3 nb^{-1} for minimum bias events. Trigger and selection criteria for these events are described in Sect. 3.1. For the $Z \to \ell\ell$ and $W \to \ell\nu$ channels, the samples analysed correspond to an integrated luminosity of approximately 36 pb^{-1}. Trigger and selection criteria, similar to those developed for the W/Z cross-section measurement [8], are applied. These criteria are described in Sects. 3.2 and 3.3.

3.1 Minimum bias and di-jet event selection

For the minimum bias events, only the early period of data taking, with a minimal pile-up contribution, is studied. Selected minimum bias events were triggered by the minimum bias trigger scintillators (MBTS), mounted at each end of the detector in front of the LAr end-cap calorimeter cryostats [9].

Events in the QCD jet sample are required to have passed the first-level calorimeter trigger, which indicates a significant energy deposit in a certain region of the calorimeter, with the most inclusive trigger with a nominal p_{T} threshold at 15 GeV. The event sample used in this analysis consists of two subsets of 300 nb^{-1} each, corresponding to

[2]The EM scale is the basic calorimeter signal scale for the ATLAS calorimeters. It provides the correct scale for energy deposited by electromagnetic showers. It does not correct for the lower energy hadron shower response nor for energy losses in the dead material.

two periods with different pile-up and trigger conditions.[3] One subset corresponds to the periods with lower pile-up conditions with, on average, 1 to 1.6 reconstructed vertices per event. The other subset corresponds to the periods with higher pileup conditions, where the peak number of visible inelastic interactions per bunch crossing goes up to 3. In the following, di-jet events are used, selected requiring the presence of exactly two jets with $p_{\mathrm{T}} > 25$ GeV and $|\eta| < 4.5$. Jets are calibrated with the local hadronic calibration (see Sect. 5.1).

For each event, at least one good primary vertex is required with a z displacement from the nominal pp interaction point less than 200 mm and with at least five associated tracks. After selection, the samples used in the analysis presented here correspond to 14 million minimum bias events and 13 million di-jet events.

3.2 $Z \to \ell\ell$ event selection

Candidate $Z \to \ell\ell$ events, where ℓ is an electron or a muon, are required to pass an e/γ or muon trigger with a p_{T} threshold between 10 and 15 GeV, where the exact trigger selection varies depending on the data period analysed. For each event, at least one good primary vertex, as defined above, is required.

The selection of $Z \to \mu\mu$ events requires the presence of exactly two good muons. A good muon is defined to be a muon reconstructed in the muon spectrometer with a matched track in the inner detector with transverse momentum above 20 GeV and $|\eta| < 2.5$ [10]. Additional requirements on the number of hits used to reconstruct the track in the inner detector are applied. The z displacement of the muon track from the primary vertex is required to be less than 10 mm. Isolation cuts are applied around the muon track.

The selection of $Z \to ee$ events requires the presence of exactly two identified electrons with $|\eta| < 2.47$, which pass the "medium" identification criteria [8, 11] and have transverse momenta above 20 GeV. Electron candidates in the electromagnetic calorimeter transition region, $1.37 < |\eta| < 1.52$, are not considered for this study. Additional cuts are applied to remove electrons falling into regions where the readout of the calorimeter was not fully operational.

In both the $Z \to ee$ and the $Z \to \mu\mu$ selections, the two leptons are required to have opposite charge and the reconstructed invariant mass of the di-lepton system, $m_{\ell\ell}$, is required to be consistent with the Z mass, $66 < m_{\ell\ell} < 116$ GeV.

With these selection criteria, about 9000 $Z \to ee$ and 13000 $Z \to \mu\mu$ events are selected. The estimated background contribution to these samples is less than 2% in both channels [8].

3.3 $W \to \ell\nu$ event selection

Lepton candidates are selected with lepton identification criteria similar to those used for the Z analysis. The differences for the selection of $W \to e\nu$ events are that the "tight" electron identification criteria [8, 11] are used and an isolation cut is applied on the electron cluster in the calorimeter to reduce contamination from QCD jet background. The event is rejected if it contains more than one reconstructed lepton. The $E_{\mathrm{T}}^{\mathrm{miss}}$, calculated as described in Sect. 5, is required to be greater than 25 GeV, and the reconstructed lepton-$\boldsymbol{E}_{\mathrm{T}}^{\mathrm{miss}}$ transverse mass, m_T, is required to be greater than 50 GeV.

With these selection criteria, about 8.5×10^4 $W \to e\nu$ and 1.05×10^5 $W \to \mu\nu$ events are selected. The background contribution to these samples is estimated to be about 5% in both channels [8].

4 Monte Carlo simulation samples

Monte Carlo (MC) events are generated using the PYTHIA6 program [12] with the ATLAS minimum bias tune (AMBT1) of the PYTHIA fragmentation and hadronisation parameters [13]. The generated events are processed with the detailed GEANT4 [14] simulation of the ATLAS detector.

The minimum bias MC event samples are generated using non-diffractive as well as single- and double-diffractive processes, where the different components are weighted according to the cross-sections given by the event generators.

The jet MC samples, generated using a 2-to-2 QCD matrix element and subsequent parton shower development, are used for comparison with the two subsets of data taken with different pile-up conditions. In the earlier sample the fraction of events with at least two observed interactions is at most of the order of 8–10%, while in the sample taken later in 2010 this fraction ranges from 10% to more than 50%. These samples are generated in the p_{T} range 8–560 GeV, in separated parton p_{T} bins to provide a larger statistics also in the high-p_{T} bins. Each sample is weighted according to its cross-section.

MC events for the study of SM backgrounds in $Z \to \ell\ell$ and $W \to \ell\nu$ analyses are also generated using PYTHIA6. The only exceptions are the $t\bar{t}$ background and the $W \to e\nu$ samples used in Sect. 8.2, which are generated with the MC@NLO program [15]. For the study of the total transverse energy of the events, samples produced with PYTHIA8 [16] are used as well.

MC samples were produced with different levels of pile-up in order to reflect the conditions in different data-taking

[3] Pile-up in the following refers to the contribution of additional pp collisions superimposed on the hard physics process.

periods. In particular, two event samples were used for jets: one was simulated with a pile-up model where only pile-up collisions originating from the primary bunch crossing are considered (in-time pile-up) and a second one was simulated with a realistic configuration of the LHC bunch group structure, where pile-up collisions from successive bunch crossings are also included in the simulation. In the case of events containing $Z \to \ell\ell$ or $W \to \ell\nu$, MC samples with in-time pile-up configuration are used, because these data correspond to periods where the contribution of out-of-time pileup is small.

The trigger and event selection criteria used for the data are also applied to the MC simulation.

5 $\boldsymbol{E}_{\mathrm{T}}^{\mathrm{miss}}$ reconstruction and calibration

The $\boldsymbol{E}_{\mathrm{T}}^{\mathrm{miss}}$ reconstruction includes contributions from energy deposits in the calorimeters and muons reconstructed in the muon spectrometer. The two $\boldsymbol{E}_{\mathrm{T}}^{\mathrm{miss}}$ components are calculated as:

$$E_{x(y)}^{\mathrm{miss}} = E_{x(y)}^{\mathrm{miss,calo}} + E_{x(y)}^{\mathrm{miss},\mu}. \tag{1}$$

Low-p_{T} tracks are used to recover low p_{T} particles which are missed in the calorimeters (see Sect. 5.3.1), and muons reconstructed from the inner detector are used to recover muons in regions not covered by the muon spectrometer (see Sect. 5.2). The two terms in the above equation are referred to as the calorimeter and muon terms, and will be described in more detail in the following sections. The values of $E_{\mathrm{T}}^{\mathrm{miss}}$ and its azimuthal coordinate (ϕ^{miss}) are then calculated as:

$$\begin{aligned} E_{\mathrm{T}}^{\mathrm{miss}} &= \sqrt{\left(E_x^{\mathrm{miss}}\right)^2 + \left(E_y^{\mathrm{miss}}\right)^2}, \\ \phi^{\mathrm{miss}} &= \arctan\left(E_y^{\mathrm{miss}}, E_x^{\mathrm{miss}}\right). \end{aligned} \tag{2}$$

5.1 Calculation of the $\boldsymbol{E}_{\mathrm{T}}^{\mathrm{miss}}$ calorimeter term

In this paper, the $\boldsymbol{E}_{\mathrm{T}}^{\mathrm{miss}}$ reconstruction uses calorimeter cells calibrated according to the reconstructed physics object to which they are associated. Calorimeter cells are associated with a reconstructed and identified high-p_{T} parent object in a chosen order: electrons, photons, hadronically decaying τ-leptons, jets and muons. Cells not associated with any such objects are also taken into account in the $\boldsymbol{E}_{\mathrm{T}}^{\mathrm{miss}}$ calculation. Their contribution, named $E_T^{\mathrm{miss,CellOut}}$ hereafter, is important for the $\boldsymbol{E}_{\mathrm{T}}^{\mathrm{miss}}$ resolution [17].

Once the cells are associated with objects as described above, the $\boldsymbol{E}_{\mathrm{T}}^{\mathrm{miss}}$ calorimeter term is calculated as follows (note that the $E_{x(y)}^{\mathrm{miss,calo},\mu}$ term is not always added, as explained in Sect. 5.2, and for that reason it is written between parentheses):

$$\begin{aligned} E_{x(y)}^{\mathrm{miss,calo}} = {} & E_{x(y)}^{\mathrm{miss},e} + E_{x(y)}^{\mathrm{miss},\gamma} + E_{x(y)}^{\mathrm{miss},\tau} + E_{x(y)}^{\mathrm{miss,jets}} \\ & + E_{x(y)}^{\mathrm{miss,softjets}} + \left(E_{x(y)}^{\mathrm{miss,calo},\mu}\right) \\ & + E_{x(y)}^{\mathrm{miss,CellOut}}, \end{aligned} \tag{3}$$

where each term is calculated from the negative sum of calibrated cell energies inside the corresponding objects, as:

$$\begin{aligned} E_x^{\mathrm{miss,term}} &= -\sum_{i=1}^{N_{\mathrm{cell}}^{\mathrm{term}}} E_i \sin\theta_i \cos\phi_i, \\ E_y^{\mathrm{miss,term}} &= -\sum_{i=1}^{N_{\mathrm{cell}}^{\mathrm{term}}} E_i \sin\theta_i \sin\phi_i, \end{aligned} \tag{4}$$

where E_i, θ_i and ϕ_i are the energy, the polar angle and the azimuthal angle, respectively. The summations are over all cells associated with specified objects in the pseudorapidity range[4] $|\eta| < 4.5$.

Because of the high granularity of the calorimeter, it is crucial to suppress noise contributions and to limit the cells used in the $\boldsymbol{E}_{\mathrm{T}}^{\mathrm{miss}}$ sum to those containing a significant signal. This is achieved by using only cells belonging to three-dimensional topological clusters, referred as topoclusters hereafter [18], with the exception of electrons and photons for which a different clustering algorithm is used [11]. The topoclusters are seeded by cells with deposited energy[5] $|E_i| > 4\sigma_{\mathrm{noise}}$, and are built by iteratively adding neighbouring cells with $|E_i| > 2\sigma_{\mathrm{noise}}$ and, finally, by adding all neighbours of the accumulated cells.

The various terms in (3) are described in the following:

- $E_{x(y)}^{\mathrm{miss},e}$, $E_{x(y)}^{\mathrm{miss},\gamma}$, $E_{x(y)}^{\mathrm{miss},\tau}$ are reconstructed from cells in clusters associated to electrons, photons and τ-jets from hadronically decaying τ-leptons, respectively;
- $E_{x(y)}^{\mathrm{miss,jets}}$ is reconstructed from cells in clusters associated to jets with calibrated $p_{\mathrm{T}} > 20$ GeV;
- $E_{x(y)}^{\mathrm{miss,softjets}}$ is reconstructed from cells in clusters associated to jets with 7 GeV $< p_{\mathrm{T}} <$ 20 GeV;
- $E_{x(y)}^{\mathrm{miss,calo},\mu}$ is the contribution to $\boldsymbol{E}_{\mathrm{T}}^{\mathrm{miss}}$ originating from the energy lost by muons in the calorimeter (see Sect. 5.2);
- the $E_{x(y)}^{\mathrm{miss,CellOut}}$ term is calculated from the cells in topoclusters which are not included in the reconstructed objects.

All these terms are calibrated independently as described in Sect. 5.3. The final $E_{x(y)}^{\mathrm{miss}}$ is calculated from (1) adding the $E_{x(y)}^{\mathrm{miss},\mu}$ term, described in Sect. 5.2.

[4] This η cut is chosen because the MC simulation does not describe data well in the very forward region.

[5] σ_{noise} is the Gaussian width of the EM cell energy distribution measured in randomly triggered events far from collision bunches.

5.2 Calculation of the $\boldsymbol{E}_{\mathrm{T}}^{\mathrm{miss}}$ muon term

The $\boldsymbol{E}_{\mathrm{T}}^{\mathrm{miss}}$ muon term is calculated from the momenta of muon tracks reconstructed with $|\eta| < 2.7$:

$$E_{x(y)}^{\mathrm{miss},\mu} = -\sum_{\mathrm{muons}} p_{x(y)}^{\mu}, \tag{5}$$

where the summation is over selected muons. In the region $|\eta| < 2.5$, only well-reconstructed muons in the muon spectrometer with a matched track in the inner detector are considered (combined muons). The matching requirement considerably reduces contributions from fake muons (reconstructed muons not corresponding to true muons). These fake muons can sometimes be created from high hit multiplicities in the muon spectrometer in events where some particles from very energetic jets punch through the calorimeter into the muon system.

In order to deal appropriately with the energy deposited by the muon in the calorimeters, $E_{x(y)}^{\mathrm{miss,calo},\mu}$, the muon term is calculated differently for isolated and non-isolated muons, with non-isolated muons defined as those within a distance $\Delta R = \sqrt{(\Delta\eta)^2 + (\Delta\phi)^2} < 0.3$ of a reconstructed jet in the event:

- The p_{T} of an isolated muon is determined from the combined measurement of the inner detector and muon spectrometer, taking into account the energy deposited in the calorimeters. In this case the energy lost by the muon in the calorimeters ($E_{x(y)}^{\mathrm{miss,calo},\mu}$) is not added to the calorimeter term (see (3)) to avoid double counting of energy.
- For a non-isolated muon, the energy deposited in the calorimeter cannot be resolved from the calorimetric energy depositions of the particles in the jet. The muon spectrometer measurement of the muon momentum after energy loss in the calorimeter is therefore used, so the $E_{x(y)}^{\mathrm{miss,calo},\mu}$ term is added to the calorimeter term (see (3)). Only in cases in which there is a significant mis-match between the spectrometer and the combined measurement, the combined measurement is used and a parameterized estimation of the muon energy loss in the calorimeter [10] is subtracted.

For higher values of pseudorapidity ($2.5 < |\eta| < 2.7$), outside the fiducial volume of the inner detector, there is no matched track requirement and the muon spectrometer p_{T} alone is used for both isolated and non-isolated muons.

Aside from the loss of muons outside the acceptance of the muon spectrometer ($|\eta| > 2.7$), muons can be lost in other small inactive regions (around $|\eta| = 0$ and $|\eta| \sim 1.2$) of the muon spectrometer. The muons which are reconstructed by segments matched to inner detector tracks extrapolated to the muon spectrometer are used to recover their contributions to $\boldsymbol{E}_{\mathrm{T}}^{\mathrm{miss}}$ in the $|\eta| \sim 1.2$ regions [10].

Although the core of the $\boldsymbol{E}_{\mathrm{T}}^{\mathrm{miss}}$ resolution is not much affected by the muon term, any muons which are not reconstructed, badly measured, or fake, can be a source of fake $E_{\mathrm{T}}^{\mathrm{miss}}$.

5.3 Calibration of $\boldsymbol{E}_{\mathrm{T}}^{\mathrm{miss}}$

The calibration of $\boldsymbol{E}_{\mathrm{T}}^{\mathrm{miss}}$ is performed using the scheme described below, where the cells are calibrated separately according to their parent object:

- The $E_{\mathrm{T}}^{\mathrm{miss},e}$ term is calculated from reconstructed electrons passing the "medium" electron identification requirements, with $p_{\mathrm{T}} > 10$ GeV and calibrated with the default electron calibration [8].
- The $E_{\mathrm{T}}^{\mathrm{miss},\gamma}$ term is calculated from photons reconstructed with the "tight" photon identification requirements [11], with $p_{\mathrm{T}} > 10$ GeV at the EM scale. Due to the low photon purity, the default photon calibration is not applied.
- The $E_{\mathrm{T}}^{\mathrm{miss},\tau}$ term is calculated from τ-jets reconstructed with the "tight" τ-identification requirements [19], with $p_{\mathrm{T}} > 10$ GeV, calibrated with the local hadronic calibration (LCW) scheme [20]. The LCW scheme uses properties of clusters to calibrate them individually. It first classifies calorimeter clusters as electromagnetic or hadronic, according to the cluster topology, and then weights each calorimeter cell in clusters according to the cluster energy and the cell energy density. Additional corrections are applied to the cluster energy for the average energy deposited in the non-active material before and between the calorimeters and for unclustered calorimeter energy.
- The $E_{\mathrm{T}}^{\mathrm{miss,softjets}}$ term is calculated from jets (reconstructed using the anti-k_t algorithm with $R = 0.6$) with $7 < p_{\mathrm{T}} < 20$ GeV calibrated with the LCW calibration.
- The $E_{\mathrm{T}}^{\mathrm{miss,jets}}$ term is calculated from jets with $p_{\mathrm{T}} > 20$ GeV calibrated with the LCW calibration and the jet energy scale (JES) factor [21] applied. The JES factor corrects the energy of jets, either at the EM-scale or after cluster calibration, back to particle level. The JES is derived as a function of reconstructed jet η and p_{T} using the generator-level information in MC simulation.
- The $E_{\mathrm{T}}^{\mathrm{miss,CellOut}}$ term is calculated from topoclusters outside reconstructed objects with the LCW calibration and from reconstructed tracks as described in Sect. 5.3.1.

Note that object classification criteria and calibration can be chosen according to specific analysis criteria, if needed.

5.3.1 Calculation of the $E_{\mathrm{T}}^{\mathrm{miss,CellOut}}$ term with a track-cluster matching algorithm

In events with W and Z boson production, the calibration of the $E_{\mathrm{T}}^{\mathrm{miss,CellOut}}$ term is of particular importance because, due to the low particle multiplicity in these events,

this $\boldsymbol{E}_{\mathrm{T}}^{\mathrm{miss}}$ contribution balances the W/Z boson p_{T} to a large extent [17]. An energy-flow algorithm is used to improve the calculation of the low-p_{T} contribution to $\boldsymbol{E}_{\mathrm{T}}^{\mathrm{miss}}$ ($E_{\mathrm{T}}^{\mathrm{miss,CellOut}}$). Tracks are added to recover the contribution from low-p_{T} particles which do not reach the calorimeter or do not seed a topocluster. Furthermore the track momentum is used instead of the topocluster energy for tracks associated to topoclusters, thus exploiting the better calibration and resolution of tracks at low momentum compared to topoclusters.

Reconstructed tracks with $p_{\mathrm{T}} > 400$ MeV, passing track quality selection criteria such as the number of hits and χ^2 of the track fit, are used for the calculation of the $E_{\mathrm{T}}^{\mathrm{miss,CellOut}}$ term. All selected tracks are extrapolated to the second layer of the electromagnetic calorimeter and very loose criteria are used for association to reconstructed objects or topoclusters, to avoid double counting. If a track is neither associated to a topocluster nor a reconstructed object, its transverse momentum is added to the calculation of $E_{\mathrm{T}}^{\mathrm{miss,CellOut}}$. In the case where the track is associated to a topocluster, its transverse momentum is used for the calculation of the $E_{\mathrm{T}}^{\mathrm{miss,CellOut}}$ and the topocluster energy is discarded, assuming that the topocluster energy corresponds to the charged particle giving the track. It has to be noticed that there is a strong correlation between the number of particles and topoclusters, so, in general no neutral energy is lost replacing the topocluster by a track, and the neutral topoclusters are kept in most of the cases. If more than one topocluster is associated to a track, only the topocluster with the largest energy is excluded from the $\boldsymbol{E}_{\mathrm{T}}^{\mathrm{miss}}$ calculation, assuming that this energy corresponds to the track.

6 Study of $\boldsymbol{E}_{\mathrm{T}}^{\mathrm{miss}}$ performance

In this section the distributions of $\boldsymbol{E}_{\mathrm{T}}^{\mathrm{miss}}$ in minimum bias, di-jet, $Z \to \ell\ell$ and $W \to \ell\nu$ events from data are compared with the expected distributions from the MC samples. The performance of $\boldsymbol{E}_{\mathrm{T}}^{\mathrm{miss}}$ in terms of resolution and scale is also derived.

Minimum bias, di-jet events and $Z \to \ell\ell$ events are used to investigate the $\boldsymbol{E}_{\mathrm{T}}^{\mathrm{miss}}$ performance without relying on MC detector simulation. In general, apart from a small contribution from the semi-leptonic decay of heavy-flavour hadrons in jets, no genuine $E_{\mathrm{T}}^{\mathrm{miss}}$ is expected in these events. Thus most of the $\boldsymbol{E}_{\mathrm{T}}^{\mathrm{miss}}$ reconstructed in these events is a direct result of imperfections in the reconstruction process or in the detector response.

6.1 $\boldsymbol{E}_{\mathrm{T}}^{\mathrm{miss}}$ performance in minimum bias and di-jet events

The distributions of E_x^{miss}, E_y^{miss}, $E_{\mathrm{T}}^{\mathrm{miss}}$ and ϕ^{miss} for data and MC simulation are shown in Fig. 1 for minimum bias events. The distributions are shown only for events with total transverse energy (see definition at the end of this section) greater than 20 GeV in order to reduce the contamination of fake triggers from the MBTS. Figure 2 shows the distributions of the same variables for the di-jet sample. The di-jet sample corresponding to the periods with higher pileup conditions (see Sect. 3.1) is used. The MC simulation expectations are superimposed, normalized to the number of events in the data.

In di-jet events a reasonable agreement is found between data and simulation for all basic quantities, while there is some disagreement in minimum bias events, attributed to imperfect modelling of soft particle activity in the MC simulation. The better agreement between data and MC simulation in the ϕ^{miss} distribution for the di-jet sample can be partly explained by the fact that the $\boldsymbol{E}_{\mathrm{T}}^{\mathrm{miss}}$ is not corrected for the primary vertex position; the primary vertex position in data is better reproduced by the MC simulation for the di-jet sample than in the case of the minimum bias sample.

Events in the tails of the $E_{\mathrm{T}}^{\mathrm{miss}}$ distributions have been carefully checked, in order to understand the origin of the large measured $E_{\mathrm{T}}^{\mathrm{miss}}$. The tails are not completely well described by MC simulation, but, both in data and in MC simulation they are in general due to mis-measured jets. In minimum bias events there are more events in the tail in MC simulation and this can be due to the fact that the MC statistics is larger than in data. In di-jet events, there are more events in the tail in data. More MC events would be desirable. In di-jet events there are 19 events with $E_{\mathrm{T}}^{\mathrm{miss}} > 110$ GeV in the data. The majority of them (13 events) are due to mis-measured jets, where in most of the cases at least one jet points to a transition region between calorimeters. Two events are due to a combination of mis-measured jets with an overlapping muon, and one event is due to a fake high-p_{T} muon. Finally two events look like good $b\bar{b}$ candidates, and one event has one reconstructed jet and no activity in the other hemisphere.

The events with fake $E_{\mathrm{T}}^{\mathrm{miss}}$ due to mis-measured jets and jets containing leptonic decays of heavy hadrons can be rejected by a cut based on the azimuthal angle between the jet and $\boldsymbol{E}_{\mathrm{T}}^{\mathrm{miss}}$, $\Delta\phi(\mathbf{jet}, \boldsymbol{E}_{\mathrm{T}}^{\mathrm{miss}})$. Since the requirement of event cleaning depends on the physics analysis, the minimal cleaning cut is applied and careful evaluation of tail events is performed in this paper. Analyses that rely on a careful understanding and reduction of the tails of the $E_{\mathrm{T}}^{\mathrm{miss}}$ distribution (e.g. SUSY searches such as Ref. [3]) have performed more detailed studies to characterize the residual tail in events containing high-p_{T} jets. These analyses use tighter jet cleaning cuts, track-jet matching, and angular cuts on $\Delta\phi(\mathbf{jet}, \boldsymbol{E}_{\mathrm{T}}^{\mathrm{miss}})$ to further reduce the fake $E_{\mathrm{T}}^{\mathrm{miss}}$ tail. In Ref. [3] a fully data-driven method (described in detail in Ref. [17]) was then employed to determine the residual fake $E_{\mathrm{T}}^{\mathrm{miss}}$ background.

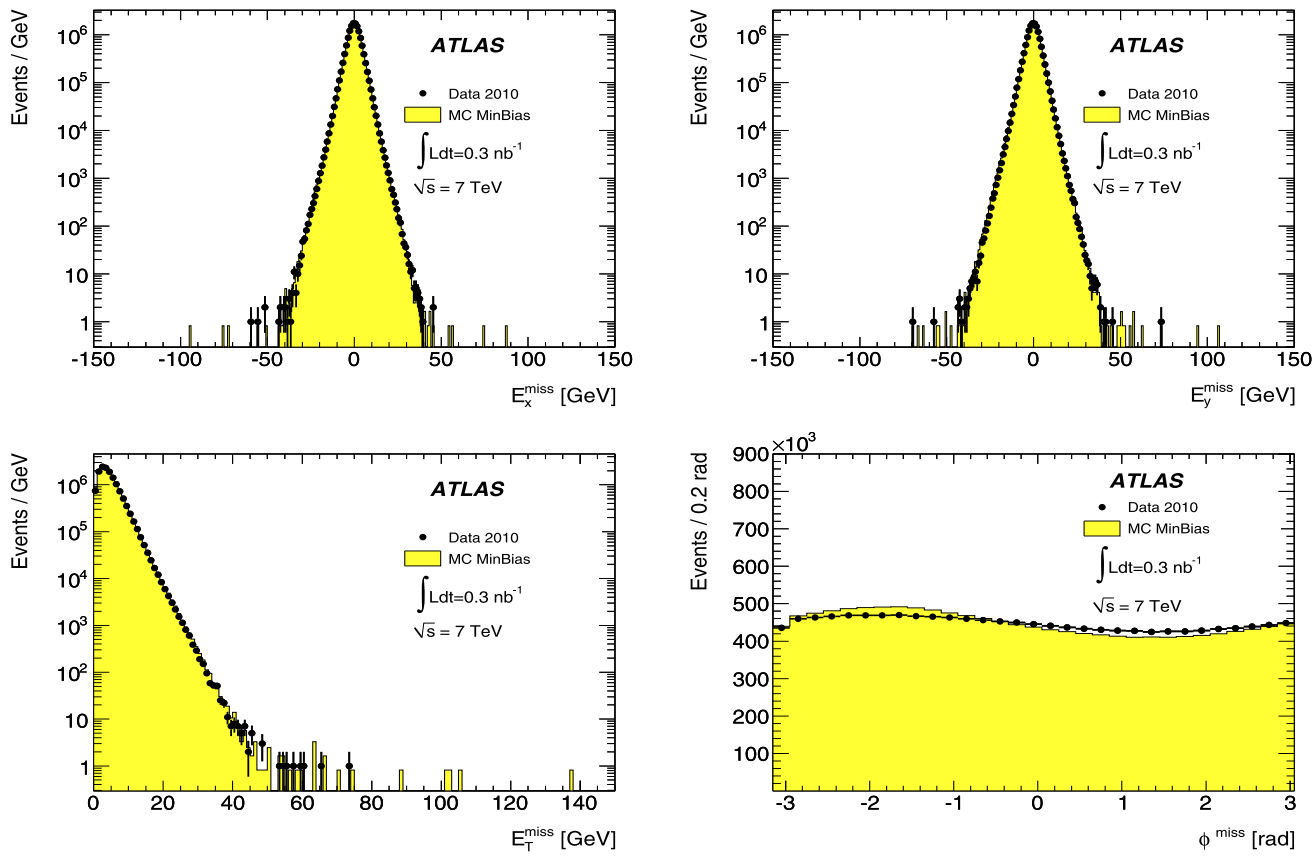

Fig. 1 Distribution of E_x^{miss} (*top left*), E_y^{miss} (*top right*), $E_{\text{T}}^{\text{miss}}$ (*bottom left*), ϕ^{miss} (*bottom right*) as measured in a data sample of minimum bias events. The expectation from MC simulation, normalized to the number of events in data, is superimposed

The contributions from jets, soft jets and topoclusters not associated to the reconstructed objects and muons are shown in Fig. 3 for the di-jet events. The data-MC agreement is good for all of the terms contributing to $\boldsymbol{E}_{\text{T}}^{\text{miss}}$. The tails observed in the muon term are mainly due to reconstructed fake muons and to one cosmic-ray muon, which can be rejected by applying a tighter selection for the muons used in the $\boldsymbol{E}_{\text{T}}^{\text{miss}}$ reconstruction, based on χ^2 criteria for the combination, isolation criteria and requirements on the number of hits in muon chambers used for the muon reconstruction.

In the following some distributions are shown for the total transverse energy, $\sum E_{\text{T}}$, which is an important quantity to parameterise and understand the $\boldsymbol{E}_{\text{T}}^{\text{miss}}$ performance. It is defined as:

$$\sum E_{\text{T}} = \sum_{i=1}^{N_{\text{cell}}} E_i \sin\theta_i, \tag{6}$$

where E_i and θ_i are the energy and the polar angle, respectively, of calorimeter cells associated to topoclusters within $|\eta| < 4.5$. Cell energies are calibrated according to the scheme described in Sect. 5.3 for $\boldsymbol{E}_{\text{T}}^{\text{miss}}$.

The data distributions of $\sum E_{\text{T}}$ for minimum bias and di-jet events from the subset corresponding to lower pileup conditions (see Sect. 3.1) are compared to MC predictions from two versions of PYTHIA in Fig. 4. The left-hand distributions show comparisons with the ATLAS tune of PYTHIA6. The right-hand distributions show the comparisons with the default tune of PYTHIA8. Due to the limited number of events simulated, the distribution for the di-jet PYTHIA8 MC sample is not smooth, and is zero in the lowest $\sum E_{\text{T}}$ bin populated by data. This is not understood, also if it can be partly explained by the fact that the low $\sum E_{\text{T}}$ region is populated by events from the jet MC sample generated in the lowest parton p_{T} bin (17–35 GeV), which is the most suppressed by the di-jet selection (a factor about 20 more than other samples) and has a large weight, due to cross-section. Moreover the PYTHIA8 jet MC sample in the 8–17 GeV parton p_{T} bin is not available. In the case of the minimum bias sample, due to the very limited number of events simulated (about a factor 25 less respect to data), the tails in the PYTHIA8 MC distribution are strongly depleted.

The PYTHIA8 MC [16] version used in this paper has not yet been tuned to the ATLAS data. The current tune [22] uses the CTEQ 6.1 parton distribution functions (PDF)

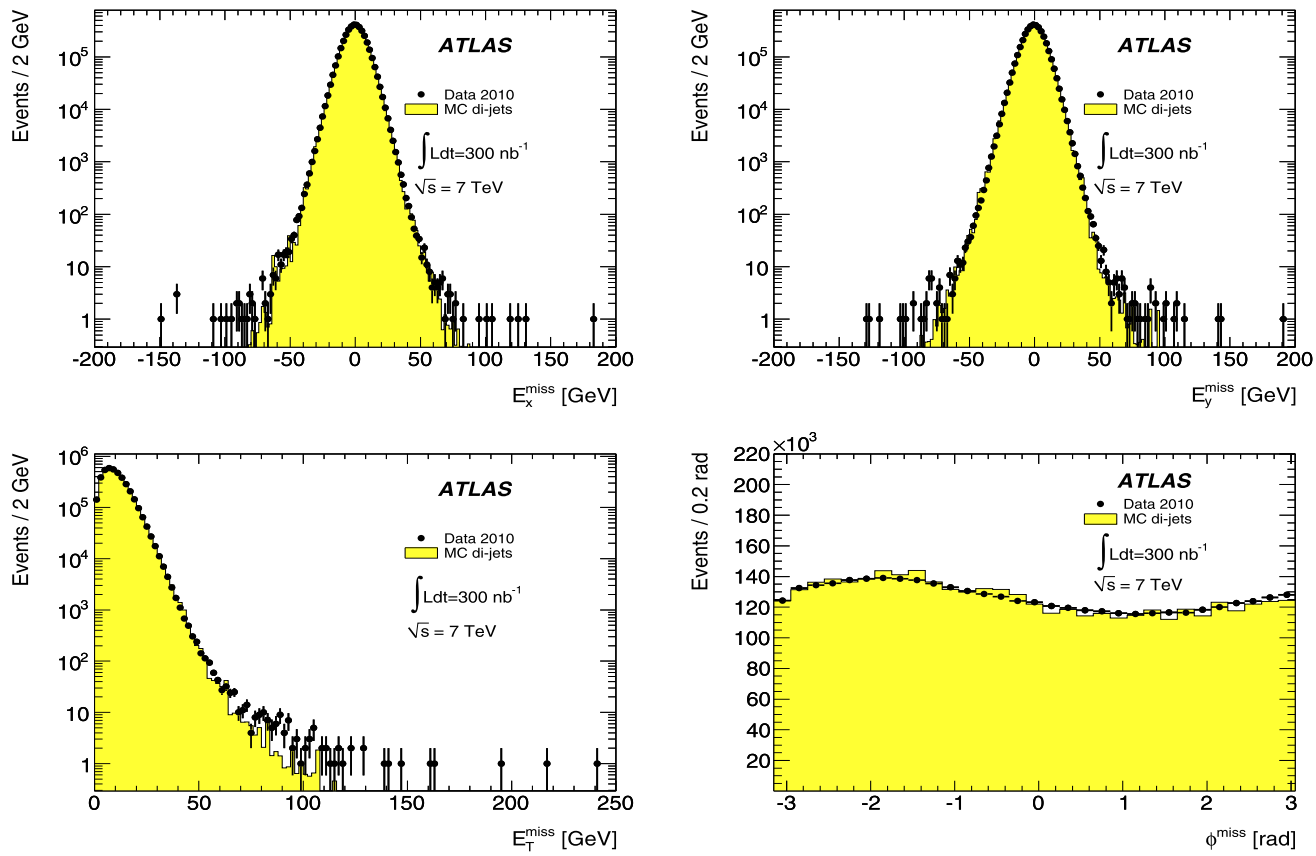

Fig. 2 Distribution of E_x^{miss} (*top left*), E_y^{miss} (*top right*), $E_{\text{T}}^{\text{miss}}$ (*bottom left*), ϕ^{miss} (*bottom right*) as measured in the data sample of di-jet events. The expectation from MC simulation, normalized to the number of events in data, is superimposed. The events in the tails are discussed in the text

instead of the MRST LO** as used in PYTHIA6, and its diffraction model differs, including higher-Q^2 diffractive processes. The comparison of the mean values and the shapes of the two different MC distributions with data seems to indicate that a better agreement is obtained with the PYTHIA8 but, due to the reduced PYTHIA8 MC statistics, no firm conclusion can be drawn. In the rest of the paper, the PYTHIA6 MC samples with the ATLAS tune are used for comparison with data; this version is used as the baseline for PYTHIA MC samples for 2010 data analyses.

6.2 $\boldsymbol{E}_{\text{T}}^{\text{miss}}$ performance in $Z \to \ell\ell$ events

The absence of genuine $E_{\text{T}}^{\text{miss}}$ in $Z \to \ell\ell$ events, coupled with the clean event signature and the relatively large cross-section, means that it is a good channel to study $\boldsymbol{E}_{\text{T}}^{\text{miss}}$ performance.

The distributions of $E_{\text{T}}^{\text{miss}}$ and ϕ^{miss} for data and MC simulation are shown in Fig. 5 for $Z \to ee$ and $Z \to \mu\mu$ events. The contributions due to muons are shown for $Z \to \mu\mu$ events in Fig. 6. Both the contributions from energy deposited in calorimeter cells associated to muons, taken at the EM scale, and the contributions from reconstructed muons are shown. For $Z \to ee$ events, the contributions from electrons, jets, soft jets and topoclusters outside the reconstructed objects are shown separately in Fig. 7. The peak at zero in the distribution of the jet term corresponds to events where there are no jets with p_{T} above 20 GeV, and the small values (<20 GeV) in the distribution are due to events with two jets whose transverse momenta balance. The MC simulation expectations, from $Z \to \ell\ell$ events and from the dominant SM backgrounds, are superimposed. Each MC sample is weighted with its corresponding cross-section and then the total MC expectation is normalized to the number of events in data. Reasonable agreement between data and MC simulation is observed in all distributions.

Events in the tails of the $E_{\text{T}}^{\text{miss}}$ distributions in Fig. 5 have been carefully checked. The 22 events with the highest $E_{\text{T}}^{\text{miss}}$ values, above 60 GeV, have been examined in detail to check whether they are related to cosmic-ray muon background, fake muons, badly measured jets or jets pointing to dead calorimeter regions. The events in the tails are found to be compatible with either signal candidates, including $t\bar{t}$, WW and WZ di-boson events, all involving real $E_{\text{T}}^{\text{miss}}$, or events in which the $\boldsymbol{E}_{\text{T}}^{\text{miss}}$ vector is close to a jet in the transverse plane. The latter category of events can arise from mis-

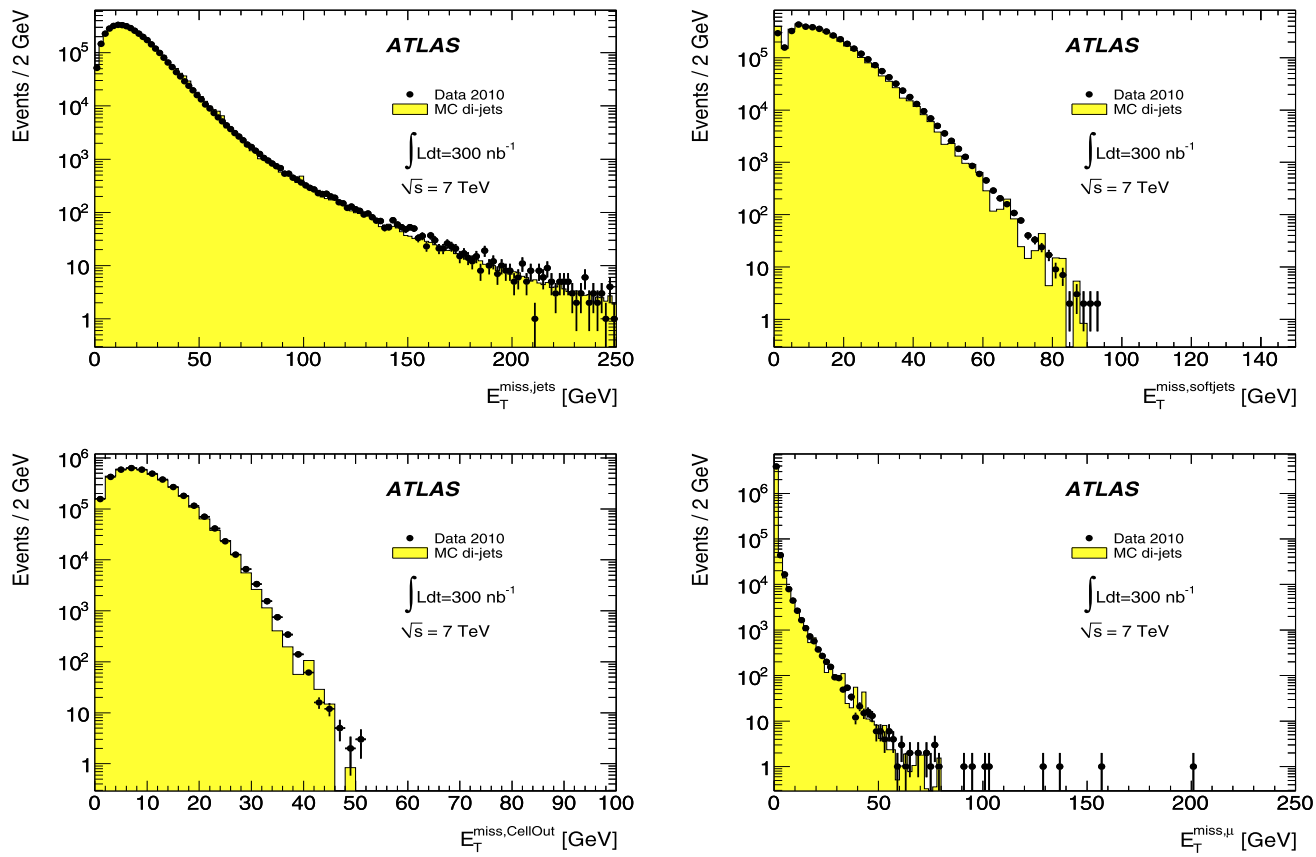

Fig. 3 Distribution of $E_{\mathrm{T}}^{\mathrm{miss}}$ computed with cells from topoclusters in jets (*top left*), in soft jets (*top right*), from topoclusters outside reconstructed objects (*bottom left*) and from reconstructed muons (*bottom right*) for data for di-jet events. The expectation from MC simulation, normalized to the number of events in data, is superimposed. The events in the tail of the $E_T^{\mathrm{miss},\mu}$ distribution are discussed in the text

measured jets, and be rejected at the analysis level with cuts on $\Delta\phi(\mathbf{jet}, \boldsymbol{E}_{\mathrm{T}}^{\mathrm{miss}})$ (see Sect. 6.1).

6.2.1 Measuring $\boldsymbol{E}_{\mathrm{T}}^{\mathrm{miss}}$ response in $Z \to \ell\ell$ events

From the event topology [17] in events with $Z \to \ell\ell$ decay one can define an axis in the transverse plane such that the component of $\boldsymbol{E}_{\mathrm{T}}^{\mathrm{miss}}$ along this axis is sensitive to detector resolution and biases. The direction of this axis, $\boldsymbol{A}_{\mathbf{Z}}$, is defined by the reconstructed momenta of the leptons:

$$\boldsymbol{A}_{\mathbf{Z}} = \left(\boldsymbol{p}_{\mathbf{T}}{}^{\ell^+} + \boldsymbol{p}_{\mathbf{T}}{}^{\ell^-}\right) / \left|\boldsymbol{p}_{\mathbf{T}}{}^{\ell^+} + \boldsymbol{p}_{\mathbf{T}}{}^{\ell^-}\right|, \tag{7}$$

where $\boldsymbol{p}_{\mathbf{T}}{}^{\ell}$ are the vector transverse momenta of the lepton and anti-lepton. The direction of $\boldsymbol{A}_{\mathbf{Z}}$ thus reconstructs the direction of motion of the Z boson. The perpendicular axis in the transverse plane, $\boldsymbol{A}_{\mathbf{AZ}}$, is a unit vector placed at right angles to $\boldsymbol{A}_{\mathbf{Z}}$, with positive direction anticlockwise from the direction of the Z boson.

The mean value of the projection of $\boldsymbol{E}_{\mathrm{T}}^{\mathrm{miss}}$ onto the longitudinal axis, $\langle \boldsymbol{E}_{\mathrm{T}}^{\mathrm{miss}} \cdot \boldsymbol{A}_{\mathbf{Z}} \rangle$, is a measure of the $\boldsymbol{E}_{\mathrm{T}}^{\mathrm{miss}}$ scale, as this axis is sensitive to the balance between the leptons and the hadronic recoil. Figure 8 shows the value of $\langle \boldsymbol{E}_{\mathrm{T}}^{\mathrm{miss}} \cdot \boldsymbol{A}_{\mathbf{Z}} \rangle$ as a function of p_{T}^{Z}. These mean values are used as a diagnostic to validate the $\boldsymbol{E}_{\mathrm{T}}^{\mathrm{miss}}$ reconstruction algorithms. If the leptons perfectly balanced the hadronic recoil, regardless of the net momentum of the lepton system, then the $\boldsymbol{E}_{\mathrm{T}}^{\mathrm{miss}} \cdot \boldsymbol{A}_{\mathbf{Z}}$ would be zero, independent of p_{T}^{Z}. Instead, $\langle \boldsymbol{E}_{\mathrm{T}}^{\mathrm{miss}} \cdot \boldsymbol{A}_{\mathbf{Z}} \rangle$ displays a small bias in both the electron and muon channels which is reasonably reproduced by the MC simulation. The observed bias is slightly negative for low values of p_{T}^{Z}, suggesting either that the p_{T} of the lepton system is overestimated or that the magnitude of the hadronic recoil is underestimated. The same sign and magnitude of bias is seen in both electron and muon channels, suggesting that the hadronic recoil, here dominated by $E_{\mathrm{T}}^{\mathrm{miss,CellOut}}$ and by soft jets, is the source of bias. The component of the $\boldsymbol{E}_{\mathrm{T}}^{\mathrm{miss}}$ along the perpendicular axis, $\boldsymbol{E}_{\mathrm{T}}^{\mathrm{miss}} \cdot \boldsymbol{A}_{\mathbf{AZ}}$, displays no bias, and, indeed there is no mechanism for generating such a bias.

In Fig. 9 the dependences of $\langle \boldsymbol{E}_{\mathrm{T}}^{\mathrm{miss}} \cdot \boldsymbol{A}_{\mathbf{Z}} \rangle$ on p_{T}^{Z} are shown separately for events with $Z \to \ell\ell$ produced in association with zero jets or with at least one jet, with the jet definition as described in Sect. 3.1. The figure demonstrates that

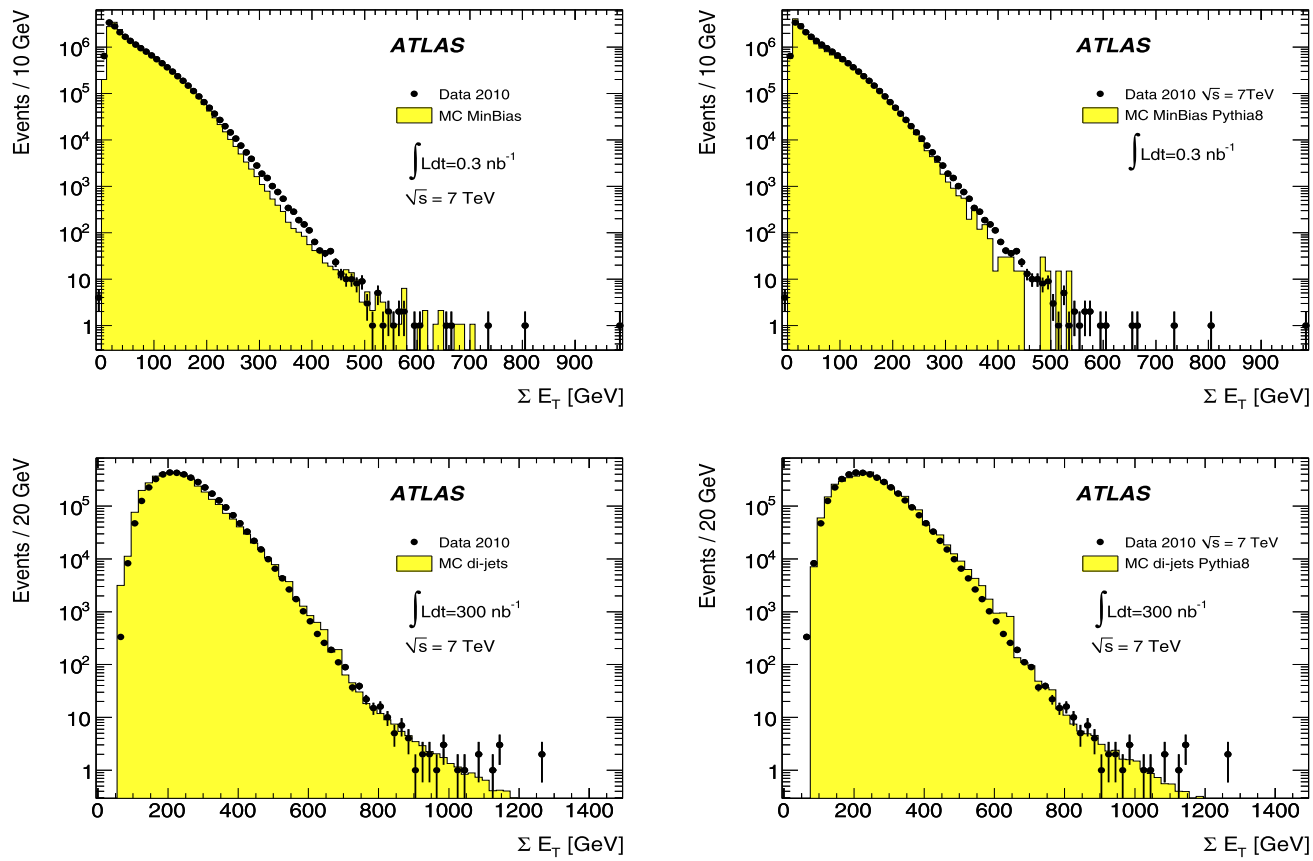

Fig. 4 Distribution of $\sum E_{\mathrm{T}}$ as measured in a data sample of minimum bias events (*top*) and di-jet events (*bottom*) selecting two jets with $p_{\mathrm{T}} > 25$ GeV. The expectation from MC simulation, normalized to the number of events in data, is superimposed. *On the left* PYTHIA6 (ATLAS tune) is compared with the data. *On the right* PYTHIA8 is compared with the data

there is a negative bias in $\langle \boldsymbol{E}_{\mathrm{T}}^{\mathrm{miss}} \cdot \boldsymbol{A}_{\mathbf{Z}} \rangle$ for events with zero jets, which increases with p_{T}^{Z} up to 6 GeV. A similar bias is observed in both electron and muon channels, hence it is interpreted as coming from imperfections in the calibration of the soft hadronic recoil (the $E_{\mathrm{T}}^{\mathrm{miss,CellOut}}$ and the $E_{\mathrm{T}}^{\mathrm{miss,softjets}}$ terms). In events with at least one jet there is a small positive bias in the electron channel at high p_{T}^{Z}, which is visible also in the muon channel for p_{T}^{Z} in the region 15–20 GeV.

Figure 10 shows $\langle \boldsymbol{E}_{\mathrm{T}}^{\mathrm{miss}} \cdot \boldsymbol{A}_{\mathbf{Z}} \rangle$ for $Z \to \ell\ell$ events where there are neither high p_{T} nor soft jets, for two cases of $\boldsymbol{E}_{\mathrm{T}}^{\mathrm{miss}}$ reconstruction: calculating the $E_{\mathrm{T}}^{\mathrm{miss,CellOut}}$ term with the track-cluster matching algorithm (see Sect. 5.3.1) or calculating this term from the calorimeter topoclusters only (denoted as $E_{\mathrm{T}}^{\mathrm{miss}}$ no tracks). The plots show a lower bias for the case with the track-cluster matching algorithm, indicating that it improves the reconstruction of the $E_{\mathrm{T}}^{\mathrm{miss,CellOut}}$ term.

6.3 $\boldsymbol{E}_{\mathrm{T}}^{\mathrm{miss}}$ performance in $W \to \ell\nu$ events

In this section the $\boldsymbol{E}_{\mathrm{T}}^{\mathrm{miss}}$ performance is studied in $W \to e\nu$ and $W \to \mu\nu$ events. In these events genuine $E_{\mathrm{T}}^{\mathrm{miss}}$ is expected due to the presence of the neutrino, therefore the $E_{\mathrm{T}}^{\mathrm{miss}}$ scale can be checked.

The distributions of $E_{\mathrm{T}}^{\mathrm{miss}}$ and ϕ^{miss} in data and in MC simulation are shown in Fig. 11 for $W \to e\nu$ and $W \to \mu\nu$ events. The contributions due to muons are shown for $W \to \mu\nu$ events in Fig. 12. Both, the $E_{\mathrm{T}}^{\mathrm{miss}}$ contribution from energy deposited in calorimeter cells associated to muons, taken at the EM scale, and the $E_{\mathrm{T}}^{\mathrm{miss}}$ contribution from reconstructed muons are shown. The contributions given by the electrons, jets, soft jets and topoclusters outside reconstructed objects are shown in Fig. 13 for $W \to e\nu$ events. The MC expectations are also shown, both from $W \to \ell\nu$ events, and from the dominant SM backgrounds. The MC simulation describes all of the quantities well, with the exception that very small data-MC discrepancies are observed in the distribution of the $E_{\mathrm{T}}^{\mathrm{miss,e}}$ at low $E_{\mathrm{T}}^{\mathrm{miss}}$ values. This can be attributed to the QCD jet background, which would predominantly populate the region of low $E_{\mathrm{T}}^{\mathrm{miss}}$ [8], but which is not included in the MC expectation shown.

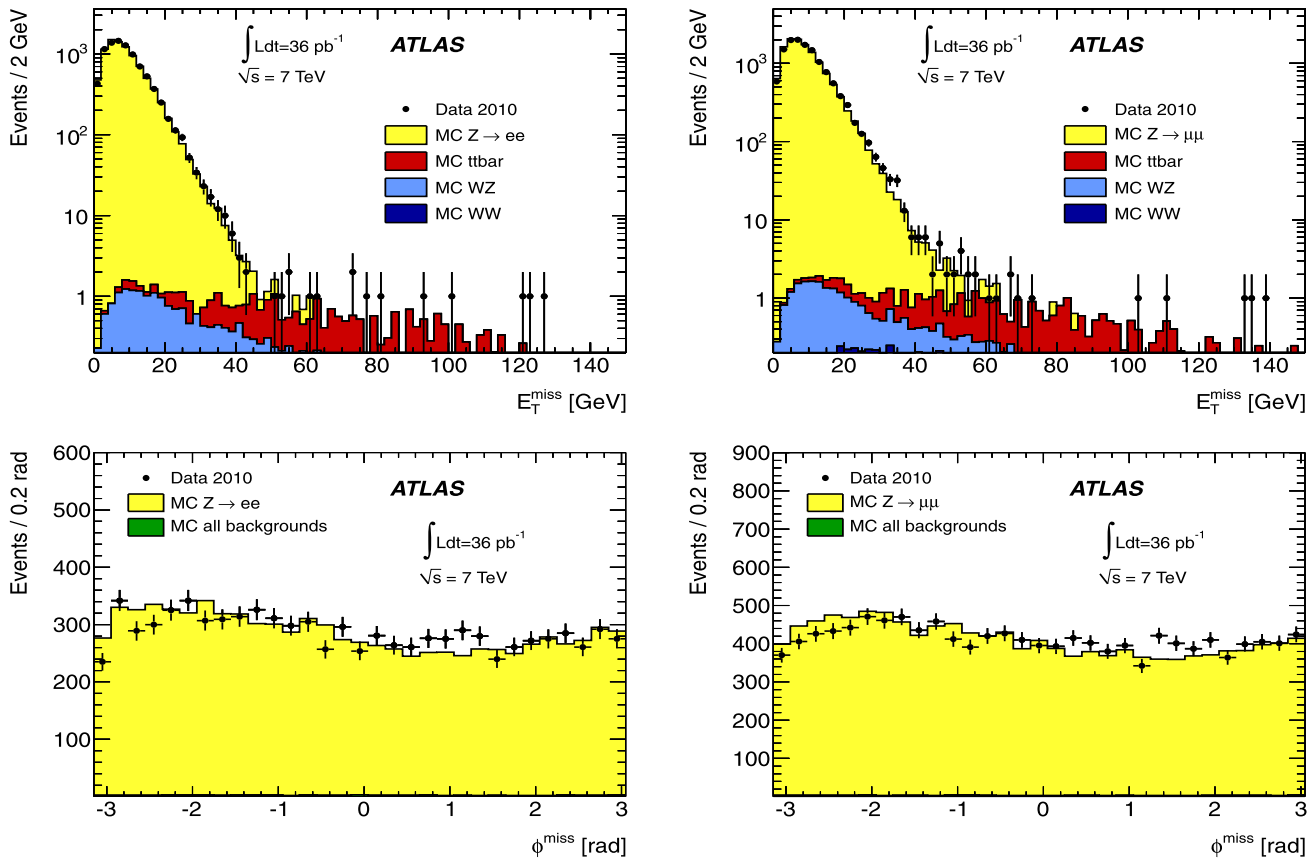

Fig. 5 Distribution of $E_{\mathrm{T}}^{\mathrm{miss}}$ (*top*) and ϕ^{miss} (*bottom*) as measured in a data sample of $Z \to ee$ (*left*) and of $Z \to \mu\mu$ (*right*). The expectation from Monte Carlo simulation is superimposed and normalized to data, after each MC sample is weighted with its corresponding cross-section. The sum of all backgrounds is shown in the lower plots

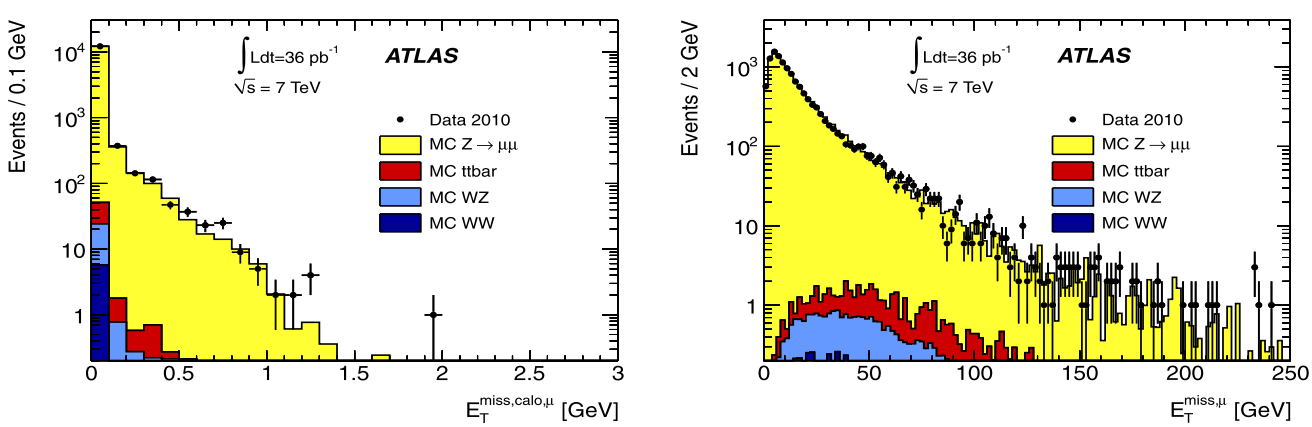

Fig. 6 Distribution of $E_{\mathrm{T}}^{\mathrm{miss}}$ computed with calorimeter cells associated to muons ($E_{\mathrm{T}}^{\mathrm{miss,calo},\mu}$) (*left*) and computed from reconstructed muons ($E_{\mathrm{T}}^{\mathrm{miss},\mu}$) (*right*) for $Z \to \mu\mu$ data. The expectation from Monte Carlo simulation is superimposed and normalized to data, after each MC sample is weighted with its corresponding cross-section

6.3.1 $E_{\mathrm{T}}^{\mathrm{miss}}$ *linearity in* $W \to \ell\nu$ *MC events*

The expected $E_{\mathrm{T}}^{\mathrm{miss}}$ linearity, which is defined as the mean value of the ratio: $(E_{\mathrm{T}}^{\mathrm{miss}} - E_{\mathrm{T}}^{\mathrm{miss,True}})/E_{\mathrm{T}}^{\mathrm{miss,True}}$, is shown as a function of $E_{\mathrm{T}}^{\mathrm{miss,True}}$ in Fig. 14 for $W \to e\nu$ and $W \to \mu\nu$ MC events. The mean value of this ratio is expected to be zero if the reconstructed $E_{\mathrm{T}}^{\mathrm{miss}}$ has the correct scale. In Fig. 14, it can be seen that there is a displacement

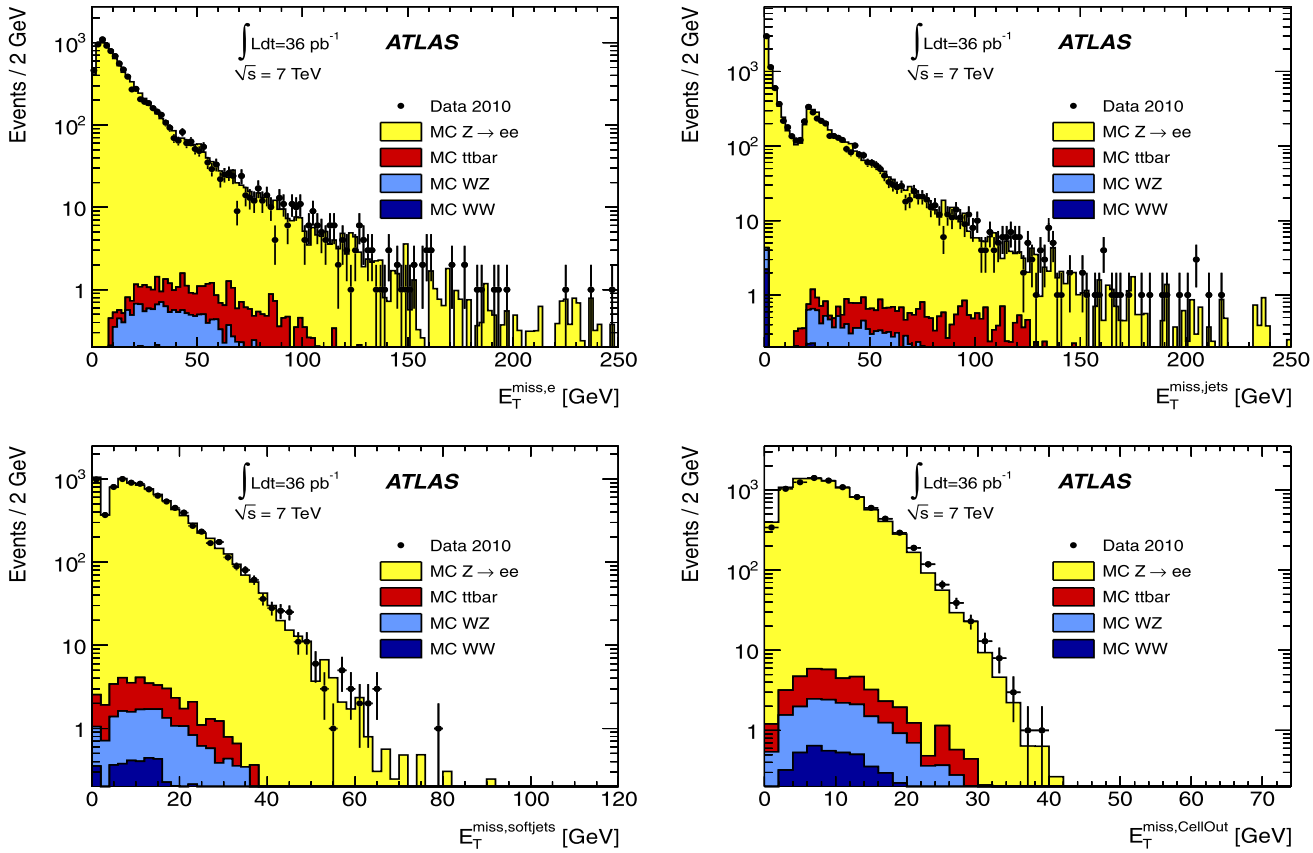

Fig. 7 Distribution of $E_{\mathrm{T}}^{\mathrm{miss}}$ computed with cells associated to electrons ($E_{\mathrm{T}}^{\mathrm{miss},e}$) (*top left*), jets with $p_{\mathrm{T}} > 20$ GeV ($E_{\mathrm{T}}^{\mathrm{miss,jets}}$) (*top right*), jets with 7 GeV $< p_{\mathrm{T}} < 20$ GeV ($E_{\mathrm{T}}^{\mathrm{miss,softjets}}$) (*bottom left*) and from topoclusters outside reconstructed objects ($E_{\mathrm{T}}^{\mathrm{miss,CellOut}}$) (*bottom right*) for $Z \to ee$ data. The expectation from Monte Carlo simulation is superimposed and normalized to data, after each MC sample is weighted with its corresponding cross-section

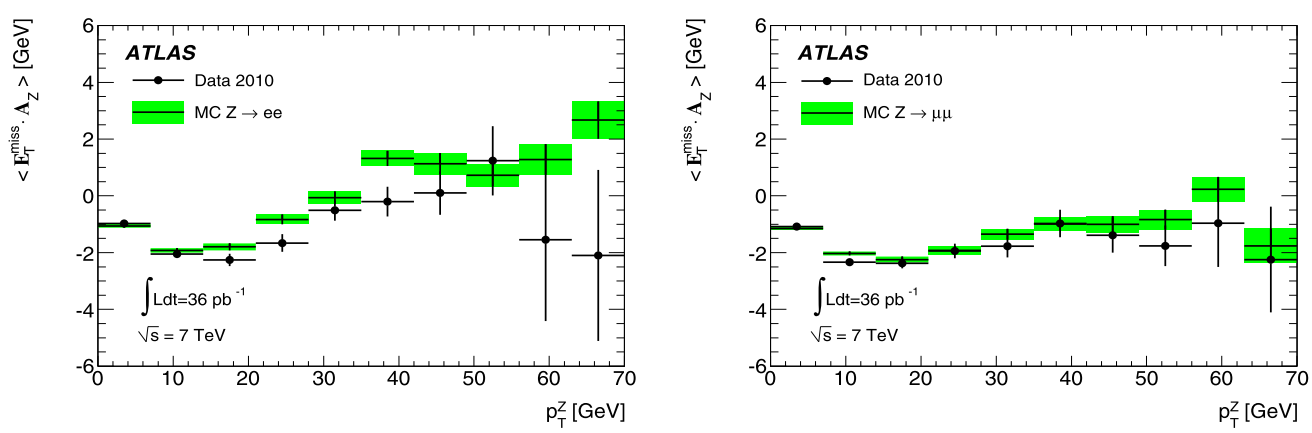

Fig. 8 Mean values of $\boldsymbol{E}_{\mathrm{T}}^{\mathrm{miss}} \cdot \boldsymbol{A}_{\mathbf{Z}}$ as a function of p_{T}^{Z} in $Z \to ee$ (*left*) and $Z \to \mu\mu$ (*right*) events

from zero which varies with the true $E_{\mathrm{T}}^{\mathrm{miss}}$. The bias at low $E_{\mathrm{T}}^{\mathrm{miss,True}}$ values is about 5% and is due to the finite resolution of the $\boldsymbol{E}_{\mathrm{T}}^{\mathrm{miss}}$ measurement. The reconstructed $E_{\mathrm{T}}^{\mathrm{miss}}$ is positive by definition, so the relative difference is positive when the $E_{\mathrm{T}}^{\mathrm{miss,True}}$ is small. The effect extends up to 40 GeV. The bias is in general larger for $W \to \mu\nu$ events than for $W \to e\nu$ events. Considering only events with $E_{\mathrm{T}}^{\mathrm{miss,True}} > 40$ GeV, the $E_{\mathrm{T}}^{\mathrm{miss}}$ linearity is better than 1% in $W \to e\nu$ events, while there is a non-linearity up to about 3% in $W \to \mu\nu$ events. This may be explained by an

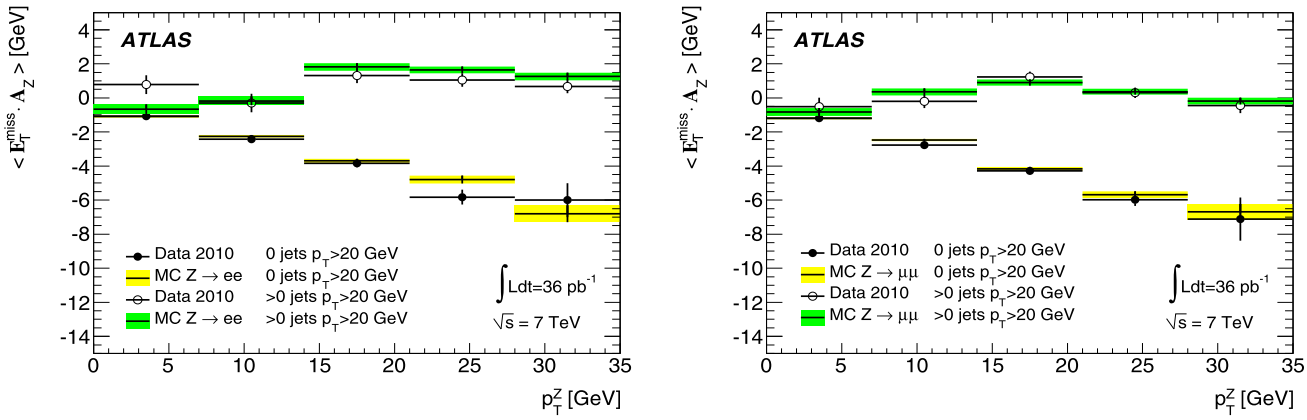

Fig. 9 Mean value of $\boldsymbol{E}_{\mathrm{T}}^{\mathrm{miss}} \cdot \boldsymbol{A_Z}$ as a function of p_{T}^{Z} requiring either zero jets with $p_{\mathrm{T}} > 20$ GeV or at least 1 jet with $p_{\mathrm{T}} > 20$ GeV in the event for $Z \to ee$ (*left*) and $Z \to \mu\mu$ (*right*) events

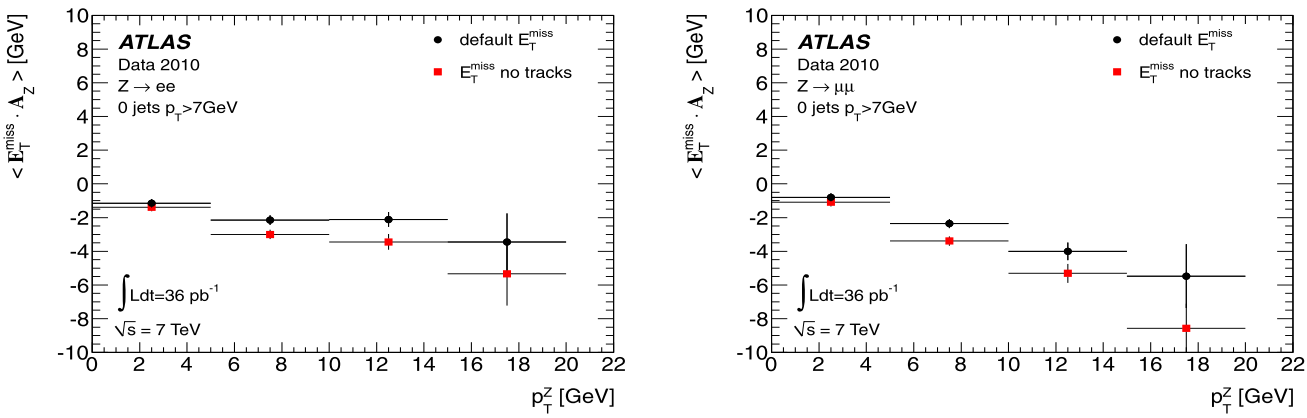

Fig. 10 Mean value of $\boldsymbol{E}_{\mathrm{T}}^{\mathrm{miss}} \cdot \boldsymbol{A_Z}$ as a function of p_{T}^{Z} in $Z \to ee$ (*left*) and $Z \to \mu\mu$ (*right*) for events with no jets with $p_{\mathrm{T}} > 7$ GeV. The default $\boldsymbol{E}_{\mathrm{T}}^{\mathrm{miss}}$ is compared with $\boldsymbol{E}_{\mathrm{T}}^{\mathrm{miss}}$ calculated in the same way with the exception that the track-cluster matching algorithm is not used for the calculation of $E_{\mathrm{T}}^{\mathrm{miss,CellOut}}$

underestimation of the $E_{\mathrm{T}}^{\mathrm{miss,calo},\mu}$ term, in which too few calorimeter cells are associated to the reconstructed muon.

6.4 $\boldsymbol{E}_{\mathrm{T}}^{\mathrm{miss}}$ resolution

A more quantitative evaluation of the $\boldsymbol{E}_{\mathrm{T}}^{\mathrm{miss}}$ performance can be obtained from a study of the $(E_x^{\mathrm{miss}}, E_y^{\mathrm{miss}})$ resolutions as a function of $\sum E_{\mathrm{T}}$. In $Z \to \ell\ell$ events, as well as in minimum bias and QCD jet events, no genuine $E_{\mathrm{T}}^{\mathrm{miss}}$ is expected, so the resolution of the two $\boldsymbol{E}_{\mathrm{T}}^{\mathrm{miss}}$ components is measured directly from reconstructed quantities, assuming that the true values of E_x^{miss} and E_y^{miss} are equal to zero. The resolution is estimated from the width of the combined distribution of E_x^{miss} and E_y^{miss} (denoted $(E_x^{\mathrm{miss}}, E_y^{\mathrm{miss}})$ distribution) in bins of $\sum E_{\mathrm{T}}$. The core of the distribution is fitted, for each $\sum E_{\mathrm{T}}$ bin, with a Gaussian over twice the expected resolution obtained from previous studies [17] and the fitted width, σ, is examined as a function of $\sum E_{\mathrm{T}}$. The $\boldsymbol{E}_{\mathrm{T}}^{\mathrm{miss}}$ resolution follows an approximately stochastic behaviour as a function of $\sum E_{\mathrm{T}}$, which can be described with the function $\sigma = k \cdot \sqrt{\Sigma E_{\mathrm{T}}}$, but deviations from this simple law are expected in the low $\sum E_{\mathrm{T}}$ region due to noise and in the very large $\sum E_{\mathrm{T}}$ region due to the constant term.

Figure 15 (left) shows the resolution from data at $\sqrt{s} = 7$ TeV for $Z \to \ell\ell$ events, minimum bias and di-jet events as a function of the total transverse energy in the event, obtained by summing the p_{T} of muons and the $\sum E_{\mathrm{T}}$ in calorimeters, calculated as described in Sect. 6.1. If the resolution is shown as a function of the $\sum E_{\mathrm{T}}$ in calorimeters, a difference between $Z \to ee$ and $Z \to \mu\mu$ events is observed due to the fact that $\sum E_{\mathrm{T}}$ includes electron momenta in $Z \to ee$ events while muon momenta are not included in $Z \to \mu\mu$ events.

The resolution of the two $\boldsymbol{E}_{\mathrm{T}}^{\mathrm{miss}}$ components is fitted with the simple function given above. The fits are acceptable and are of similar quality for all different channels studied. This allows to use the parameter k as an estimator for the resolution and to compare it in various physics channels in

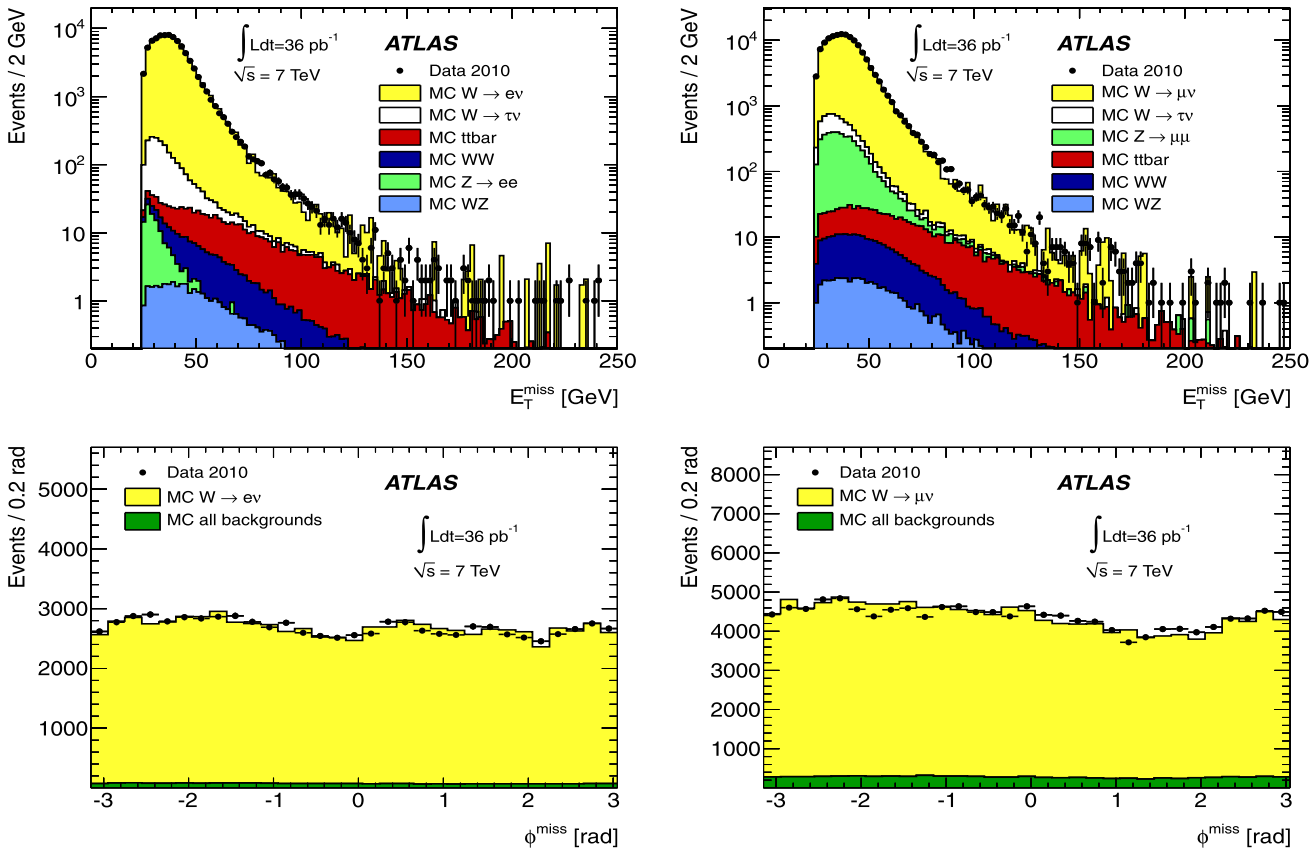

Fig. 11 Distribution of $E_{\mathrm{T}}^{\mathrm{miss}}$ (*top*) and ϕ^{miss} (*bottom*) as measured in a data sample of $W \to e\nu$ (*left*) and $W \to \mu\nu$ (*right*) events. The expectation from Monte Carlo simulation is superimposed and normalized to data, after each MC sample is weighted with its corresponding cross-section. The sum of all backgrounds is shown in the lower plots

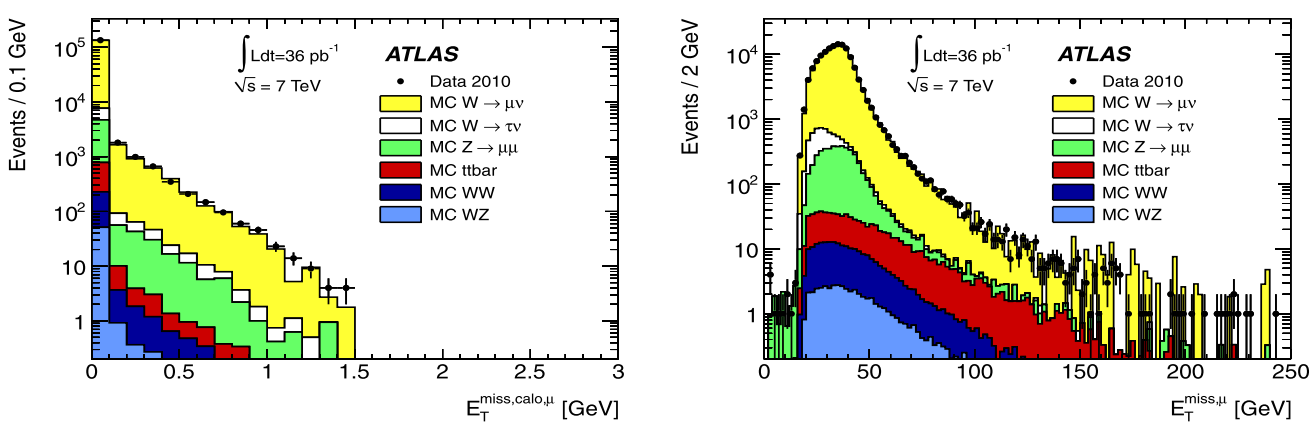

Fig. 12 Distribution of $E_{\mathrm{T}}^{\mathrm{miss}}$ computed with cells from muons ($E_{\mathrm{T}}^{\mathrm{miss,calo},\mu}$) (*left*) and reconstructed muons ($E_{\mathrm{T}}^{\mathrm{miss,muon}}$) (*right*) for $W \to \mu\nu$ data. The expectation from Monte Carlo simulation is superimposed and normalized to data, after each MC sample is weighted with its corresponding cross-section

data and MC simulation. There is a reasonable agreement in the $\boldsymbol{E}_{\mathrm{T}}^{\mathrm{miss}}$ resolution in the different physics channels, as can be seen from the fit parameters k reported in the figure. The k parameter has fit values ranging from 0.42 GeV$^{1/2}$ for $Z \to \ell\ell$ events to 0.51 GeV$^{1/2}$ for di-jet events. The $\boldsymbol{E}_{\mathrm{T}}^{\mathrm{miss}}$ resolution is better in $Z \to \ell\ell$ events because the lepton momenta are measured with better precision than jets.

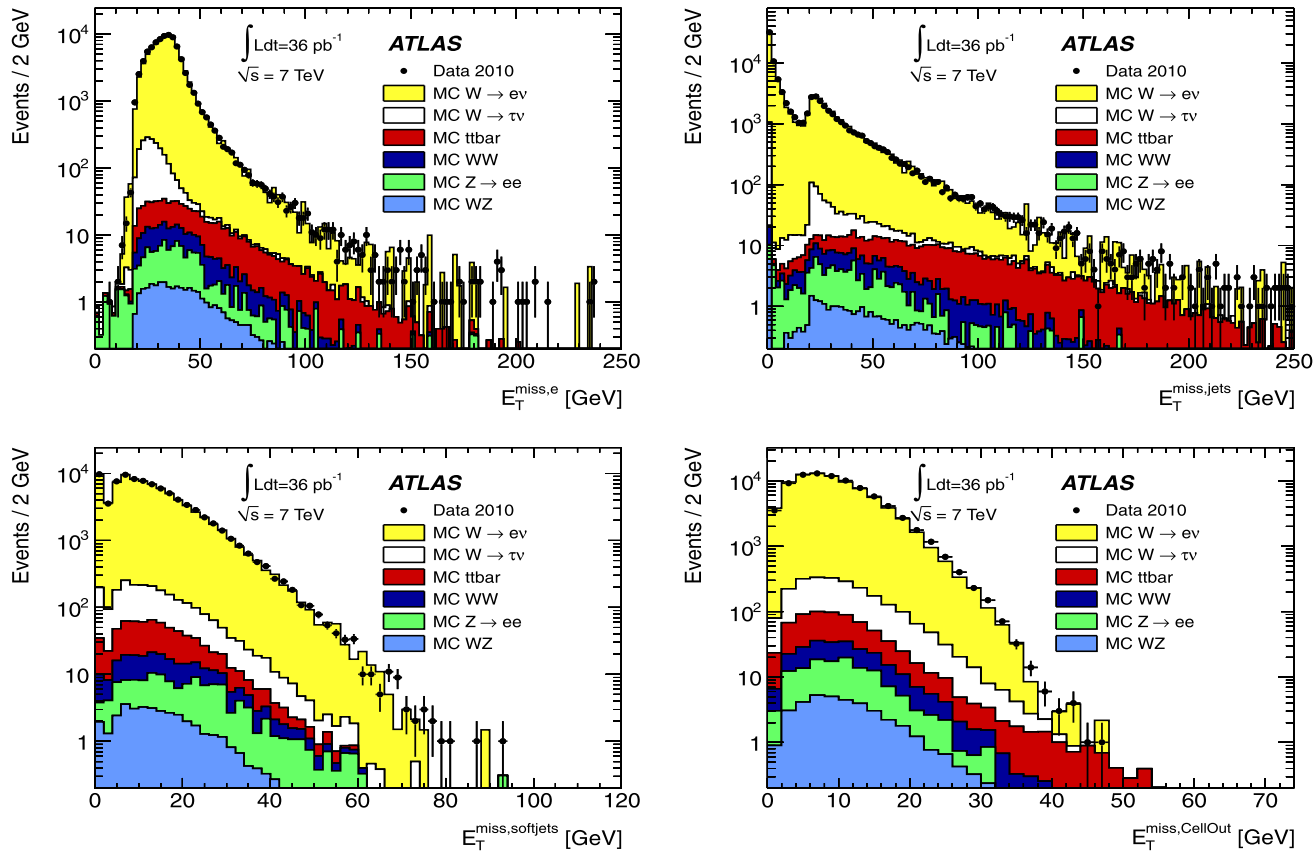

Fig. 13 Distribution of $E_{\mathrm{T}}^{\mathrm{miss}}$ computed with cells associated to electrons ($E_{\mathrm{T}}^{\mathrm{miss},e}$) (*top left*), jets with $p_{\mathrm{T}} > 20$ GeV ($E_{\mathrm{T}}^{\mathrm{miss,jets}}$) (*top right*), jets with $p_{\mathrm{T}} < 20$ GeV ($E_{\mathrm{T}}^{\mathrm{miss,softjets}}$) (*bottom left*) and from topoclusters outside reconstructed objects ($E_{\mathrm{T}}^{\mathrm{miss,CellOut}}$) (*bottom right*) for data. The expectation from Monte Carlo simulation is superimposed and normalized to data, after each MC sample is weighted with its corresponding cross-section

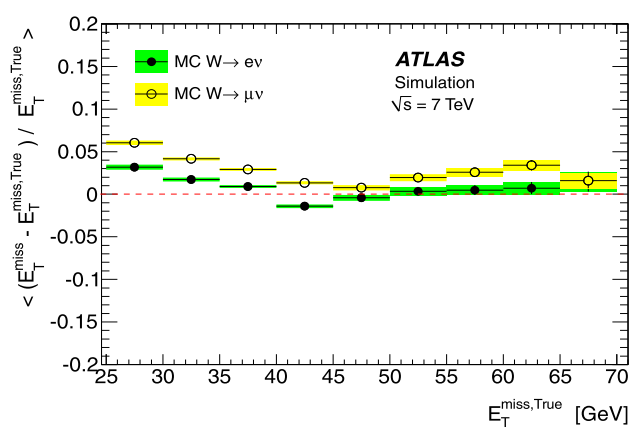

Fig. 14 $E_{\mathrm{T}}^{\mathrm{miss}}$ linearity in $W \to e\nu$ and $W \to \mu\nu$ MC events as a function of $E_{\mathrm{T}}^{\mathrm{miss,True}}$

In Fig. 15 (right) the $\boldsymbol{E}_{\mathrm{T}}^{\mathrm{miss}}$ resolution is shown for MC events. In addition to the $Z \to \ell\ell$, minimum bias and di-jet events, the resolution is also shown for $W \to \ell\nu$ MC events. In W events the resolution of the two $\boldsymbol{E}_{\mathrm{T}}^{\mathrm{miss}}$ components is estimated from the width of ($E_x^{\mathrm{miss}} - E_x^{\mathrm{miss,True}}$, $E_y^{\mathrm{miss}} - E_y^{\mathrm{miss,True}}$) in bins of $\sum E_{\mathrm{T}}$, fitted with a Gaussian as explained above. There is a reasonable agreement in the $\boldsymbol{E}_{\mathrm{T}}^{\mathrm{miss}}$ resolution in the different MC channels studied with the fitted value of k ranging from 0.42 GeV$^{1/2}$ for $Z \to \ell\ell$ events to 0.50 GeV$^{1/2}$ for di-jet events. As observed for data, the $\boldsymbol{E}_{\mathrm{T}}^{\mathrm{miss}}$ resolution is better in $Z \to \ell\ell$ events and slightly better in $W \to \ell\nu$ events, due to the presence of the leptons which are more precisely measured.

The resolution in MC minimum bias events is slightly worse than in data. This is probably due to imperfections of the modelling of soft particle activity in MC simulation, while there is a good data-MC agreement in the resolution for other channels.

7 Evaluation of the systematic uncertainty on the $\boldsymbol{E}_{\mathrm{T}}^{\mathrm{miss}}$ scale

For any analysis using $\boldsymbol{E}_{\mathrm{T}}^{\mathrm{miss}}$, it is necessary to be able to evaluate the systematic uncertainty on the $E_{\mathrm{T}}^{\mathrm{miss}}$ scale. The

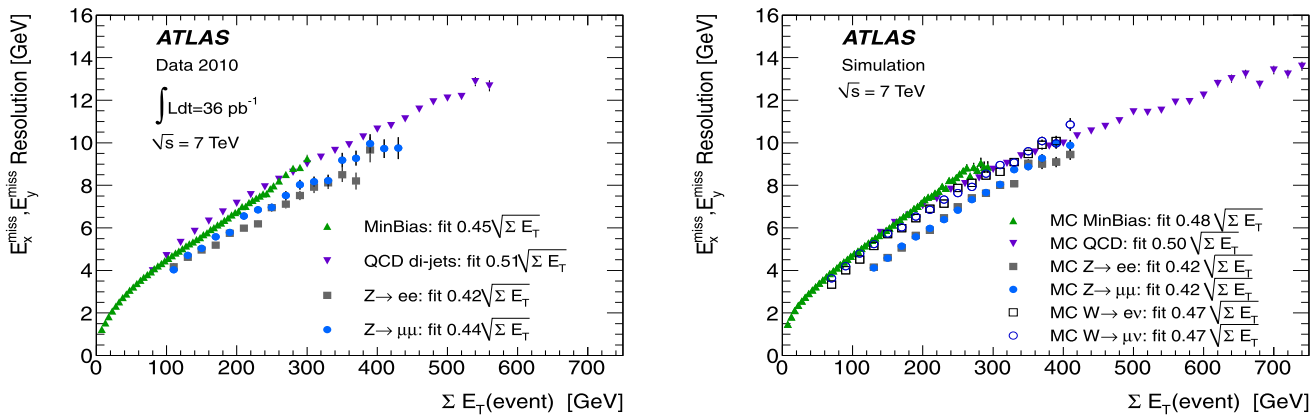

Fig. 15 E_x^{miss} and E_y^{miss} resolution as a function of the total transverse energy in the event calculated by summing the p_{T} of muons and the total transverse energy in the calorimeter in data at $\sqrt{s} = 7$ TeV (*left*) and MC (*right*). The resolution of the two $\boldsymbol{E}_{\text{T}}^{\text{miss}}$ components is fitted with a function $\sigma = k \cdot \sqrt{\Sigma E_{\text{T}}}$ and the fitted values of the parameter k, expressed in $\text{GeV}^{1/2}$, are reported in the figure

Table 1 Variations of the default simulation settings used for the estimate of the $E_{\text{T}}^{\text{miss,CellOut}}$ term systematic uncertainty. See Ref. [21] for details of the parameters

Variation	Description
Dead Material	5% increase in the inner detector material
	0.1 X_0 in front of the cryostat of the EM barrel calorimeter
	0.05 X_0 between presampler and EM barrel calorimeter
	0.1 X_0 in the cryostat after the EM barrel calorimeter
	density of material in barrel-endcap transition of the EM calorimeter $\times 1.5$
FTFP_BERT	An alternative shower model for hadronic interaction in GEANT4
QGSP	An alternative shower model for hadronic interaction in GEANT4
PYTHIA Perugia 2010 tune	An alternative setting of the PYTHIA parameters with increased final state radiation and more soft particles

$\boldsymbol{E}_{\text{T}}^{\text{miss}}$, as defined in Sect. 5.3, is the sum of several terms corresponding to different types of reconstructed objects. The uncertainty on each individual term can be evaluated given the knowledge of the reconstructed objects [8, 23] that are used to build it and this uncertainty can be propagated to $E_{\text{T}}^{\text{miss}}$. The overall systematic uncertainty on the $E_{\text{T}}^{\text{miss}}$ scale is then calculated by combining the uncertainties on each term.

The relative impact of the uncertainty of the constituent terms on $E_{\text{T}}^{\text{miss}}$ differs from one analysis to another depending on the final state being studied. In particular, in events containing W and Z bosons decaying to leptons, uncertainties on the scale and resolution in the measurements of the charged leptons, together with uncertainties on the jet energy scale, need to be propagated to the systematic uncertainty estimate of $E_{\text{T}}^{\text{miss}}$. Another significant contribution to the $E_{\text{T}}^{\text{miss}}$ scale uncertainty in W and Z boson final states comes from the contribution of topoclusters outside reconstructed objects and from soft jets. In the next three subsections, two complementary methods for the evaluation of the systematic uncertainty on the $E_{\text{T}}^{\text{miss,CellOut}}$ and the $E_{\text{T}}^{\text{miss,softjets}}$ terms are described. Finally the overall $E_{\text{T}}^{\text{miss}}$ uncertainty for $W \to \ell\nu$ events is calculated.

7.1 Evaluation of the systematic uncertainty on the $\boldsymbol{E}_{\text{T}}^{\text{miss,CellOut}}$ scale using Monte Carlo simulation

There are several possible sources of systematic uncertainty in the calculation of $E_{\text{T}}^{\text{miss,CellOut}}$. These sources include inaccuracies in the description of the detector material, the choice of shower model and the model for the underlying event in the simulation. The systematic uncertainty due to each of these sources is estimated with dedicated MC simulations. The MC jet samples, generated with PYTHIA, are those used to assess the systematic uncertainty on the jet energy scale [21]. Table 1 lists the simulation samples considered, referred to in the following as "variations" with respect to the nominal sample.

The estimate of the uncertainty on $E_{\text{T}}^{\text{miss,CellOut}}$ for a variation i is determined by calculating the percentage difference between the mean value of this term for the nominal sample, labelled μ_0, and that for the variation sample, labelled μ_i. This approach assumes that the variations affect the total scale and none of the variations introduces a shape dependence in the $E_{\text{T}}^{\text{miss,CellOut}}$ term, as verified in Ref. [24]. In order to cross-check for a possible dependence

on the event total transverse energy, the relative difference $R_i = (\mu_i - \mu_0)/\mu_0$ between different variations is computed in bins of $\sum E_{\mathrm{T}}$ for the jet samples. No significant dependence of R_i on $\sum E_{\mathrm{T}}$ is observed. A cross-check on the topology dependence is done using $W \to \ell\nu$ samples simulated by introducing the variations i. Table 2 shows the R_i values as computed in both the QCD jet samples and the $W \to \ell\nu$ samples. The results are consistent, showing that the estimated uncertainty does not have a large dependence on the event topology.

A symmetric systematic uncertainty on the $E_{\mathrm{T}}^{\mathrm{miss,CellOut}}$ scale is obtained by summing in quadrature the estimated uncertainties averaged between simulated jet and W events. The total estimated uncertainty[6] on the $E_{\mathrm{T}}^{\mathrm{miss,CellOut}}$ term is 2.6%.

7.2 Evaluation of the systematic uncertainty on the $\boldsymbol{E}_{\mathrm{T}}^{\mathrm{miss,CellOut}}$ scale from the topocluster energy scale uncertainty

The uncertainty on the scale of the $E_{\mathrm{T}}^{\mathrm{miss,CellOut}}$ term, which is built from topoclusters with a correction based on tracks (see Sect. 5.3.1), can also be calculated from the topocluster energy scale uncertainties. These uncertainties can be estimated from comparisons between data and MC simulation using the E/p response from single tracks, measured by summing the energies of all calorimeter clusters around a single isolated track [25]. The effects of these uncertainties on the $E_{\mathrm{T}}^{\mathrm{miss,CellOut}}$ term can be evaluated by varying the energy scale of topoclusters that contribute to the $E_{\mathrm{T}}^{\mathrm{miss,CellOut}}$ term in $W \to e\nu$ MC samples, as was done in Ref. [8].

The shift in the topocluster energy scale is applied by multiplying the topocluster energy by the function:

$$1 \pm a \times (1 + b/p_T), \tag{8}$$

Table 2 Systematic uncertainties (R_i) on $E_{\mathrm{T}}^{\mathrm{miss,CellOut}}$ associated with variations in the dead material (all the variations listed in Table 1 are applied at the same time), in the calorimeter shower modelling (FTFP_BERT, QGSP) and in the event generator settings (PYTHIA Perugia 2010 tune)

Variation	jet events	W production
Dead Material	$(-0.5 \pm 0.1)\%$	$(-0.6 \pm 0.2)\%$
FTFP_BERT	$(0.1 \pm 0.4)\%$	$(0.5 \pm 0.2)\%$
QGSP	$(-1.6 \pm 0.4)\%$	$(-2.2 \pm 0.2)\%$
PYTHIA Perugia 2010 tune	$(-1.7 \pm 0.1)\%$	$(-1.5 \pm 0.2)\%$

[6]In this uncertainty evaluation using MC simulation, the uncertainty on the absolute electromagnetic energy scale in the calorimeters should also be taken into account. For the bulk of the LAr barrel electromagnetic calorimeter a 1.5% uncertainty is found on the cell energy measurement, increasing to 5% for the presampler and 3% for the tile calorimeter [25].

with $a = 3(10)\%$ for $|\eta| < (>)3.2$ and $b = 1.2$ GeV.

The a parameter in (8) addresses the uncertainty on the cluster energy scale, obtained by comparing the ratio of the cluster energy and the measured track momentum, E/p, in data and MC simulation [25]. The value in the forward region, where tracks cannot be used to validate the energy scale, is estimated from the transverse momentum balance of one jet in the central region and one jet in the forward region in events with only two jets at high transverse momenta.

The b parameter in (8) addresses the possible change in the clustering efficiency and scale in a non-isolated environment. To go from the response for single isolated particles to the cluster energy scale, possible effects from the noise thresholds in the configuration with nearby particles are taken into account.

Because of threshold effects, more energy is clustered for nearby particles than for isolated ones. In an hypothetic worst case scenario, the environment is so busy that the clustering algorithm is forced to cluster all the deposited energy, with no bias due to the noise thresholds. Therefore, the maximal size of the noise threshold effect can be evaluated by comparing the ratio E_{cell}/p of the total energy E_{cell} deposited into all cells around an isolated track to the track momentum, to the ratio E/p of the clustered energy E to the track momentum, in data and MC simulation.

The fractional $E_{\mathrm{T}}^{\mathrm{miss,CellOut}}$ uncertainty is evaluated from:

$$\left(\Delta^{\mathrm{CellOut}+} + \Delta^{\mathrm{CellOut}-}\right) / \left(2 \times E_{\mathrm{T}}^{\mathrm{miss,CellOut}}\right), \tag{9}$$

where

$$\begin{aligned} \Delta^{\mathrm{CellOut}+} &= \left|E_{\mathrm{T}}^{\mathrm{miss,CellOut}+} - E_{\mathrm{T}}^{\mathrm{miss,CellOut}}\right|, \\ \Delta^{\mathrm{CellOut}-} &= \left|E_{\mathrm{T}}^{\mathrm{miss,CellOut}-} - E_{\mathrm{T}}^{\mathrm{miss,CellOut}}\right|, \end{aligned} \tag{10}$$

with $E_{\mathrm{T}}^{\mathrm{miss,CellOut}+}$ and $E_{\mathrm{T}}^{\mathrm{miss,CellOut}-}$ obtained by shifting the topocluster energies up and down, respectively, using (8). The value of the fractional $E_{\mathrm{T}}^{\mathrm{miss,CellOut}}$ uncertainty is found to be approximately 13%, decreasing slightly with increasing $\sum E_{\mathrm{T}}^{\mathrm{CellOut}}$. This uncertainty is much larger than the uncertainty due to the detector description estimated from the first three lines of Table 2. The main reason is that the values of a and b which enter into (8) are conservative, to include the effects described above. In particular the cluster energy uncertainty in the forward region is conservatively estimated, since the uncertainty cannot be evaluated using tracks. Moreover, the procedure does not take into account the fact that when the clusters are shifted up in p_{T}, some of them can form jets above threshold and they are therefore included in the soft jet term in $E_{\mathrm{T}}^{\mathrm{miss}}$. These clusters should be removed from the $E_{\mathrm{T}}^{\mathrm{miss,CellOut}}$, they are in fact kept and this increases the uncertainty. It should also be noted that in the calculation of $E_{\mathrm{T}}^{\mathrm{miss,CellOut}}$ the track momentum is

used instead of the topocluster energy when there is a track-topocluster matching (see Sect. 5.3.1). This would result in a reduced uncertainty due to the more precise measurement of the track momentum, which is not taken into account here. Further study is expected to provide a reduction in this uncertainty in future, by considering the described effects in detail.

To give an estimate of the $E_{\mathrm{T}}^{\mathrm{miss,CellOut}}$ systematic uncertainty, the calorimeter contribution can be taken from Sect. 7.2, and the uncertainty from the event generator settings from Sect. 7.1 (PYTHIA Perugia 2010 tune). This results in a total systematic uncertainty on the scale of $E_{\mathrm{T}}^{\mathrm{miss,CellOut}}$ of about 13%, which slightly decreases when $\sum E_{\mathrm{T}}{}^{\mathrm{CellOut}}$ increases.

7.3 Evaluation of the systematic uncertainty on the $\boldsymbol{E}_{\mathrm{T}}^{\mathrm{miss,softjets}}$ scale

The same procedure described in the previous sections is used to assess the systematic uncertainty on the $E_{\mathrm{T}}^{\mathrm{miss}}$ term calculated from soft jets (see Sect. 5.1).

Using the MC approach described in Sect. 7.1, it is found that the uncertainty on $E_{\mathrm{T}}^{\mathrm{miss,softjets}}$ does not exhibit a large dependence on the event $\sum E_{\mathrm{T}}$, as was also found for the uncertainty on the $E_{\mathrm{T}}^{\mathrm{miss,CellOut}}$ scale. The results are consistent between the QCD jet samples and the W samples, as can be seen from Table 3 which gives the systematic uncertainties R_i as computed in jet samples and in $W \to \ell\nu$ samples.

A total, symmetric, systematic uncertainty of about 3.3% on the $E_{\mathrm{T}}^{\mathrm{miss,softjets}}$ term is obtained by combining the results in Table 3, as was done in Sect. 7.1. With the same data-driven approach utilising the uncertainty on the topocluster energy scale described in Sect. 7.2, the systematic uncertainty on $E_{\mathrm{T}}^{\mathrm{miss,softjets}}$ is evaluated to be about 10%.

As for $E_{\mathrm{T}}^{\mathrm{miss,CellOut}}$, the uncertainty on the $E_{\mathrm{T}}^{\mathrm{miss,softjets}}$ scale found by shifting the topocluster energies is larger than the uncertainty estimated from MC simulation. To give an estimate of the systematic uncertainty on $E_{\mathrm{T}}^{\mathrm{miss,softjets}}$, the contribution from the calorimeter response can be taken from the data-driven evaluation and the contribution from the event generator settings from Table 3. This results in an overall systematic uncertainty of about 10% on $E_{\mathrm{T}}^{\mathrm{miss,softjets}}$, slightly increasing as $\sum E_{\mathrm{T}}$ increases.

Table 3 Systematic uncertainties (R_i) on $E_{\mathrm{T}}^{\mathrm{miss,softjets}}$ associated with variations in the dead material (all the variations listed in Table 1 are applied at the same time), in the calorimeter shower modelling (FTFP_BERT, QGSP) and in the event generator settings (PYTHIA Perugia 2010 tune)

Variation	jet events	W production
Dead Material	$(-1.5 \pm 0.1)\%$	$(-1.5 \pm 0.2)\%$
FTFP_BERT	$(0.3 \pm 0.4)\%$	$(0.8 \pm 0.2)\%$
QGSP	$(-2.6 \pm 0.4)\%$	$(-2.5 \pm 0.2)\%$
PYTHIA Perugia 2010 tune	$(-1.4 \pm 0.1)\%$	$(-1.0 \pm 0.2)\%$

7.4 Evaluation of the overall systematic uncertainty on the $\boldsymbol{E}_{\mathrm{T}}^{\mathrm{miss}}$ scale in $W \to e\nu$ and $W \to \mu\nu$ events

Using as inputs the systematic uncertainties on the different reconstructed objects [8, 21] and on $E_{\mathrm{T}}^{\mathrm{miss,CellOut}}$ and $E_{\mathrm{T}}^{\mathrm{miss,softjets}}$ evaluated in the previous sections, the overall $E_{\mathrm{T}}^{\mathrm{miss}}$ systematic uncertainty in $W \to e\nu$ and $W \to \mu\nu$ events is estimated. The same method can be applied to any final state event topology. Figure 16 shows, for both $W \to e\nu$ and $W \to \mu\nu$ events, the systematic uncertainties on each of the terms $E_{\mathrm{T}}^{\mathrm{miss},e}$ ($E_{\mathrm{T}}^{\mathrm{miss},\mu}$), $E_{\mathrm{T}}^{\mathrm{miss,jets}}$, $E_{\mathrm{T}}^{\mathrm{miss,softjets}}$ and $E_{\mathrm{T}}^{\mathrm{miss,CellOut}}$ as a function of their individual contribution to $\sum E_{\mathrm{T}}$ labelled $\sum E_{\mathrm{T}}{}^{\mathrm{term}}$. All the uncertainties are calculated with the formulae in (9) and (10). In the same figure the uncertainty on $E_{\mathrm{T}}^{\mathrm{miss}}$ due to the uncertainties on the different terms is also shown as a function of the total $\sum E_{\mathrm{T}}$, together with the overall uncertainty on $\boldsymbol{E}_{\mathrm{T}}^{\mathrm{miss}}$, obtained by combining the partial terms. The uncertainties on $E_{\mathrm{T}}^{\mathrm{miss,softjets}}$ and $E_{\mathrm{T}}^{\mathrm{miss,CellOut}}$ are considered to be fully correlated. In $W \to e\nu$ and $W \to \mu\nu$ events, selected as described in Sect. 3.3, the overall uncertainty on the $E_{\mathrm{T}}^{\mathrm{miss}}$ scale increases with $\sum E_{\mathrm{T}}$ from ~1% to ~7%. It is estimated to be, on average, about 2.6% for both channels.

The $E_{\mathrm{T}}^{\mathrm{miss}}$ scale uncertainty depends on the event topology because the contribution of a given $E_{\mathrm{T}}^{\mathrm{miss}}$ term can vary for different final states.

8 Determination of the $\boldsymbol{E}_{\mathrm{T}}^{\mathrm{miss}}$ scale from $W \to \ell\nu$ events

The determination of the absolute $E_{\mathrm{T}}^{\mathrm{miss}}$ scale is important in a range of analyses involving $E_{\mathrm{T}}^{\mathrm{miss}}$ measurements, ranging from precision measurements to searches for new physics.

In this section two complementary methods to determine the absolute scale of $E_{\mathrm{T}}^{\mathrm{miss}}$ using $W \to \ell\nu$ events are described. The first method uses a fit to the distribution of the transverse mass, m_{T}, of the lepton-$E_{\mathrm{T}}^{\mathrm{miss}}$ system, and is sensitive both to the scale and the resolution of $E_{\mathrm{T}}^{\mathrm{miss}}$. The second method uses the interdependence of the neutrino and lepton momenta in the $W \to e\nu$ channel, and the $E_{\mathrm{T}}^{\mathrm{miss}}$ scale is determined as a function of the reconstructed electron transverse momentum. Both methods allow checks on the agreement between data and MC simulation for the $E_{\mathrm{T}}^{\mathrm{miss}}$ scale.

8.1 Reconstructed transverse mass method

The method described in this section uses the shape of the m_{T} distribution and is sensitive to both the $E_{\mathrm{T}}^{\mathrm{miss}}$ resolution and scale. The lepton transverse momentum, p_{T}^{ℓ}, and

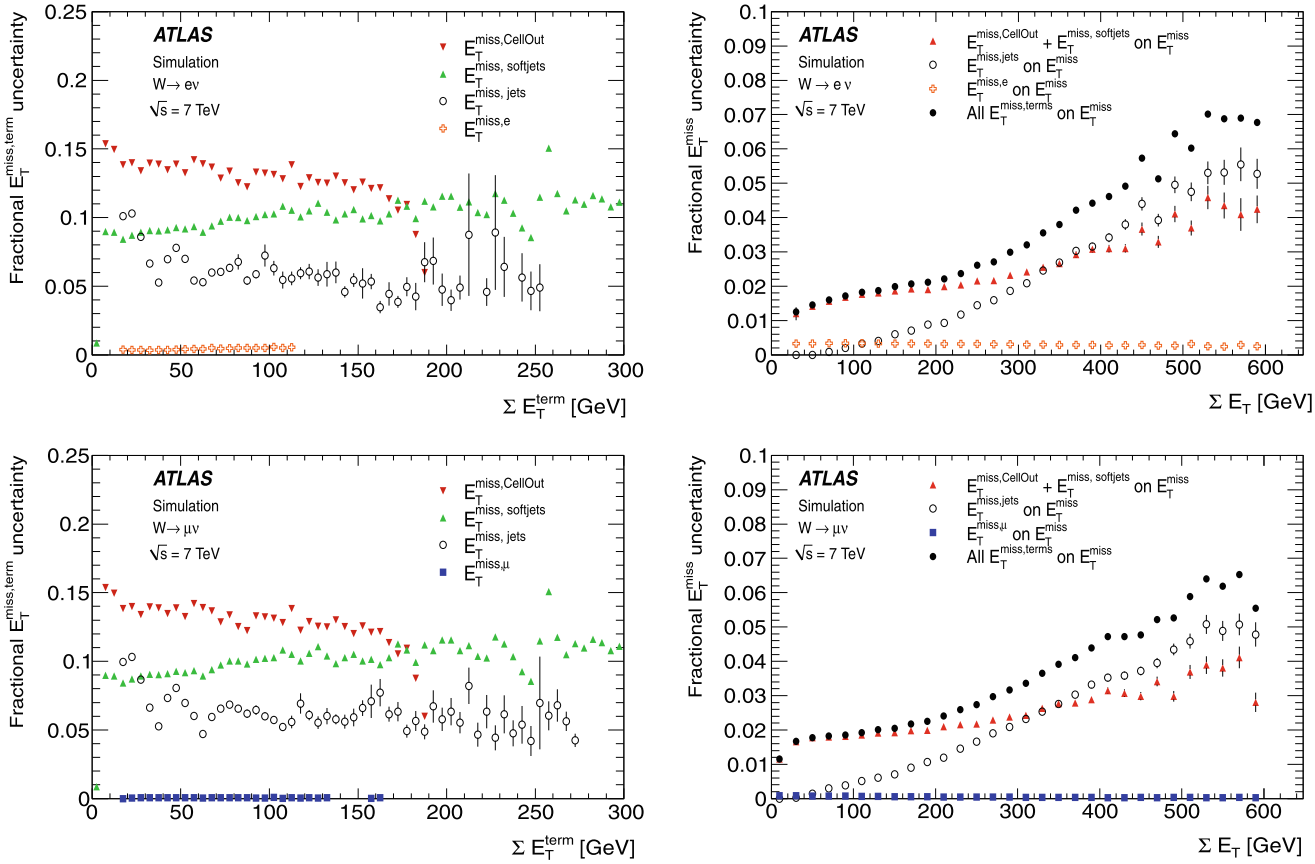

Fig. 16 Fractional systematic uncertainty (calculated as in (9) and (10)) on different $E_{\mathrm{T}}^{\mathrm{miss}}$ terms as a function of respective $\sum E_{\mathrm{T}}^{\mathrm{term}}$ (*left*) and contributions of different term uncertainties on $E_{\mathrm{T}}^{\mathrm{miss}}$ uncertainty as a function of $\sum E_{\mathrm{T}}$ (*right*) in MC $W \to e\nu$ events (*top*) and $W \to \mu\nu$ events (*bottom*). The overall systematic uncertainty on the $E_{\mathrm{T}}^{\mathrm{miss}}$ scale, obtained combining the various contributions is shown in the right plots (*filled circles*). The uncertainties on $E_{\mathrm{T}}^{\mathrm{miss,softjets}}$ and $E_{\mathrm{T}}^{\mathrm{miss,CellOut}}$ are considered to be fully correlated

the $E_{\mathrm{T}}^{\mathrm{miss}}$ are used to calculate m_{T} as:

$$m_T = \sqrt{2p_{\mathrm{T}}^{\ell} E_{\mathrm{T}}^{\mathrm{miss}}(1-\cos\phi)}, \tag{11}$$

where ϕ is the azimuthal angle between the lepton momentum and $E_{\mathrm{T}}^{\mathrm{miss}}$ directions. The true m_{T} is reconstructed from the simulation under the hypothesis that $E_{\mathrm{T}}^{\mathrm{miss}}$ is entirely due to the neutrino momentum, p_{T}^{ν}. Template histograms of the m_{T} distributions are generated by convoluting the true transverse mass distribution with a Gaussian function:

$$E_{x(y)}^{\mathrm{miss,smeared}} = \alpha\, E_{x(y)}^{\mathrm{miss,True}} * Gauss\big(0, k\cdot\sqrt{\Sigma E_{\mathrm{T}}}\big), \tag{12}$$

where the parameters α and k are the $E_{\mathrm{T}}^{\mathrm{miss}}$ scale and resolution respectively.

The α and k parameters are determined through a fit of the m_{T} distribution to data using a linear combination of signal and background m_{T} distributions obtained from simulation. All the backgrounds, with the exception of the jet background, are evaluated from the same MC samples used in Sect. 6.3 and the normalization is fixed according to their cross-sections. The shape of the jet background is also evaluated from MC simulation and its normalization is obtained from the fit, in addition to α and k.

To select $W \to \mu\nu$ events, the same criteria as described in Sect. 3.3 are used, with the exception that no cut on $E_{\mathrm{T}}^{\mathrm{miss}}$ is applied and a looser cut, $m_{\mathrm{T}} > 30$ GeV, is applied in order that the background normalization can be fitted. The α and k parameters obtained from the fit are shown in Table 4, together with the numbers of events for the signal and backgrounds and the χ^2/ndof of the fit. In the table, instead of the values of α, the values of $\alpha - 1 = \langle (E_{x(y)}^{\mathrm{miss}} - E_{x(y)}^{\mathrm{miss,True}})/E_{x(y)}^{\mathrm{miss,True}} \rangle$ are reported, in order to compare with the result in Sects. 6.3.1 and 8.2. The results for the α and k parameters using the m_{T} distribution of the simulated signal are also shown in Table 4, and they are in good agreement with the results from data. The result of the fit to data and MC simulation is shown in Fig. 17.

To select $W \to e\nu$ events, the selection described in Sect. 3.3 is used with the addition of tighter cuts. A cut $E_{\mathrm{T}}^{\mathrm{miss}} > 36$ GeV is applied to exclude the region where the $E_{\mathrm{T}}^{\mathrm{miss}}$ response is not linear (see Fig. 14). A cut $m_{\mathrm{T}} > 40$

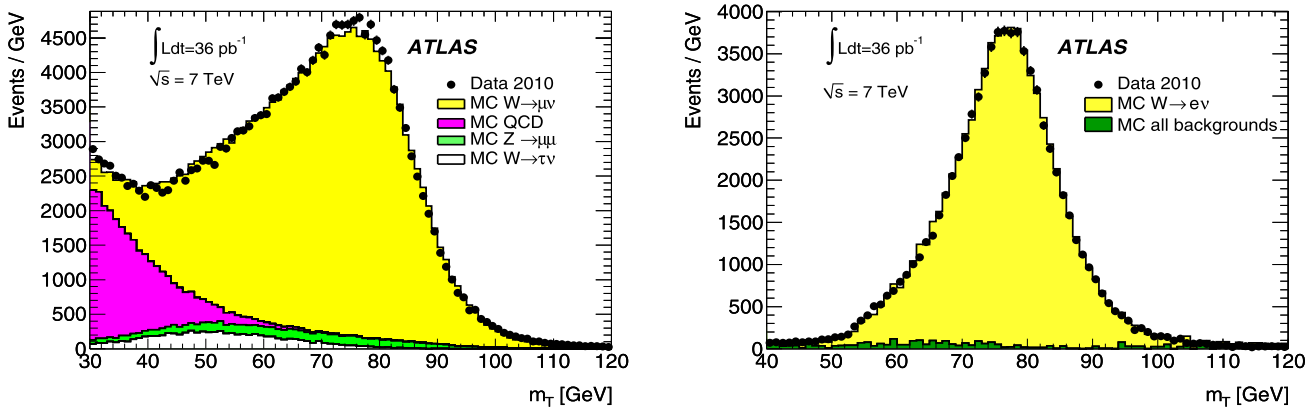

Fig. 17 Distributions of the transverse mass, m_{T}, of the muon-$E_{\mathrm{T}}^{\mathrm{miss}}$ system (*left*) and of the electron-$E_{\mathrm{T}}^{\mathrm{miss}}$ system (*right*) for data. The m_{T} distributions from Monte Carlo simulation are superimposed, after each background sample is weighted as explained in the text. The main backgrounds are shown for $W \to \mu\nu$, the sum of all backgrounds is shown for $W \to e\nu$. The $W \to \ell\nu$ MC signal histogram is obtained using the true $E_{\mathrm{T}}^{\mathrm{miss}}$ smeared as in (12) with the scale and resolution parameters obtained from the fit

GeV is also applied. The α and k parameters obtained from the fit are shown in Table 4, together with the results obtained from the MC, which are in good agreement with data. The result of the fit to data and MC simulation is shown in Fig. 17.

The results obtained with this method are compatible, at the few percent level, with the results shown in Fig. 14 and Fig. 15, which were derived using only simulation. From those figures, for the $W \to \mu\nu$ channel $\alpha - 1$ has values up to 3% and the resolution is $0.47\sqrt{\sum E_{\mathrm{T}}}$; for the $W \to e\nu$ channel $\alpha - 1$ is close to zero for high $E_{\mathrm{T}}^{\mathrm{miss}}$ values and the resolution is $0.47\sqrt{\sum E_{\mathrm{T}}}$.

The uncertainty due to background subtraction is already included in the uncertainty reported in Table 4. The systematic uncertainty on $\alpha - 1$ is determined to be about 1% for each channel, by checking the stability of the results using different cuts on $E_{\mathrm{T}}^{\mathrm{miss}}$ and using a different generator, MC@NLO. In summary, with this method the $E_{\mathrm{T}}^{\mathrm{miss}}$ absolute scale is determined from $W \to \ell\nu$ events, in a data sample corresponding to an integrated luminosity of about 36 pb^{-1}, with an uncertainty (adding the uncertainties reported in Table 4 with the systematic uncertainty) of about 1.5% and about 2% for the $W \to \mu\nu$ and $W \to e\nu$ decay channels, respectively.

8.2 Method based on the correlation between electron and neutrino transverse momenta in $W \to e\nu$

In this section the correlation between the transverse momenta of charged and neutral leptons from W boson decays is used to determine the $E_{\mathrm{T}}^{\mathrm{miss}}$ scale. The mean measured $E_{\mathrm{T}}^{\mathrm{miss}}$ is compared to the mean true $E_{\mathrm{T}}^{\mathrm{miss}}$ from signal MC events. The relative bias in the reconstructed $E_{\mathrm{T}}^{\mathrm{miss}}$, $(\langle E_{\mathrm{T}}^{\mathrm{miss}}\rangle - \langle E_{\mathrm{T}}^{\mathrm{miss,True}}\rangle)/\langle E_{\mathrm{T}}^{\mathrm{miss,True}}\rangle$, is studied as a function of p_{T}^{e} because the MC simulation of the electron response is more accurate than that for hadrons.

This method is shown for $W \to e\nu$ events by applying selection criteria similar to the ones described in Sect. 3.3, but with isolation requirements both on the electron track and calorimeter signal. The $E_{\mathrm{T}}^{\mathrm{miss}}$ is required to be greater than 20 GeV and no cut is applied on m_{T}.

MC samples are generated with MC@NLO [15]. A next-to-leading-order (NLO) generator is used for this study because in this approach the $E_{\mathrm{T}}^{\mathrm{miss}}$ scale is validated on the

Table 4 Results of m_{T} fit in $W \to \ell\nu$ events. The second and third columns show the scale and resolution parameters obtained. The numbers of events for the signal, the electroweak and QCD backgrounds obtained from the fit are shown in the fourth, fifth and sixth columns for data. In the last column the χ^2/ndof of the fit is reported. The errors are statistical and take into account background subtraction uncertainties and correlations

Channel	$\alpha - 1$ (%)	k	Signal	EW (fixed)	QCD	$\chi^2/ndof$
$W \to \mu\nu$ data	5.1 ± 0.8	0.52 ± 0.01	164920 ± 840	14760	24870 ± 840	68/87
$W \to \mu\nu$ MC	5.5 ± 0.8	0.50 ± 0.01				70/78
$W \to e\nu$ data	-0.8 ± 1.6	0.49 ± 0.01	75660 ± 180	1210	980 ± 180	54/75
$W \to e\nu$ MC	1.8 ± 1.7	0.50 ± 0.01				38/54

basis of the known decay properties of the W boson. The correlation between p_{T}^{ν} and p_{T}^{e} is important for this study, and is poorly described by leading-order generators such as PYTHIA, whereas it is much improved in MC@NLO. The MC events are weighted such that the true W boson transverse momentum, p_{T}^{W}, and pseudorapidity η^{W} agree with that generated using the RESBOS [26] generator which is more accurate in describing p_{T}^{W} at low values. Finally, an additional smearing is applied to the reconstructed electron momentum in the MC samples, to match the electron resolution measured in data, and the correction is propagated to $E_{\mathrm{T}}^{\mathrm{miss}}$.

A data-driven technique is used to estimate the impact of jet background, which is small (see Fig. 18 left) and concentrated at low p_{T}^{e}. $W \to \tau\nu$ events, where the τ decays to an electron, are the second largest background, but the impact on the mean value of $E_{\mathrm{T}}^{\mathrm{miss}}$ is found to be negligible.

The distribution of p_{T}^{e} is shown in Fig. 18. The distribution from data after event selection is fitted by varying the normalization of signal MC and QCD background distributions. A satisfactory description of data is achieved except for the first bin, which is excluded from the fit. For each p_{T}^{e} bin, the corrected distribution of $E_{\mathrm{T}}^{\mathrm{miss}}$ is obtained by subtracting that of the background sample (after normalizing it according to the fit) from the data distribution. The largest impact of background corresponds to $p_{\mathrm{T}}^{e} = 20$ GeV, with an effect of about 2 GeV on the mean value of $E_{\mathrm{T}}^{\mathrm{miss}}$; the effect decreases quickly to 0.2 GeV at $p_{\mathrm{T}}^{e} = 30$ GeV.

Since a cut on $E_{\mathrm{T}}^{\mathrm{miss}}$ is used for the event selection and the $\boldsymbol{E}_{\mathrm{T}}^{\mathrm{miss}}$ resolution is finite, the results are biased. To correct for the bias in signal MC events the requirement of reconstructed $E_{\mathrm{T}}^{\mathrm{miss}} > 20$ GeV is replaced by a cut on true $E_{\mathrm{T}}^{\mathrm{miss}} > 20$ GeV.

The mean measured $E_{\mathrm{T}}^{\mathrm{miss}}$, corrected for background and for the event selection bias, is used to calculate the relative bias in the reconstructed $E_{\mathrm{T}}^{\mathrm{miss}}$, $(\langle E_{\mathrm{T}}^{\mathrm{miss}}\rangle - \langle E_{\mathrm{T}}^{\mathrm{miss,True}}\rangle)/\langle E_{\mathrm{T}}^{\mathrm{miss,True}}\rangle$, which is shown in Fig. 18 as a function of p_{T}^{e}. The figure shows that the $E_{\mathrm{T}}^{\mathrm{miss}}$ scale is correct at low values of p_{T}^{e} while it is overestimated at high values of p_{T}^{e}.

The bias on $E_{\mathrm{T}}^{\mathrm{miss}}$ is on the percent level between 25 and 35 GeV, then it rises up to 7% and it is $2 \pm 0.1\%$ on average. For comparison, if the entire calculation is performed on signal MC events alone, the resulting average bias in $E_{\mathrm{T}}^{\mathrm{miss}}$ is $2.9 \pm 0.1\%$. The method relies on simulation to derive the correlation between $E_{\mathrm{T}}^{\mathrm{miss,True}}$ and p_{T}^{e}, so it can be sensitive to details of the simulation. In particular, the jet factorization and renormalization scales, as well as the choice of PDF, can affect the results, but all these also change the p_{T}^{W} distribution. Therefore the shape of the p_{T}^{W} distribution was distorted by $\pm 10\%$, justified by the comparison of a recent measurement of the p_{T}^{Z} distribution [27] with RESBOS predictions, and the relative bias was calculated again. A systematic uncertainty on the relative $E_{\mathrm{T}}^{\mathrm{miss}}$ scale bias of $\pm 2\%$ is evaluated. The results for the average $E_{\mathrm{T}}^{\mathrm{miss}}$ scale are summarized in Table 5. These results agree within errors with the values of $\alpha - 1$ shown in Table 4.

9 Conclusion

The missing transverse momentum ($\boldsymbol{E}_{\mathrm{T}}^{\mathrm{miss}}$) has been measured in minimum bias, di-jet, $Z \to \ell\ell$ and $W \to \ell\nu$ events in 7 TeV pp collisions recorded with the ATLAS detector in 2010.

The value of $\boldsymbol{E}_{\mathrm{T}}^{\mathrm{miss}}$ is reconstructed from calorimeter cells in topological clusters, with the exception of electrons and photons for which a different clustering algorithm is used, and from reconstructed muons. The cells are calibrated according to their parent particle type. The scheme yielding the best performance is evaluated to be that in which electrons are calibrated with the default electron calibration and photons are used at the EM scale, the τ-jets and jets are calibrated with the local hadronic calibration (LCW), the jets

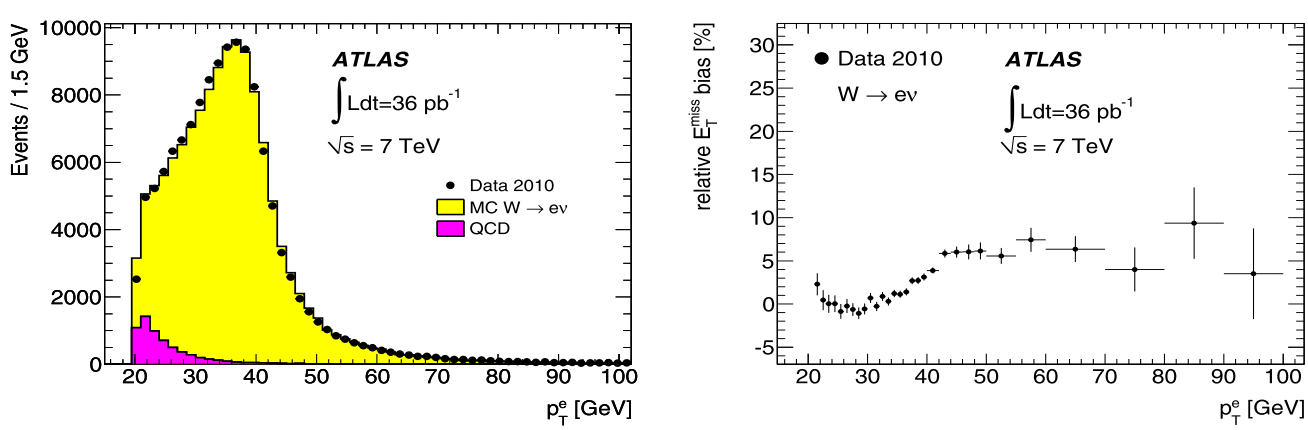

Fig. 18 Transverse momentum distribution of electron candidates in data, in signal MC with nominal event selection and with reversed cuts for background (QCD) from data (*left*). Relative bias in the reconstructed $E_{\mathrm{T}}^{\mathrm{miss}}$ (*right*). Only statistical uncertainties are shown

Table 5 Average relative $E_{\mathrm{T}}^{\mathrm{miss}}$ scale bias obtained from data and MC simulation from the electron-neutrino correlation method. The statistical and the systematic uncertainties are given for data

source	scale bias (%)
data	$2.0 \pm 0.1 \pm 2.0$
MC	2.9 ± 0.1

with p_{T} greater than 20 GeV are scaled to the jet energy scale, and the contribution from topoclusters not associated to high-p_{T} objects is calculated with LCW calibration combined with tracking information.

Monte Carlo simulation is found to describe the data in general rather well. No large tails are observed in the $E_{\mathrm{T}}^{\mathrm{miss}}$ distribution in minimum bias, di-jet and $Z \to \ell\ell$ events, where no significant $E_{\mathrm{T}}^{\mathrm{miss}}$ is expected. The tails are not completely well described by MC simulation especially in di-jets events, where there are more events in the tail in data.

There is some difference observed between data and MC simulation for the reconstructed total transverse energy. The precise difference is dependent on the model used to simulate soft-physics processes.

The $\boldsymbol{E}_{\mathrm{T}}^{\mathrm{miss}}$ resolution is similar in the different channels studied and in agreement with the resolution in the MC simulation. The resolution follows a function $\sigma = k \cdot \sqrt{\Sigma E_{\mathrm{T}}}$, where the parameter k is about 0.5 $\mathrm{GeV}^{1/2}$.

The linearity of the $\boldsymbol{E}_{\mathrm{T}}^{\mathrm{miss}}$ measurement in $W \to \ell\nu$ events is studied in MC simulation as a function of the true $E_{\mathrm{T}}^{\mathrm{miss}}$. Except for the bias observed at small true $E_{\mathrm{T}}^{\mathrm{miss}}$ values (visible up to 40 GeV), due to the finite $\boldsymbol{E}_{\mathrm{T}}^{\mathrm{miss}}$ resolution, the linearity is better than 1% in $W \to e\nu$ events, while a small non-linearity up to about 3% is observed in $W \to \mu\nu$ events.

The $\boldsymbol{E}_{\mathrm{T}}^{\mathrm{miss}}$ projected along the Z direction in $Z \to \ell\ell$ events is observed to have a bias up to 6 GeV at large values of p_T^Z in events with no jets, suggesting that some improvements are still needed in the calibration of low-p_{T} objects.

The overall systematic uncertainty on $E_{\mathrm{T}}^{\mathrm{miss}}$ scale, calculated by combining the uncertainties on the various terms entering the full $\boldsymbol{E}_{\mathrm{T}}^{\mathrm{miss}}$ calculation, is estimated to be, on average, 2.6% in events with a W decaying to a lepton (electron or muon) and neutrino. The uncertainty is larger at large $\sum E_{\mathrm{T}}$.

Two methods are used for determining the $E_{\mathrm{T}}^{\mathrm{miss}}$ scale from $W \to \ell\nu$ events in data, giving results in agreement with that evaluated using MC simulation. The resulting uncertainty on the $E_{\mathrm{T}}^{\mathrm{miss}}$ scale determined in-situ with 36 pb^{-1} of data is, on average, about 2%.

Acknowledgements We thank CERN for the very successful operation of the LHC, as well as the support staff from our institutions without whom ATLAS could not be operated efficiently.

We acknowledge the support of ANPCyT, Argentina; YerPhI, Armenia; ARC, Australia; BMWF, Austria; ANAS, Azerbaijan; SSTC, Belarus; CNPq and FAPESP, Brazil; NSERC, NRC and CFI, Canada; CERN; CONICYT, Chile; CAS, MOST and NSFC, China; COLCIENCIAS, Colombia; MSMT CR, MPO CR and VSC CR, Czech Republic; DNRF, DNSRC and Lundbeck Foundation, Denmark; ARTEMIS, European Union; IN2P3-CNRS, CEA-DSM/IRFU, France; GNAS, Georgia; BMBF, DFG, HGF, MPG and AvH Foundation, Germany; GSRT, Greece; ISF, MINERVA, GIF, DIP and Benoziyo Center, Israel; INFN, Italy; MEXT and JSPS, Japan; CNRST, Morocco; FOM and NWO, Netherlands; RCN, Norway; MNiSW, Poland; GRICES and FCT, Portugal; MERYS (MECTS), Romania; MES of Russia and ROSATOM, Russian Federation; JINR; MSTD, Serbia; MSSR, Slovakia; ARRS and MVZT, Slovenia; DST/NRF, South Africa; MICINN, Spain; SRC and Wallenberg Foundation, Sweden; SER, SNSF and Cantons of Bern and Geneva, Switzerland; NSC, Taiwan; TAEK, Turkey; STFC, the Royal Society and Leverhulme Trust, United Kingdom; DOE and NSF, United States of America.

The crucial computing support from all WLCG partners is acknowledged gratefully, in particular from CERN and the ATLAS Tier-1 facilities at TRIUMF (Canada), NDGF (Denmark, Norway, Sweden), CC-IN2P3 (France), KIT/GridKA (Germany), INFN-CNAF (Italy), NL-T1 (Netherlands), PIC (Spain), ASGC (Taiwan), RAL (UK) and BNL (USA) and in the Tier-2 facilities worldwide.

Open Access This article is distributed under the terms of the Creative Commons Attribution Noncommercial License which permits any noncommercial use, distribution, and reproduction in any medium, provided the original author(s) and source are credited.

References

1. The ATLAS Collaboration, The ATLAS experiment at the CERN large hadron collider. J. Instrum. **3**, S08003 (2008)
2. The ATLAS Collaboration, Performance of the ATLAS detector using first collision data. J. High Energy Phys. **09**, 056 (2010)
3. The ATLAS Collaboration, Search for squarks and gluinos using final states with jets and missing transverse momentum with the ATLAS detector in 7 TeV proton-proton collisions. Phys. Lett. B **701**, 186 (2011)
4. The ATLAS Collaboration, Properties of jets and inputs to jets reconstruction and calibration with the ATLAS detector using proton-proton collisions at $\sqrt{s} = 7$ TeV. ATLAS-CONF-2010-053
5. M. Cacciari, G.P. Salam, G. Soyez, The anti-k_t jet clustering algorithm. J. High Energy Phys. **05**, 063 (2008). arXiv:0802.1189
6. The ATLAS Collaboration, Luminosity determination in pp collisions at 7 TeV using the ATLAS detector at the LHC. Eur. Phys. J. C **071**, 1630 (2011). arXiv:1101.2185
7. The ATLAS Collaboration, Updated luminosity determination in pp collisions at sqrt(s) = 7 TeV using the ATLAS detector. ATLAS-CONF-2011-011
8. The ATLAS Collaboration, Measurement of the $W \to l\nu$ and $Z \to ll$ production cross sections in proton-proton collisions at $\sqrt{s} = 7$ TeV with the ATLAS detector. J. High Energy Phys. **12**, 060 (2010). arXiv:1010.2130
9. The ATLAS Collaboration, Charged-particle multiplicities in pp interactions measured with the ATLAS detector at the LHC. New J. Phys. **13**, 053033 (2011)
10. The ATLAS Collaboration, Muon reconstruction performance. ATLAS-CONF-2010-064
11. The ATLAS Collaboration, Electron and photon reconstruction and identification in ATLAS: expected performance at high energy and results at 900 GeV. ATLAS-CONF-2010-005

12. T. Sjostrand, S. Mrenna, P. Skands, PYTHIA 6.4 physics and manual. J. High Energy Phys. **05**, 026 (2006)
13. The ATLAS Collaboration, Charged particle multiplicities in pp interactions at sqrt(s) = 0.9 and 7 TeV in a diffractive limited phase-space measured with the ATLAS detector at the LHC and new PYTHIA6 tune. ATLAS-CONF-2010-031
14. S. Agostinelli et al., GEANT4: A simulation toolkit. Nucl. Instrum. Methods A **506**, 250 (2003)
15. S. Frixione, B.R. Webber, Matching NLO QCD computations and parton shower simulations. J. High Energy Phys. **06**, 029 (2002)
16. T. Sjostrand, S. Mrenna, P. Skands, Brief introduction to PYTHIA8.1. Comput. Phys. Commun. **178**, 852 (2008). arXiv:0710.3820
17. The ATLAS Collaboration, Expected performance of the ATLAS experiment—Detector, trigger and physics (Jet and $E_{\mathrm{T}}^{\mathrm{miss}}$chapter). arXiv:0901.0512
18. W. Lampl et al., Calorimeter clustering algorithms: Description and performance. ATL-LARG-PUB-2008-002
19. The ATLAS Collaboration, Tau reconstruction and identification performance in ATLAS. ATLAS-CONF-2010-086
20. T. Barillari et al., Local hadron calibration properties. ATL-LARG-PUB-2009-001
21. The ATLAS Collaboration, Jet energy scale and its systematic uncertainty in proton-proton collisions at $\sqrt{s} = 7$ TeV in ATLAS 2010 data. ATLAS-CONF-2011-032
22. R. Corke, T. Sjostrand, Interleaved parton showers and tuning prospects. J. High Energy Phys. **032**, 1103 (2011). arXiv:1011.1759
23. The ATLAS Collaboration, Measurement of inclusive jet and dijet cross sections in proton-proton collisions at 7 TeV centre-of-mass energy with the ATLAS detector. Eur. Phys. J. C **71**, 1512 (2011). arXiv:1009.5908
24. The ATLAS Collaboration, Reconstruction and calibration of missing transverse energy and performance in Z and W events in ATLAS proton-proton collisions at $\sqrt{s} = 7$ TeV. ATLAS-CONF-2011-080
25. The ATLAS Collaboration, ATLAS calorimeter response to single isolated hadrons and estimation of the calorimeter jet scale uncertainty. ATLAS-CONF-2011-028
26. C. Balazs, C.P. Yuan, Soft gluon effects on lepton pairs at hadron colliders. Phys. Rev. D **56**, 5558–5583 (1997)
27. The ATLAS Collaboration, Measurement of the transverse momentum distribution of Z/γ bosons in proton-proton collisions at $\sqrt{s} = 7$ TeV with the ATLAS detector. Phys. Lett. B **705**, 415–434 (2011). arXiv:1107.2381

The ATLAS Collaboration

G. Aad[48], B. Abbott[111], J. Abdallah[11], A.A. Abdelalim[49], A. Abdesselam[118], O. Abdinov[10], B. Abi[112], M. Abolins[88], H. Abramowicz[153], H. Abreu[115], E. Acerbi[89a,89b], B.S. Acharya[164a,164b], D.L. Adams[24], T.N. Addy[56], J. Adelman[175], M. Aderholz[99], S. Adomeit[98], P. Adragna[75], T. Adye[129], S. Aefsky[22], J.A. Aguilar-Saavedra[124b,a], M. Aharrouche[81], S.P. Ahlen[21], F. Ahles[48], A. Ahmad[148], M. Ahsan[40], G. Aielli[133a,133b], T. Akdogan[18a], T.P.A. Åkesson[79], G. Akimoto[155], A.V. Akimov[94], A. Akiyama[67], M.S. Alam[1], M.A. Alam[76], J. Albert[169], S. Albrand[55], M. Aleksa[29], I.N. Aleksandrov[65], F. Alessandria[89a], C. Alexa[25a], G. Alexander[153], G. Alexandre[49], T. Alexopoulos[9], M. Alhroob[20], M. Aliev[15], G. Alimonti[89a], J. Alison[120], M. Aliyev[10], P.P. Allport[73], S.E. Allwood-Spiers[53], J. Almond[82], A. Aloisio[102a,102b], R. Alon[171], A. Alonso[79], M.G. Alviggi[102a,102b], K. Amako[66], P. Amaral[29], C. Amelung[22], V.V. Ammosov[128], A. Amorim[124a,b], G. Amorós[167], N. Amram[153], C. Anastopoulos[29], L.S. Ancu[16], N. Andari[115], T. Andeen[34], C.F. Anders[20], G. Anders[58a], K.J. Anderson[30], A. Andreazza[89a,89b], V. Andrei[58a], M-L. Andrieux[55], X.S. Anduaga[70], A. Angerami[34], F. Anghinolfi[29], N. Anjos[124a], A. Annovi[47], A. Antonaki[8], M. Antonelli[47], A. Antonov[96], J. Antos[144b], F. Anulli[132a], S. Aoun[83], L. Aperio Bella[4], R. Apolle[118,c], G. Arabidze[88], I. Aracena[143], Y. Arai[66], A.T.H. Arce[44], J.P. Archambault[28], S. Arfaoui[29,d], J-F. Arguin[14], E. Arik[18a,*], M. Arik[18a], A.J. Armbruster[87], O. Arnaez[81], C. Arnault[115], A. Artamonov[95], G. Artoni[132a,132b], D. Arutinov[20], S. Asai[155], R. Asfandiyarov[172], S. Ask[27], B. Åsman[146a,146b], L. Asquith[5], K. Assamagan[24], A. Astbury[169], A. Astvatsatourov[52], G. Atoian[175], B. Aubert[4], B. Auerbach[175], E. Auge[115], K. Augsten[127], M. Aurousseau[145a], N. Austin[73], G. Avolio[163], R. Avramidou[9], D. Axen[168], C. Ay[54], G. Azuelos[93,e], Y. Azuma[155], M.A. Baak[29], G. Baccaglioni[89a], C. Bacci[134a,134b], A.M. Bach[14], H. Bachacou[136], K. Bachas[29], G. Bachy[29], M. Backes[49], M. Backhaus[20], E. Badescu[25a], P. Bagnaia[132a,132b], S. Bahinipati[2], Y. Bai[32a], D.C. Bailey[158], T. Bain[158], J.T. Baines[129], O.K. Baker[175], M.D. Baker[24], S. Baker[77], E. Banas[38], P. Banerjee[93], Sw. Banerjee[172], D. Banfi[29], A. Bangert[137], V. Bansal[169], H.S. Bansil[17], L. Barak[171], S.P. Baranov[94], A. Barashkou[65], A. Barbaro Galtieri[14], T. Barber[27], E.L. Barberio[86], D. Barberis[50a,50b], M. Barbero[20], D.Y. Bardin[65], T. Barillari[99], M. Barisonzi[174], T. Barklow[143], N. Barlow[27], B.M. Barnett[129], R.M. Barnett[14], A. Baroncelli[134a], G. Barone[49], A.J. Barr[118], F. Barreiro[80], J. Barreiro Guimarães da Costa[57], P. Barrillon[115], R. Bartoldus[143], A.E. Barton[71], D. Bartsch[20], V. Bartsch[149], R.L. Bates[53], L. Batkova[144a], J.R. Batley[27], A. Battaglia[16], M. Battistin[29],

G. Battistoni[89a], F. Bauer[136], H.S. Bawa[143,f], B. Beare[158], T. Beau[78], P.H. Beauchemin[118], R. Beccherle[50a], P. Bechtle[41], H.P. Beck[16], M. Beckingham[48], K.H. Becks[174], A.J. Beddall[18c], A. Beddall[18c], S. Bedikian[175], V.A. Bednyakov[65], C.P. Bee[83], M. Begel[24], S. Behar Harpaz[152], P.K. Behera[63], M. Beimforde[99], C. Belanger-Champagne[85], P.J. Bell[49], W.H. Bell[49], G. Bella[153], L. Bellagamba[19a], F. Bellina[29], M. Bellomo[29], A. Belloni[57], O. Beloborodova[107], K. Belotskiy[96], O. Beltramello[29], S. Ben Ami[152], O. Benary[153], D. Benchekroun[135a], C. Benchouk[83], M. Bendel[81], N. Benekos[165], Y. Benhammou[153], D.P. Benjamin[44], M. Benoit[115], J.R. Bensinger[22], K. Benslama[130], S. Bentvelsen[105], D. Berge[29], E. Bergeaas Kuutmann[41], N. Berger[4], F. Berghaus[169], E. Berglund[49], J. Beringer[14], K. Bernardet[83], P. Bernat[77], R. Bernhard[48], C. Bernius[24], T. Berry[76], A. Bertin[19a,19b], F. Bertinelli[29], F. Bertolucci[122a,122b], M.I. Besana[89a,89b], N. Besson[136], S. Bethke[99], W. Bhimji[45], R.M. Bianchi[29], M. Bianco[72a,72b], O. Biebel[98], S.P. Bieniek[77], K. Bierwagen[54], J. Biesiada[14], M. Biglietti[134a,134b], H. Bilokon[47], M. Bindi[19a,19b], S. Binet[115], A. Bingul[18c], C. Bini[132a,132b], C. Biscarat[177], U. Bitenc[48], K.M. Black[21], R.E. Blair[5], J.-B. Blanchard[115], G. Blanchot[29], T. Blazek[144a], C. Blocker[22], J. Blocki[38], A. Blondel[49], W. Blum[81], U. Blumenschein[54], G.J. Bobbink[105], V.B. Bobrovnikov[107], S.S. Bocchetta[79], A. Bocci[44], C.R. Boddy[118], M. Boehler[41], J. Boek[174], N. Boelaert[35], S. Böser[77], J.A. Bogaerts[29], A. Bogdanchikov[107], A. Bogouch[90,*], C. Bohm[146a], V. Boisvert[76], T. Bold[163,g], V. Boldea[25a], N.M. Bolnet[136], M. Bona[75], V.G. Bondarenko[96], M. Boonekamp[136], G. Boorman[76], C.N. Booth[139], S. Bordoni[78], C. Borer[16], A. Borisov[128], G. Borissov[71], I. Borjanovic[12a], S. Borroni[132a,132b], K. Bos[105], D. Boscherini[19a], M. Bosman[11], H. Boterenbrood[105], D. Botterill[129], J. Bouchami[93], J. Boudreau[123], E.V. Bouhova-Thacker[71], C. Bourdarios[115], N. Bousson[83], A. Boveia[30], J. Boyd[29], I.R. Boyko[65], N.I. Bozhko[128], I. Bozovic-Jelisavcic[12b], J. Bracinik[17], A. Braem[29], P. Branchini[134a], G.W. Brandenburg[57], A. Brandt[7], G. Brandt[15], O. Brandt[54], U. Bratzler[156], B. Brau[84], J.E. Brau[114], H.M. Braun[174], B. Brelier[158], J. Bremer[29], R. Brenner[166], S. Bressler[152], D. Breton[115], D. Britton[53], F.M. Brochu[27], I. Brock[20], R. Brock[88], T.J. Brodbeck[71], E. Brodet[153], F. Broggi[89a], C. Bromberg[88], G. Brooijmans[34], W.K. Brooks[31b], G. Brown[82], H. Brown[7], P.A. Bruckman de Renstrom[38], D. Bruncko[144b], R. Bruneliere[48], S. Brunet[61], A. Bruni[19a], G. Bruni[19a], M. Bruschi[19a], T. Buanes[13], F. Bucci[49], J. Buchanan[118], N.J. Buchanan[2], P. Buchholz[141], R.M. Buckingham[118], A.G. Buckley[45], S.I. Buda[25a], I.A. Budagov[65], B. Budick[108], V. Büscher[81], L. Bugge[117], D. Buira-Clark[118], O. Bulekov[96], M. Bunse[42], T. Buran[117], H. Burckhart[29], S. Burdin[73], T. Burgess[13], S. Burke[129], E. Busato[33], P. Bussey[53], C.P. Buszello[166], F. Butin[29], B. Butler[143], J.M. Butler[21], C.M. Buttar[53], J.M. Butterworth[77], W. Buttinger[27], T. Byatt[77], S. Cabrera Urbán[167], D. Caforio[19a,19b], O. Cakir[3a], P. Calafiura[14], G. Calderini[78], P. Calfayan[98], R. Calkins[106], L.P. Caloba[23a], R. Caloi[132a,132b], D. Calvet[33], S. Calvet[33], R. Camacho Toro[33], P. Camarri[133a,133b], M. Cambiaghi[119a,119b], D. Cameron[117], S. Campana[29], M. Campanelli[77], V. Canale[102a,102b], F. Canelli[30], A. Canepa[159a], J. Cantero[80], L. Capasso[102a,102b], M.D.M. Capeans Garrido[29], I. Caprini[25a], M. Caprini[25a], D. Capriotti[99], M. Capua[36a,36b], R. Caputo[148], C. Caramarcu[25a], R. Cardarelli[133a], T. Carli[29], G. Carlino[102a], L. Carminati[89a,89b], B. Caron[159a], S. Caron[48], G.D. Carrillo Montoya[172], A.A. Carter[75], J.R. Carter[27], J. Carvalho[124a,h], D. Casadei[108], M.P. Casado[11], M. Cascella[122a,122b], C. Caso[50a,50b,*], A.M. Castaneda Hernandez[172], E. Castaneda-Miranda[172], V. Castillo Gimenez[167], N.F. Castro[124a], G. Cataldi[72a], F. Cataneo[29], A. Catinaccio[29], J.R. Catmore[71], A. Cattai[29], G. Cattani[133a,133b], S. Caughron[88], D. Cauz[164a,164c], P. Cavalleri[78], D. Cavalli[89a], M. Cavalli-Sforza[11], V. Cavasinni[122a,122b], F. Ceradini[134a,134b], A.S. Cerqueira[23a], A. Cerri[29], L. Cerrito[75], F. Cerutti[47], S.A. Cetin[18b], F. Cevenini[102a,102b], A. Chafaq[135a], D. Chakraborty[106], K. Chan[2], B. Chapleau[85], J.D. Chapman[27], J.W. Chapman[87], E. Chareyre[78], D.G. Charlton[17], V. Chavda[82], C.A. Chavez Barajas[29], S. Cheatham[85], S. Chekanov[5], S.V. Chekulaev[159a], G.A. Chelkov[65], M.A. Chelstowska[104], C. Chen[64], H. Chen[24], S. Chen[32c], T. Chen[32c], X. Chen[172], S. Cheng[32a], A. Cheplakov[65], V.F. Chepurnov[65], R. Cherkaoui El Moursli[135e], V. Chernyatin[24], E. Cheu[6], S.L. Cheung[158], L. Chevalier[136], G. Chiefari[102a,102b], L. Chikovani[51], J.T. Childers[58a], A. Chilingarov[71], G. Chiodini[72a], M.V. Chizhov[65], G. Choudalakis[30], S. Chouridou[137], I.A. Christidi[77], A. Christov[48], D. Chromek-Burckhart[29], M.L. Chu[151], J. Chudoba[125], G. Ciapetti[132a,132b], K. Ciba[37], A.K. Ciftci[3a], R. Ciftci[3a], D. Cinca[33], V. Cindro[74], M.D. Ciobotaru[163], C. Ciocca[19a,19b], A. Ciocio[14], M. Cirilli[87], M. Ciubancan[25a], A. Clark[49], P.J. Clark[45], W. Cleland[123], J.C. Clemens[83], B. Clement[55], C. Clement[146a,146b], R.W. Clifft[129], Y. Coadou[83], M. Cobal[164a,164c], A. Coccaro[50a,50b], J. Cochran[64], P. Coe[118], J.G. Cogan[143], J. Coggeshall[165], E. Cogneras[177], C.D. Cojocaru[28], J. Colas[4], A.P. Colijn[105], C. Collard[115], N.J. Collins[17], C. Collins-Tooth[53], J. Collot[55], G. Colon[84], P. Conde Muiño[124a], E. Coniavitis[118], M.C. Conidi[11], M. Consonni[104], V. Consorti[48], S. Constantinescu[25a], C. Conta[119a,119b], F. Conventi[102a,i], J. Cook[29], M. Cooke[14], B.D. Cooper[77], A.M. Cooper-Sarkar[118], N.J. Cooper-Smith[76], K. Copic[34], T. Cornelissen[50a,50b], M. Corradi[19a], F. Corriveau[85,j], A. Cortes-Gonzalez[165], G. Cortiana[99], G. Costa[89a], M.J. Costa[167], D. Costanzo[139], T. Costin[30], D. Côté[29], R. Coura Torres[23a], L. Courneyea[169], G. Cowan[76], C. Cowden[27], B.E. Cox[82], K. Cranmer[108], F. Crescioli[122a,122b], M. Cristinziani[20], G. Crosetti[36a,36b], R. Crupi[72a,72b], S. Crépé-Renaudin[55], C.-M. Cuciuc[25a], C. Cuenca Almenar[175], T. Cuhadar Donszelmann[139], M. Curatolo[47], C.J. Curtis[17], P. Cwetanski[61], H. Czirr[141], Z. Czyczula[117], S. D'Auria[53], M. D'Onofrio[73], A. D'Orazio[132a,132b], P.V.M. Da Silva[23a], C. Da Via[82], W. Dabrowski[37], T. Dai[87], C. Dallapiccola[84], M. Dam[35], M. Dameri[50a,50b], D.S. Damiani[137], H.O. Danielsson[29], D. Dannheim[99], V. Dao[49], G. Darbo[50a],

G.L. Darlea[25b], C. Daum[105], J.P. Dauvergne[29], W. Davey[86], T. Davidek[126], N. Davidson[86], R. Davidson[71], E. Davies[118,c], M. Davies[93], A.R. Davison[77], Y. Davygora[58a], E. Dawe[142], I. Dawson[139], J.W. Dawson[5,*], R.K. Daya[39], K. De[7], R. de Asmundis[102a], S. De Castro[19a,19b], P.E. De Castro Faria Salgado[24], S. De Cecco[78], J. de Graat[98], N. De Groot[104], P. de Jong[105], C. De La Taille[115], H. De la Torre[80], B. De Lotto[164a,164c], L. De Mora[71], L. De Nooij[105], M. De Oliveira Branco[29], D. De Pedis[132a], A. De Salvo[132a], U. De Sanctis[164a,164c], A. De Santo[149], J.B. De Vivie De Regie[115], S. Dean[77], D.V. Dedovich[65], J. Degenhardt[120], M. Dehchar[118], C. Del Papa[164a,164c], J. Del Peso[80], T. Del Prete[122a,122b], M. Deliyergiyev[74], A. Dell'Acqua[29], L. Dell'Asta[89a,89b], M. Della Pietra[102a,i], D. della Volpe[102a,102b], M. Delmastro[29], P. Delpierre[83], N. Delruelle[29], P.A. Delsart[55], C. Deluca[148], S. Demers[175], M. Demichev[65], B. Demirkoz[11,k], J. Deng[163], S.P. Denisov[128], D. Derendarz[38], J.E. Derkaoui[135d], F. Derue[78], P. Dervan[73], K. Desch[20], E. Devetak[148], P.O. Deviveiros[158], A. Dewhurst[129], B. DeWilde[148], S. Dhaliwal[158], R. Dhullipudi[24,l], A. Di Ciaccio[133a,133b], L. Di Ciaccio[4], A. Di Girolamo[29], B. Di Girolamo[29], S. Di Luise[134a,134b], A. Di Mattia[88], B. Di Micco[29], R. Di Nardo[133a,133b], A. Di Simone[133a,133b], R. Di Sipio[19a,19b], M.A. Diaz[31a], F. Diblen[18c], E.B. Diehl[87], J. Dietrich[41], T.A. Dietzsch[58a], S. Diglio[115], K. Dindar Yagci[39], J. Dingfelder[20], C. Dionisi[132a,132b], P. Dita[25a], S. Dita[25a], F. Dittus[29], F. Djama[83], T. Djobava[51], M.A.B. do Vale[23a], A. Do Valle Wemans[124a], T.K.O. Doan[4], M. Dobbs[85], R. Dobinson[29,*], D. Dobos[42], E. Dobson[29], M. Dobson[163], J. Dodd[34], C. Doglioni[118], T. Doherty[53], Y. Doi[66,*], J. Dolejsi[126], I. Dolenc[74], Z. Dolezal[126], B.A. Dolgoshein[96,*], T. Dohmae[155], M. Donadelli[23d], M. Donega[120], J. Donini[55], J. Dopke[29], A. Doria[102a], A. Dos Anjos[172], M. Dosil[11], A. Dotti[122a,122b], M.T. Dova[70], J.D. Dowell[17], A.D. Doxiadis[105], A.T. Doyle[53], Z. Drasal[126], J. Drees[174], N. Dressnandt[120], H. Drevermann[29], C. Driouichi[35], M. Dris[9], J. Dubbert[99], T. Dubbs[137], S. Dube[14], E. Duchovni[171], G. Duckeck[98], A. Dudarev[29], F. Dudziak[64], M. Dührssen[29], I.P. Duerdoth[82], L. Duflot[115], M-A. Dufour[85], M. Dunford[29], H. Duran Yildiz[3b], R. Duxfield[139], M. Dwuznik[37], F. Dydak[29], D. Dzahini[55], M. Düren[52], W.L. Ebenstein[44], J. Ebke[98], S. Eckert[48], S. Eckweiler[81], K. Edmonds[81], C.A. Edwards[76], N.C. Edwards[53], W. Ehrenfeld[41], T. Ehrich[99], T. Eifert[29], G. Eigen[13], K. Einsweiler[14], E. Eisenhandler[75], T. Ekelof[166], M. El Kacimi[135c], M. Ellert[166], S. Elles[4], F. Ellinghaus[81], K. Ellis[75], N. Ellis[29], J. Elmsheuser[98], M. Elsing[29], D. Emeliyanov[129], R. Engelmann[148], A. Engl[98], B. Epp[62], A. Eppig[87], J. Erdmann[54], A. Ereditato[16], D. Eriksson[146a], J. Ernst[1], M. Ernst[24], J. Ernwein[136], D. Errede[165], S. Errede[165], E. Ertel[81], M. Escalier[115], C. Escobar[167], X. Espinal Curull[11], B. Esposito[47], F. Etienne[83], A.I. Etienvre[136], E. Etzion[153], D. Evangelakou[54], H. Evans[61], L. Fabbri[19a,19b], C. Fabre[29], R.M. Fakhrutdinov[128], S. Falciano[132a], Y. Fang[172], M. Fanti[89a,89b], A. Farbin[7], A. Farilla[134a], J. Farley[148], T. Farooque[158], S.M. Farrington[118], P. Farthouat[29], P. Fassnacht[29], D. Fassouliotis[8], B. Fatholahzadeh[158], A. Favareto[89a,89b], L. Fayard[115], S. Fazio[36a,36b], R. Febbraro[33], P. Federic[144a], O.L. Fedin[121], W. Fedorko[88], M. Fehling-Kaschek[48], L. Feligioni[83], D. Fellmann[5], C.U. Felzmann[86], C. Feng[32d], E.J. Feng[30], A.B. Fenyuk[128], J. Ferencei[144b], J. Ferland[93], W. Fernando[109], S. Ferrag[53], J. Ferrando[53], V. Ferrara[41], A. Ferrari[166], P. Ferrari[105], R. Ferrari[119a], A. Ferrer[167], M.L. Ferrer[47], D. Ferrere[49], C. Ferretti[87], A. Ferretto Parodi[50a,50b], M. Fiascaris[30], F. Fiedler[81], A. Filipčič[74], A. Filippas[9], F. Filthaut[104], M. Fincke-Keeler[169], M.C.N. Fiolhais[124a,h], L. Fiorini[167], A. Firan[39], G. Fischer[41], P. Fischer[20], M.J. Fisher[109], S.M. Fisher[129], M. Flechl[48], I. Fleck[141], J. Fleckner[81], P. Fleischmann[173], S. Fleischmann[174], T. Flick[174], L.R. Flores Castillo[172], M.J. Flowerdew[99], M. Fokitis[9], T. Fonseca Martin[16], D.A. Forbush[138], A. Formica[136], A. Forti[82], D. Fortin[159a], J.M. Foster[82], D. Fournier[115], A. Foussat[29], A.J. Fowler[44], K. Fowler[137], H. Fox[71], P. Francavilla[122a,122b], S. Franchino[119a,119b], D. Francis[29], T. Frank[171], M. Franklin[57], S. Franz[29], M. Fraternali[119a,119b], S. Fratina[120], S.T. French[27], F. Friedrich[43], R. Froeschl[29], D. Froidevaux[29], J.A. Frost[27], C. Fukunaga[156], E. Fullana Torregrosa[29], J. Fuster[167], C. Gabaldon[29], O. Gabizon[171], T. Gadfort[24], S. Gadomski[49], G. Gagliardi[50a,50b], P. Gagnon[61], C. Galea[98], E.J. Gallas[118], M.V. Gallas[29], V. Gallo[16], B.J. Gallop[129], P. Gallus[125], E. Galyaev[40], K.K. Gan[109], Y.S. Gao[143,f], V.A. Gapienko[128], A. Gaponenko[14], F. Garberson[175], M. Garcia-Sciveres[14], C. García[167], J.E. García Navarro[49], R.W. Gardner[30], N. Garelli[29], H. Garitaonandia[105], V. Garonne[29], J. Garvey[17], C. Gatti[47], G. Gaudio[119a], O. Gaumer[49], B. Gaur[141], L. Gauthier[136], I.L. Gavrilenko[94], C. Gay[168], G. Gaycken[20], J.-C. Gayde[29], E.N. Gazis[9], P. Ge[32d], C.N.P. Gee[129], D.A.A. Geerts[105], Ch. Geich-Gimbel[20], K. Gellerstedt[146a,146b], C. Gemme[50a], A. Gemmell[53], M.H. Genest[98], S. Gentile[132a,132b], M. George[54], S. George[76], P. Gerlach[174], A. Gershon[153], C. Geweniger[58a], H. Ghazlane[135b], P. Ghez[4], N. Ghodbane[33], B. Giacobbe[19a], S. Giagu[132a,132b], V. Giakoumopoulou[8], V. Giangiobbe[122a,122b], F. Gianotti[29], B. Gibbard[24], A. Gibson[158], S.M. Gibson[29], L.M. Gilbert[118], M. Gilchriese[14], V. Gilewsky[91], D. Gillberg[28], A.R. Gillman[129], D.M. Gingrich[2,e], J. Ginzburg[153], N. Giokaris[8], R. Giordano[102a,102b], F.M. Giorgi[15], P. Giovannini[99], P.F. Giraud[136], D. Giugni[89a], M. Giunta[132a,132b], P. Giusti[19a], B.K. Gjelsten[117], L.K. Gladilin[97], C. Glasman[80], J. Glatzer[48], A. Glazov[41], K.W. Glitza[174], G.L. Glonti[65], J. Godfrey[142], J. Godlewski[29], M. Goebel[41], T. Göpfert[43], C. Goeringer[81], C. Gössling[42], T. Göttfert[99], S. Goldfarb[87], D. Goldin[39], T. Golling[175], S.N. Golovnia[128], A. Gomes[124a,b], L.S. Gomez Fajardo[41], R. Gonçalo[76], J. Goncalves Pinto Firmino Da Costa[41], L. Gonella[20], A. Gonidec[29], S. Gonzalez[172], S. González de la Hoz[167], M.L. Gonzalez Silva[26], S. Gonzalez-Sevilla[49], J.J. Goodson[148], L. Goossens[29], P.A. Gorbounov[95], H.A. Gordon[24], I. Gorelov[103], G. Gorfine[174], B. Gorini[29], E. Gorini[72a,72b], A. Gorišek[74], E. Gornicki[38], S.A. Gorokhov[128], V.N. Goryachev[128], B. Gosdzik[41], M. Gosselink[105], M.I. Gostkin[65], I. Gough Eschrich[163],

M. Gouighri[135a], D. Goujdami[135c], M.P. Goulette[49], A.G. Goussiou[138], C. Goy[4], I. Grabowska-Bold[163,g], V. Grabski[176], P. Grafström[29], C. Grah[174], K.-J. Grahn[41], F. Grancagnolo[72a], S. Grancagnolo[15], V. Grassi[148], V. Gratchev[121], N. Grau[34], H.M. Gray[29], J.A. Gray[148], E. Graziani[134a], O.G. Grebenyuk[121], D. Greenfield[129], T. Greenshaw[73], Z.D. Greenwood[24,l], K. Gregersen[35], I.M. Gregor[41], P. Grenier[143], J. Griffiths[138], N. Grigalashvili[65], A.A. Grillo[137], S. Grinstein[11], Y.V. Grishkevich[97], J.-F. Grivaz[115], J. Grognuz[29], M. Groh[99], E. Gross[171], J. Grosse-Knetter[54], J. Groth-Jensen[171], K. Grybel[141], V.J. Guarino[5], D. Guest[175], C. Guicheney[33], A. Guida[72a,72b], T. Guillemin[4], S. Guindon[54], H. Guler[85,m], J. Gunther[125], B. Guo[158], J. Guo[34], A. Gupta[30], Y. Gusakov[65], V.N. Gushchin[128], A. Gutierrez[93], P. Gutierrez[111], N. Guttman[153], O. Gutzwiller[172], C. Guyot[136], C. Gwenlan[118], C.B. Gwilliam[73], A. Haas[143], S. Haas[29], C. Haber[14], R. Hackenburg[24], H.K. Hadavand[39], D.R. Hadley[17], P. Haefner[99], F. Hahn[29], S. Haider[29], Z. Hajduk[38], H. Hakobyan[176], J. Haller[54], K. Hamacher[174], P. Hamal[113], A. Hamilton[49], S. Hamilton[161], H. Han[32a], L. Han[32b], K. Hanagaki[116], M. Hance[120], C. Handel[81], P. Hanke[58a], J.R. Hansen[35], J.B. Hansen[35], J.D. Hansen[35], P.H. Hansen[35], P. Hansson[143], K. Hara[160], G.A. Hare[137], T. Harenberg[174], S. Harkusha[90], D. Harper[87], R.D. Harrington[21], O.M. Harris[138], K. Harrison[17], J. Hartert[48], F. Hartjes[105], T. Haruyama[66], A. Harvey[56], S. Hasegawa[101], Y. Hasegawa[140], S. Hassani[136], M. Hatch[29], D. Hauff[99], S. Haug[16], M. Hauschild[29], R. Hauser[88], M. Havranek[20], B.M. Hawes[118], C.M. Hawkes[17], R.J. Hawkings[29], D. Hawkins[163], T. Hayakawa[67], D. Hayden[76], H.S. Hayward[73], S.J. Haywood[129], E. Hazen[21], M. He[32d], S.J. Head[17], V. Hedberg[79], L. Heelan[7], S. Heim[88], B. Heinemann[14], S. Heisterkamp[35], L. Helary[4], M. Heller[115], S. Hellman[146a,146b], D. Hellmich[20], C. Helsens[11], R.C.W. Henderson[71], M. Henke[58a], A. Henrichs[54], A.M. Henriques Correia[29], S. Henrot-Versille[115], F. Henry-Couannier[83], C. Hensel[54], T. Henß[174], C.M. Hernandez[7], Y. Hernández Jiménez[167], R. Herrberg[15], A.D. Hershenhorn[152], G. Herten[48], R. Hertenberger[98], L. Hervas[29], N.P. Hessey[105], A. Hidvegi[146a], E. Higón-Rodriguez[167], D. Hill[5,*], J.C. Hill[27], N. Hill[5], K.H. Hiller[41], S. Hillert[20], S.J. Hillier[17], I. Hinchliffe[14], E. Hines[120], M. Hirose[116], F. Hirsch[42], D. Hirschbuehl[174], J. Hobbs[148], N. Hod[153], M.C. Hodgkinson[139], P. Hodgson[139], A. Hoecker[29], M.R. Hoeferkamp[103], J. Hoffman[39], D. Hoffmann[83], M. Hohlfeld[81], M. Holder[141], S.O. Holmgren[146a], T. Holy[127], J.L. Holzbauer[88], Y. Homma[67], T.M. Hong[120], L. Hooft van Huysduynen[108], T. Horazdovsky[127], C. Horn[143], S. Horner[48], K. Horton[118], J.-Y. Hostachy[55], S. Hou[151], M.A. Houlden[73], A. Hoummada[135a], J. Howarth[82], D.F. Howell[118], I. Hristova[15], J. Hrivnac[115], I. Hruska[125], T. Hryn'ova[4], P.J. Hsu[175], S.-C. Hsu[14], G.S. Huang[111], Z. Hubacek[127], F. Hubaut[83], F. Huegging[20], T.B. Huffman[118], E.W. Hughes[34], G. Hughes[71], R.E. Hughes-Jones[82], M. Huhtinen[29], P. Hurst[57], M. Hurwitz[14], U. Husemann[41], N. Huseynov[65,n], J. Huston[88], J. Huth[57], G. Iacobucci[49], G. Iakovidis[9], M. Ibbotson[82], I. Ibragimov[141], R. Ichimiya[67], L. Iconomidou-Fayard[115], J. Idarraga[115], M. Idzik[37], P. Iengo[102a,102b], O. Igonkina[105], Y. Ikegami[66], M. Ikeno[66], Y. Ilchenko[39], D. Iliadis[154], N. Ilic[158], D. Imbault[78], M. Imhaeuser[174], M. Imori[155], T. Ince[20], J. Inigo-Golfin[29], P. Ioannou[8], M. Iodice[134a], G. Ionescu[4], A. Irles Quiles[167], K. Ishii[66], A. Ishikawa[67], M. Ishino[68], R. Ishmukhametov[39], C. Issever[118], S. Istin[18a], A.V. Ivashin[128], W. Iwanski[38], H. Iwasaki[66], J.M. Izen[40], V. Izzo[102a], B. Jackson[120], J.N. Jackson[73], P. Jackson[143], M.R. Jaekel[29], V. Jain[61], K. Jakobs[48], S. Jakobsen[35], J. Jakubek[127], D.K. Jana[111], E. Jankowski[158], E. Jansen[77], A. Jantsch[99], M. Janus[20], G. Jarlskog[79], L. Jeanty[57], K. Jelen[37], I. Jen-La Plante[30], P. Jenni[29], A. Jeremie[4], P. Jež[35], S. Jézéquel[4], M.K. Jha[19a], H. Ji[172], W. Ji[81], J. Jia[148], Y. Jiang[32b], M. Jimenez Belenguer[41], G. Jin[32b], S. Jin[32a], O. Jinnouchi[157], M.D. Joergensen[35], D. Joffe[39], L.G. Johansen[13], M. Johansen[146a,146b], K.E. Johansson[146a], P. Johansson[139], S. Johnert[41], K.A. Johns[6], K. Jon-And[146a,146b], G. Jones[82], R.W.L. Jones[71], T.W. Jones[77], T.J. Jones[73], O. Jonsson[29], C. Joram[29], P.M. Jorge[124a,b], J. Joseph[14], T. Jovin[12b], X. Ju[130], V. Juranek[125], P. Jussel[62], A. Juste Rozas[11], V.V. Kabachenko[128], S. Kabana[16], M. Kaci[167], A. Kaczmarska[38], P. Kadlecik[35], M. Kado[115], H. Kagan[109], M. Kagan[57], S. Kaiser[99], E. Kajomovitz[152], S. Kalinin[174], L.V. Kalinovskaya[65], S. Kama[39], N. Kanaya[155], M. Kaneda[29], T. Kanno[157], V.A. Kantserov[96], J. Kanzaki[66], B. Kaplan[175], A. Kapliy[30], J. Kaplon[29], D. Kar[43], M. Karagoz[118], M. Karnevskiy[41], K. Karr[5], V. Kartvelishvili[71], A.N. Karyukhin[128], L. Kashif[172], A. Kasmi[39], R.D. Kass[109], A. Kastanas[13], M. Kataoka[4], Y. Kataoka[155], E. Katsoufis[9], J. Katzy[41], V. Kaushik[6], K. Kawagoe[67], T. Kawamoto[155], G. Kawamura[81], M.S. Kayl[105], V.A. Kazanin[107], M.Y. Kazarinov[65], J.R. Keates[82], R. Keeler[169], R. Kehoe[39], M. Keil[54], G.D. Kekelidze[65], M. Kelly[82], J. Kennedy[98], C.J. Kenney[143], M. Kenyon[53], O. Kepka[125], N. Kerschen[29], B.P. Kerševan[74], S. Kersten[174], K. Kessoku[155], C. Ketterer[48], J. Keung[158], M. Khakzad[28], F. Khalil-zada[10], H. Khandanyan[165], A. Khanov[112], D. Kharchenko[65], A. Khodinov[96], A.G. Kholodenko[128], A. Khomich[58a], T.J. Khoo[27], G. Khoriauli[20], A. Khoroshilov[174], N. Khovanskiy[65], V. Khovanskiy[95], E. Khramov[65], J. Khubua[51], H. Kim[7], M.S. Kim[2], P.C. Kim[143], S.H. Kim[160], N. Kimura[170], O. Kind[15], B.T. King[73], M. King[67], R.S.B. King[118], J. Kirk[129], G.P. Kirsch[118], L.E. Kirsch[22], A.E. Kiryunin[99], T. Kishimoto[67], D. Kisielewska[37], T. Kittelmann[123], A.M. Kiver[128], H. Kiyamura[67], E. Kladiva[144b], J. Klaiber-Lodewigs[42], M. Klein[73], U. Klein[73], K. Kleinknecht[81], M. Klemetti[85], A. Klier[171], A. Klimentov[24], R. Klingenberg[42], E.B. Klinkby[35], T. Klioutchnikova[29], P.F. Klok[104], S. Klous[105], E.-E. Kluge[58a], T. Kluge[73], P. Kluit[105], S. Kluth[99], N.S. Knecht[158], E. Kneringer[62], J. Knobloch[29], E.B.F.G. Knoops[83], A. Knue[54], B.R. Ko[44], T. Kobayashi[155], M. Kobel[43], M. Kocian[143], A. Kocnar[113], P. Kodys[126], K. Köneke[29], A.C. König[104], S. Koenig[81], L. Köpke[81], F. Koetsveld[104], P. Koevesarki[20], T. Koffas[29], E. Koffeman[105], F. Kohn[54], Z. Kohout[127], T. Kohriki[66], T. Koi[143],

T. Kokott[20], G.M. Kolachev[107], H. Kolanoski[15], V. Kolesnikov[65], I. Koletsou[89a], J. Koll[88], D. Kollar[29], M. Kollefrath[48], S.D. Kolya[82], A.A. Komar[94], J.R. Komaragiri[142], Y. Komori[155], T. Kondo[66], T. Kono[41,o], A.I. Kononov[48], R. Konoplich[108,p], N. Konstantinidis[77], A. Kootz[174], S. Koperny[37], S.V. Kopikov[128], K. Korcyl[38], K. Kordas[154], V. Koreshev[128], A. Korn[14], A. Korol[107], I. Korolkov[11], E.V. Korolkova[139], V.A. Korotkov[128], O. Kortner[99], S. Kortner[99], V.V. Kostyukhin[20], M.J. Kotamäki[29], S. Kotov[99], V.M. Kotov[65], A. Kotwal[44], C. Kourkoumelis[8], V. Kouskoura[154], A. Koutsman[105], R. Kowalewski[169], T.Z. Kowalski[37], W. Kozanecki[136], A.S. Kozhin[128], V. Kral[127], V.A. Kramarenko[97], G. Kramberger[74], M.W. Krasny[78], A. Krasznahorkay[108], J. Kraus[88], A. Kreisel[153], F. Krejci[127], J. Kretzschmar[73], N. Krieger[54], P. Krieger[158], K. Kroeninger[54], H. Kroha[99], J. Kroll[120], J. Kroseberg[20], J. Krstic[12a], U. Kruchonak[65], H. Krüger[20], T. Kruker[16], Z.V. Krumshteyn[65], A. Kruth[20], T. Kubota[86], S. Kuehn[48], A. Kugel[58c], T. Kuhl[41], D. Kuhn[62], V. Kukhtin[65], Y. Kulchitsky[90], S. Kuleshov[31b], C. Kummer[98], M. Kuna[78], N. Kundu[118], J. Kunkle[120], A. Kupco[125], H. Kurashige[67], M. Kurata[160], Y.A. Kurochkin[90], V. Kus[125], W. Kuykendall[138], M. Kuze[157], P. Kuzhir[91], J. Kvita[29], R. Kwee[15], A. La Rosa[172], L. La Rotonda[36a,36b], L. Labarga[80], J. Labbe[4], S. Lablak[135a], C. Lacasta[167], F. Lacava[132a,132b], H. Lacker[15], D. Lacour[78], V.R. Lacuesta[167], E. Ladygin[65], R. Lafaye[4], B. Laforge[78], T. Lagouri[80], S. Lai[48], E. Laisne[55], M. Lamanna[29], C.L. Lampen[6], W. Lampl[6], E. Lancon[136], U. Landgraf[48], M.P.J. Landon[75], H. Landsman[152], J.L. Lane[82], C. Lange[41], A.J. Lankford[163], F. Lanni[24], K. Lantzsch[29], S. Laplace[78], C. Lapoire[20], J.F. Laporte[136], T. Lari[89a], A.V. Larionov[128], A. Larner[118], C. Lasseur[29], M. Lassnig[29], P. Laurelli[47], A. Lavorato[118], W. Lavrijsen[14], P. Laycock[73], A.B. Lazarev[65], O. Le Dortz[78], E. Le Guirriec[83], C. Le Maner[158], E. Le Menedeu[136], C. Lebel[93], T. LeCompte[5], F. Ledroit-Guillon[55], H. Lee[105], J.S.H. Lee[150], S.C. Lee[151], L. Lee[175], M. Lefebvre[169], M. Legendre[136], A. Leger[49], B.C. LeGeyt[120], F. Legger[98], C. Leggett[14], M. Lehmacher[20], G. Lehmann Miotto[29], X. Lei[6], M.A.L. Leite[23d], R. Leitner[126], D. Lellouch[171], M. Leltchouk[34], B. Lemmer[54], V. Lendermann[58a], K.J.C. Leney[145b], T. Lenz[105], G. Lenzen[174], B. Lenzi[29], K. Leonhardt[43], S. Leontsinis[9], C. Leroy[93], J.-R. Lessard[169], J. Lesser[146a], C.G. Lester[27], A. Leung Fook Cheong[172], J. Levêque[4], D. Levin[87], L.J. Levinson[171], M.S. Levitski[128], M. Lewandowska[21], A. Lewis[118], G.H. Lewis[108], A.M. Leyko[20], M. Leyton[15], B. Li[83], H. Li[172], S. Li[32b,d], X. Li[87], Z. Liang[39], Z. Liang[118,q], B. Liberti[133a], P. Lichard[29], M. Lichtnecker[98], K. Lie[165], W. Liebig[13], R. Lifshitz[152], J.N. Lilley[17], C. Limbach[20], A. Limosani[86], M. Limper[63], S.C. Lin[151,r], F. Linde[105], J.T. Linnemann[88], E. Lipeles[120], L. Lipinsky[125], A. Lipniacka[13], T.M. Liss[165], D. Lissauer[24], A. Lister[49], A.M. Litke[137], C. Liu[28], D. Liu[151,s], H. Liu[87], J.B. Liu[87], M. Liu[32b], S. Liu[2], Y. Liu[32b], M. Livan[119a,119b], S.S.A. Livermore[118], A. Lleres[55], J. Llorente Merino[80], S.L. Lloyd[75], E. Lobodzinska[41], P. Loch[6], W.S. Lockman[137], S. Lockwitz[175], T. Loddenkoetter[20], F.K. Loebinger[82], A. Loginov[175], C.W. Loh[168], T. Lohse[15], K. Lohwasser[48], M. Lokajicek[125], J. Loken[118], V.P. Lombardo[4], R.E. Long[71], L. Lopes[124a,b], D. Lopez Mateos[57], M. Losada[162], P. Loscutoff[14], F. Lo Sterzo[132a,132b], M.J. Losty[159a], X. Lou[40], A. Lounis[115], K.F. Loureiro[162], J. Love[21], P.A. Love[71], A.J. Lowe[143,f], F. Lu[32a], H.J. Lubatti[138], C. Luci[132a,132b], A. Lucotte[55], A. Ludwig[43], D. Ludwig[41], I. Ludwig[48], J. Ludwig[48], F. Luehring[61], G. Luijckx[105], D. Lumb[48], L. Luminari[132a], E. Lund[117], B. Lund-Jensen[147], B. Lundberg[79], J. Lundberg[146a,146b], J. Lundquist[35], M. Lungwitz[81], A. Lupi[122a,122b], G. Lutz[99], D. Lynn[24], J. Lys[14], E. Lytken[79], H. Ma[24], L.L. Ma[172], J.A. Macana Goia[93], G. Maccarrone[47], A. Macchiolo[99], B. Maček[74], J. Machado Miguens[124a], R. Mackeprang[35], R.J. Madaras[14], W.F. Mader[43], R. Maenner[58c], T. Maeno[24], P. Mättig[174], S. Mättig[41], P.J. Magalhaes Martins[124a,h], L. Magnoni[29], E. Magradze[54], Y. Mahalalel[153], K. Mahboubi[48], G. Mahout[17], C. Maiani[132a,132b], C. Maidantchik[23a], A. Maio[124a,b], S. Majewski[24], Y. Makida[66], N. Makovec[115], P. Mal[6], Pa. Malecki[38], P. Malecki[38], V.P. Maleev[121], F. Malek[55], U. Mallik[63], D. Malon[5], S. Maltezos[9], V. Malyshev[107], S. Malyukov[29], R. Mameghani[98], J. Mamuzic[12b], A. Manabe[66], L. Mandelli[89a], I. Mandić[74], R. Mandrysch[15], J. Maneira[124a], P.S. Mangeard[88], I.D. Manjavidze[65], A. Mann[54], P.M. Manning[137], A. Manousakis-Katsikakis[8], B. Mansoulie[136], A. Manz[99], A. Mapelli[29], L. Mapelli[29], L. March[80], J.F. Marchand[29], F. Marchese[133a,133b], G. Marchiori[78], M. Marcisovsky[125], A. Marin[21,*], C.P. Marino[61], F. Marroquim[23a], R. Marshall[82], Z. Marshall[29], F.K. Martens[158], S. Marti-Garcia[167], A.J. Martin[175], B. Martin[29], B. Martin[88], F.F. Martin[120], J.P. Martin[93], Ph. Martin[55], T.A. Martin[17], B. Martin dit Latour[49], S. Martin-Haugh[149], M. Martinez[11], V. Martinez Outschoorn[57], A.C. Martyniuk[82], M. Marx[82], F. Marzano[132a], A. Marzin[111], L. Masetti[81], T. Mashimo[155], R. Mashinistov[94], J. Masik[82], A.L. Maslennikov[107], I. Massa[19a,19b], G. Massaro[105], N. Massol[4], P. Mastrandrea[132a,132b], A. Mastroberardino[36a,36b], T. Masubuchi[155], M. Mathes[20], P. Matricon[115], H. Matsumoto[155], H. Matsunaga[155], T. Matsushita[67], C. Mattravers[118,c], J.M. Maugain[29], S.J. Maxfield[73], D.A. Maximov[107], E.N. May[5], A. Mayne[139], R. Mazini[151], M. Mazur[20], M. Mazzanti[89a], E. Mazzoni[122a,122b], S.P. Mc Kee[87], A. McCarn[165], R.L. McCarthy[148], T.G. McCarthy[28], N.A. McCubbin[129], K.W. McFarlane[56], J.A. Mcfayden[139], H. McGlone[53], G. Mchedlidze[51], R.A. McLaren[29], T. Mclaughlan[17], S.J. McMahon[129], R.A. McPherson[169,j], A. Meade[84], J. Mechnich[105], M. Mechtel[174], M. Medinnis[41], R. Meera-Lebbai[111], T. Meguro[116], R. Mehdiyev[93], S. Mehlhase[35], A. Mehta[73], K. Meier[58a], J. Meinhardt[48], B. Meirose[79], C. Melachrinos[30], B.R. Mellado Garcia[172], L. Mendoza Navas[162], Z. Meng[151,s], A. Mengarelli[19a,19b], S. Menke[99], C. Menot[29], E. Meoni[11], K.M. Mercurio[57], P. Mermod[118], L. Merola[102a,102b], C. Meroni[89a], F.S. Merritt[30], A. Messina[29], J. Metcalfe[103], A.S. Mete[64], S. Meuser[20], C. Meyer[81], J-P. Meyer[136], J. Meyer[173], J. Meyer[54], T.C. Meyer[29], W.T. Meyer[64], J. Miao[32d],

S. Michal[29], L. Micu[25a], R.P. Middleton[129], P. Miele[29], S. Migas[73], L. Mijović[41], G. Mikenberg[171], M. Mikestikova[125], M. Mikuž[74], D.W. Miller[143], R.J. Miller[88], W.J. Mills[168], C. Mills[57], A. Milov[171], D.A. Milstead[146a,146b], D. Milstein[171], A.A. Minaenko[128], M. Miñano[167], I.A. Minashvili[65], A.I. Mincer[108], B. Mindur[37], M. Mineev[65], Y. Ming[130], L.M. Mir[11], G. Mirabelli[132a], L. Miralles Verge[11], A. Misiejuk[76], J. Mitrevski[137], G.Y. Mitrofanov[128], V.A. Mitsou[167], S. Mitsui[66], P.S. Miyagawa[139], K. Miyazaki[67], J.U. Mjörnmark[79], T. Moa[146a,146b], P. Mockett[138], S. Moed[57], V. Moeller[27], K. Mönig[41], N. Möser[20], S. Mohapatra[148], W. Mohr[48], S. Mohrdieck-Möck[99], A.M. Moisseev[128,*], R. Moles-Valls[167], J. Molina-Perez[29], J. Monk[77], E. Monnier[83], S. Montesano[89a,89b], F. Monticelli[70], S. Monzani[19a,19b], R.W. Moore[2], G.F. Moorhead[86], C. Mora Herrera[49], A. Moraes[53], N. Morange[136], J. Morel[54], G. Morello[36a,36b], D. Moreno[81], M. Moreno Llácer[167], P. Morettini[50a], M. Morii[57], J. Morin[75], Y. Morita[66], A.K. Morley[29], G. Mornacchi[29], S.V. Morozov[96], J.D. Morris[75], L. Morvaj[101], H.G. Moser[99], M. Mosidze[51], J. Moss[109], R. Mount[143], E. Mountricha[136], S.V. Mouraviev[94], E.J.W. Moyse[84], M. Mudrinic[12b], F. Mueller[58a], J. Mueller[123], K. Mueller[20], T.A. Müller[98], D. Muenstermann[29], A. Muir[168], Y. Munwes[153], W.J. Murray[129], I. Mussche[105], E. Musto[102a,102b], A.G. Myagkov[128], M. Myska[125], J. Nadal[11], K. Nagai[160], K. Nagano[66], Y. Nagasaka[60], A.M. Nairz[29], Y. Nakahama[29], K. Nakamura[155], I. Nakano[110], G. Nanava[20], A. Napier[161], M. Nash[77,c], N.R. Nation[21], T. Nattermann[20], T. Naumann[41], G. Navarro[162], H.A. Neal[87], E. Nebot[80], P.Yu. Nechaeva[94], A. Negri[119a,119b], G. Negri[29], S. Nektarijevic[49], S. Nelson[143], T.K. Nelson[143], S. Nemecek[125], P. Nemethy[108], A.A. Nepomuceno[23a], M. Nessi[29,t], S.Y. Nesterov[121], M.S. Neubauer[165], A. Neusiedl[81], R.M. Neves[108], P. Nevski[24], P.R. Newman[17], V. Nguyen Thi Hong[136], R.B. Nickerson[118], R. Nicolaidou[136], L. Nicolas[139], B. Nicquevert[29], F. Niedercorn[115], J. Nielsen[137], T. Niinikoski[29], N. Nikiforou[34], A. Nikiforov[15], V. Nikolaenko[128], K. Nikolaev[65], I. Nikolic-Audit[78], K. Nikolics[49], K. Nikolopoulos[24], H. Nilsen[48], P. Nilsson[7], Y. Ninomiya[155], A. Nisati[132a], T. Nishiyama[67], R. Nisius[99], L. Nodulman[5], M. Nomachi[116], I. Nomidis[154], M. Nordberg[29], B. Nordkvist[146a,146b], P.R. Norton[129], J. Novakova[126], M. Nozaki[66], M. Nožička[41], L. Nozka[113], I.M. Nugent[159a], A.-E. Nuncio-Quiroz[20], G. Nunes Hanninger[86], T. Nunnemann[98], E. Nurse[77], T. Nyman[29], B.J. O'Brien[45], S.W. O'Neale[17,*], D.C. O'Neil[142], V. O'Shea[53], F.G. Oakham[28,e], H. Oberlack[99], J. Ocariz[78], A. Ochi[67], S. Oda[155], S. Odaka[66], J. Odier[83], H. Ogren[61], A. Oh[82], S.H. Oh[44], C.C. Ohm[146a,146b], T. Ohshima[101], H. Ohshita[140], T.K. Ohska[66], T. Ohsugi[59], S. Okada[67], H. Okawa[163], Y. Okumura[101], T. Okuyama[155], M. Olcese[50a], A.G. Olchevski[65], M. Oliveira[124a,h], D. Oliveira Damazio[24], E. Oliver Garcia[167], D. Olivito[120], A. Olszewski[38], J. Olszowska[38], C. Omachi[67], A. Onofre[124a,u], P.U.E. Onyisi[30], C.J. Oram[159a], M.J. Oreglia[30], Y. Oren[153], D. Orestano[134a,134b], I. Orlov[107], C. Oropeza Barrera[53], R.S. Orr[158], B. Osculati[50a,50b], R. Ospanov[120], C. Osuna[11], G. Otero y Garzon[26], J.P. Ottersbach[105], M. Ouchrif[135d], F. Ould-Saada[117], A. Ouraou[136], Q. Ouyang[32a], M. Owen[82], S. Owen[139], V.E. Ozcan[18a], N. Ozturk[7], A. Pacheco Pages[11], C. Padilla Aranda[11], S. Pagan Griso[14], E. Paganis[139], F. Paige[24], K. Pajchel[117], G. Palacino[159b], C.P. Paleari[6], S. Palestini[29], D. Pallin[33], A. Palma[124a,b], J.D. Palmer[17], Y.B. Pan[172], E. Panagiotopoulou[9], B. Panes[31a], N. Panikashvili[87], S. Panitkin[24], D. Pantea[25a], M. Panuskova[125], V. Paolone[123], A. Papadelis[146a], Th.D. Papadopoulou[9], A. Paramonov[5], W. Park[24,v], M.A. Parker[27], F. Parodi[50a,50b], J.A. Parsons[34], U. Parzefall[48], E. Pasqualucci[132a], A. Passeri[134a], F. Pastore[134a,134b], Fr. Pastore[29], G. Pásztor[49,w], S. Pataraia[172], N. Patel[150], J.R. Pater[82], S. Patricelli[102a,102b], T. Pauly[29], M. Pecsy[144a], M.I. Pedraza Morales[172], S.V. Peleganchuk[107], H. Peng[32b], R. Pengo[29], A. Penson[34], J. Penwell[61], M. Perantoni[23a], K. Perez[34,x], T. Perez Cavalcanti[41], E. Perez Codina[11], M.T. Pérez García-Estañ[167], V. Perez Reale[34], L. Perini[89a,89b], H. Pernegger[29], R. Perrino[72a], P. Perrodo[4], S. Persembe[3a], V.D. Peshekhonov[65], B.A. Petersen[29], J. Petersen[29], T.C. Petersen[35], E. Petit[83], A. Petridis[154], C. Petridou[154], E. Petrolo[132a], F. Petrucci[134a,134b], D. Petschull[41], M. Petteni[142], R. Pezoa[31b], A. Phan[86], A.W. Phillips[27], P.W. Phillips[129], G. Piacquadio[29], E. Piccaro[75], M. Piccinini[19a,19b], A. Pickford[53], S.M. Piec[41], R. Piegaia[26], J.E. Pilcher[30], A.D. Pilkington[82], J. Pina[124a,b], M. Pinamonti[164a,164c], A. Pinder[118], J.L. Pinfold[2], J. Ping[32c], B. Pinto[124a,b], O. Pirotte[29], C. Pizio[89a,89b], R. Placakyte[41], M. Plamondon[169], W.G. Plano[82], M.-A. Pleier[24], A.V. Pleskach[128], A. Poblaguev[24], S. Poddar[58a], F. Podlyski[33], L. Poggioli[115], T. Poghosyan[20], M. Pohl[49], F. Polci[55], G. Polesello[119a], A. Policicchio[138], A. Polini[19a], J. Poll[75], V. Polychronakos[24], D.M. Pomarede[136], D. Pomeroy[22], K. Pommès[29], L. Pontecorvo[132a], B.G. Pope[88], G.A. Popeneciu[25a], D.S. Popovic[12a], A. Poppleton[29], X. Portell Bueso[29], R. Porter[163], C. Posch[21], G.E. Pospelov[99], S. Pospisil[127], I.N. Potrap[99], C.J. Potter[149], C.T. Potter[114], G. Poulard[29], J. Poveda[172], R. Prabhu[77], P. Pralavorio[83], S. Prasad[57], R. Pravahan[7], S. Prell[64], K. Pretzl[16], L. Pribyl[29], D. Price[61], L.E. Price[5], M.J. Price[29], P.M. Prichard[73], D. Prieur[123], M. Primavera[72a], K. Prokofiev[108], F. Prokoshin[31b], S. Protopopescu[24], J. Proudfoot[5], X. Prudent[43], H. Przysiezniak[4], S. Psoroulas[20], E. Ptacek[114], E. Pueschel[84], J. Purdham[87], M. Purohit[24,v], P. Puzo[115], Y. Pylypchenko[117], J. Qian[87], Z. Qian[83], Z. Qin[41], A. Quadt[54], D.R. Quarrie[14], W.B. Quayle[172], F. Quinonez[31a], M. Raas[104], V. Radescu[58b], B. Radics[20], T. Rador[18a], F. Ragusa[89a,89b], G. Rahal[177], A.M. Rahimi[109], D. Rahm[24], S. Rajagopalan[24], M. Rammensee[48], M. Rammes[141], M. Ramstedt[146a,146b], A.S. Randle-Conde[39], K. Randrianarivony[28], P.N. Ratoff[71], F. Rauscher[98], E. Rauter[99], M. Raymond[29], A.L. Read[117], D.M. Rebuzzi[119a,119b], A. Redelbach[173], G. Redlinger[24], R. Reece[120], K. Reeves[40], A. Reichold[105], E. Reinherz-Aronis[153], A. Reinsch[114], I. Reisinger[42], D. Reljic[12a], C. Rembser[29], Z.L. Ren[151], A. Renaud[115], P. Renkel[39], M. Rescigno[132a], S. Resconi[89a], B. Resende[136],

P. Reznicek[98], R. Rezvani[158], A. Richards[77], R. Richter[99], E. Richter-Was[38,y], M. Ridel[78], S. Rieke[81], M. Rijpstra[105], M. Rijssenbeek[148], A. Rimoldi[119a,119b], L. Rinaldi[19a], R.R. Rios[39], I. Riu[11], G. Rivoltella[89a,89b], F. Rizatdinova[112], E. Rizvi[75], S.H. Robertson[85,j], A. Robichaud-Veronneau[49], D. Robinson[27], J.E.M. Robinson[77], M. Robinson[114], A. Robson[53], J.G. Rocha de Lima[106], C. Roda[122a,122b], D. Roda Dos Santos[29], S. Rodier[80], D. Rodriguez[162], A. Roe[54], S. Roe[29], O. Røhne[117], V. Rojo[1], S. Rolli[161], A. Romaniouk[96], V.M. Romanov[65], G. Romeo[26], L. Roos[78], E. Ros[167], S. Rosati[132a,132b], K. Rosbach[49], A. Rose[149], M. Rose[76], G.A. Rosenbaum[158], E.I. Rosenberg[64], P.L. Rosendahl[13], O. Rosenthal[141], L. Rosselet[49], V. Rossetti[11], E. Rossi[102a,102b], L.P. Rossi[50a], L. Rossi[89a,89b], M. Rotaru[25a], I. Roth[171], J. Rothberg[138], D. Rousseau[115], C.R. Royon[136], A. Rozanov[83], Y. Rozen[152], X. Ruan[115], I. Rubinskiy[41], B. Ruckert[98], N. Ruckstuhl[105], V.I. Rud[97], C. Rudolph[43], G. Rudolph[62], F. Rühr[6], F. Ruggieri[134a,134b], A. Ruiz-Martinez[64], E. Rulikowska-Zarebska[37], V. Rumiantsev[91,*], L. Rumyantsev[65], K. Runge[48], O. Runolfsson[20], Z. Rurikova[48], N.A. Rusakovich[65], D.R. Rust[61], J.P. Rutherfoord[6], C. Ruwiedel[14], P. Ruzicka[125], Y.F. Ryabov[121], V. Ryadovikov[128], P. Ryan[88], M. Rybar[126], G. Rybkin[115], N.C. Ryder[118], S. Rzaeva[10], A.F. Saavedra[150], I. Sadeh[153], H.F-W. Sadrozinski[137], R. Sadykov[65], F. Safai Tehrani[132a,132b], H. Sakamoto[155], G. Salamanna[75], A. Salamon[133a], M. Saleem[111], D. Salihagic[99], A. Salnikov[143], J. Salt[167], B.M. Salvachua Ferrando[5], D. Salvatore[36a,36b], F. Salvatore[149], A. Salvucci[104], A. Salzburger[29], D. Sampsonidis[154], B.H. Samset[117], A. Sanchez[102a,102b], H. Sandaker[13], H.G. Sander[81], M.P. Sanders[98], M. Sandhoff[174], T. Sandoval[27], C. Sandoval[162], R. Sandstroem[99], S. Sandvoss[174], D.P.C. Sankey[129], A. Sansoni[47], C. Santamarina Rios[85], C. Santoni[33], R. Santonico[133a,133b], H. Santos[124a], J.G. Saraiva[124a,b], T. Sarangi[172], E. Sarkisyan-Grinbaum[7], F. Sarri[122a,122b], G. Sartisohn[174], O. Sasaki[66], T. Sasaki[66], N. Sasao[68], I. Satsounkevitch[90], G. Sauvage[4], E. Sauvan[4], J.B. Sauvan[115], P. Savard[158,e], V. Savinov[123], D.O. Savu[29], P. Savva[9], L. Sawyer[24,l], D.H. Saxon[53], L.P. Says[33], C. Sbarra[19a,19b], A. Sbrizzi[19a,19b], O. Scallon[93], D.A. Scannicchio[163], J. Schaarschmidt[115], P. Schacht[99], U. Schäfer[81], S. Schaepe[20], S. Schaetzel[58b], A.C. Schaffer[115], D. Schaile[98], R.D. Schamberger[148], A.G. Schamov[107], V. Scharf[58a], V.A. Schegelsky[121], D. Scheirich[87], M. Schernau[163], M.I. Scherzer[14], C. Schiavi[50a,50b], J. Schieck[98], M. Schioppa[36a,36b], S. Schlenker[29], J.L. Schlereth[5], E. Schmidt[48], K. Schmieden[20], C. Schmitt[81], S. Schmitt[58b], M. Schmitz[20], A. Schöning[58b], M. Schott[29], D. Schouten[142], J. Schovancova[125], M. Schram[85], C. Schroeder[81], N. Schroer[58c], S. Schuh[29], G. Schuler[29], J. Schultes[174], H.-C. Schultz-Coulon[58a], H. Schulz[15], J.W. Schumacher[20], M. Schumacher[48], B.A. Schumm[137], Ph. Schune[136], C. Schwanenberger[82], A. Schwartzman[143], Ph. Schwemling[78], R. Schwienhorst[88], R. Schwierz[43], J. Schwindling[136], T. Schwindt[20], W.G. Scott[129], J. Searcy[114], E. Sedykh[121], E. Segura[11], S.C. Seidel[103], A. Seiden[137], F. Seifert[43], J.M. Seixas[23a], G. Sekhniaidze[102a], D.M. Seliverstov[121], B. Sellden[146a], G. Sellers[73], M. Seman[144b], N. Semprini-Cesari[19a,19b], C. Serfon[98], L. Serin[115], R. Seuster[99], H. Severini[111], M.E. Sevior[86], A. Sfyrla[29], E. Shabalina[54], M. Shamim[114], L.Y. Shan[32a], J.T. Shank[21], Q.T. Shao[86], M. Shapiro[14], P.B. Shatalov[95], L. Shaver[6], K. Shaw[164a,164c], D. Sherman[175], P. Sherwood[77], A. Shibata[108], H. Shichi[101], S. Shimizu[29], M. Shimojima[100], T. Shin[56], A. Shmeleva[94], M.J. Shochet[30], D. Short[118], M.A. Shupe[6], P. Sicho[125], A. Sidoti[132a,132b], A. Siebel[174], F. Siegert[48], J. Siegrist[14], Dj. Sijacki[12a], O. Silbert[171], J. Silva[124a,b], Y. Silver[153], D. Silverstein[143], S.B. Silverstein[146a], V. Simak[127], O. Simard[136], Lj. Simic[12a], S. Simion[115], B. Simmons[77], R. Simoniello[89a,89b], M. Simonyan[35], P. Sinervo[158], N.B. Sinev[114], V. Sipica[141], G. Siragusa[173], A. Sircar[24], A.N. Sisakyan[65], S.Yu. Sivoklokov[97], J. Sjölin[146a,146b], T.B. Sjursen[13], L.A. Skinnari[14], K. Skovpen[107], P. Skubic[111], N. Skvorodnev[22], M. Slater[17], T. Slavicek[127], K. Sliwa[161], T.J. Sloan[71], J. Sloper[29], V. Smakhtin[171], S.Yu. Smirnov[96], L.N. Smirnova[97], O. Smirnova[79], B.C. Smith[57], D. Smith[143], K.M. Smith[53], M. Smizanska[71], K. Smolek[127], A.A. Snesarev[94], S.W. Snow[82], J. Snow[111], J. Snuverink[105], S. Snyder[24], M. Soares[124a], R. Sobie[169,j], J. Sodomka[127], A. Soffer[153], C.A. Solans[167], M. Solar[127], J. Solc[127], E. Soldatov[96], U. Soldevila[167], E. Solfaroli Camillocci[132a,132b], A.A. Solodkov[128], O.V. Solovyanov[128], J. Sondericker[24], N. Soni[2], V. Sopko[127], B. Sopko[127], M. Sorbi[89a,89b], M. Sosebee[7], A. Soukharev[107], S. Spagnolo[72a,72b], F. Spanò[76], R. Spighi[19a], G. Spigo[29], F. Spila[132a,132b], E. Spiriti[134a], R. Spiwoks[29], M. Spousta[126], T. Spreitzer[158], B. Spurlock[7], R.D. St. Denis[53], T. Stahl[141], J. Stahlman[120], R. Stamen[58a], E. Stanecka[29], R.W. Stanek[5], C. Stanescu[134a], S. Stapnes[117], E.A. Starchenko[128], J. Stark[55], P. Staroba[125], P. Starovoitov[91], A. Staude[98], P. Stavina[144a], G. Stavropoulos[14], G. Steele[53], P. Steinbach[43], P. Steinberg[24], I. Stekl[127], B. Stelzer[142], H.J. Stelzer[88], O. Stelzer-Chilton[159a], H. Stenzel[52], K. Stevenson[75], G.A. Stewart[29], J.A. Stillings[20], T. Stockmanns[20], M.C. Stockton[29], K. Stoerig[48], G. Stoicea[25a], S. Stonjek[99], P. Strachota[126], A.R. Stradling[7], A. Straessner[43], J. Strandberg[147], S. Strandberg[146a,146b], A. Strandlie[117], M. Strang[109], E. Strauss[143], M. Strauss[111], P. Strizenec[144b], R. Ströhmer[173], D.M. Strom[114], J.A. Strong[76,*], R. Stroynowski[39], J. Strube[129], B. Stugu[13], I. Stumer[24,*], J. Stupak[148], P. Sturm[174], D.A. Soh[151,q], D. Su[143], H.S. Subramania[2], A. Succurro[11], Y. Sugaya[116], T. Sugimoto[101], C. Suhr[106], K. Suita[67], M. Suk[126], V.V. Sulin[94], S. Sultansoy[3d], T. Sumida[29], X. Sun[55], J.E. Sundermann[48], K. Suruliz[139], S. Sushkov[11], G. Susinno[36a,36b], M.R. Sutton[149], Y. Suzuki[66], Y. Suzuki[67], M. Svatos[125], Yu.M. Sviridov[128], S. Swedish[168], I. Sykora[144a], T. Sykora[126], B. Szeless[29], J. Sánchez[167], D. Ta[105], K. Tackmann[41], A. Taffard[163], R. Tafirout[159a], A. Taga[117], N. Taiblum[153], Y. Takahashi[101], H. Takai[24], R. Takashima[69], H. Takeda[67], T. Takeshita[140], M. Talby[83], A. Talyshev[107], M.C. Tamsett[24], J. Tanaka[155], R. Tanaka[115], S. Tanaka[131], S. Tanaka[66], Y. Tanaka[100], K. Tani[67],

N. Tannoury[83], G.P. Tappern[29], S. Tapprogge[81], D. Tardif[158], S. Tarem[152], F. Tarrade[28], G.F. Tartarelli[89a], P. Tas[126], M. Tasevsky[125], E. Tassi[36a,36b], M. Tatarkhanov[14], C. Taylor[77], F.E. Taylor[92], G.N. Taylor[86], W. Taylor[159b], M. Teinturier[115], M. Teixeira Dias Castanheira[75], P. Teixeira-Dias[76], K.K. Temming[48], H. Ten Kate[29], P.K. Teng[151], S. Terada[66], K. Terashi[155], J. Terron[80], M. Terwort[41,o], M. Testa[47], R.J. Teuscher[158,j], J. Thadome[174], J. Therhaag[20], T. Theveneaux-Pelzer[78], M. Thioye[175], S. Thoma[48], J.P. Thomas[17], E.N. Thompson[84], P.D. Thompson[17], P.D. Thompson[158], A.S. Thompson[53], E. Thomson[120], M. Thomson[27], R.P. Thun[87], F. Tian[34], T. Tic[125], V.O. Tikhomirov[94], Y.A. Tikhonov[107], C.J.W.P. Timmermans[104], P. Tipton[175], F.J. Tique Aires Viegas[29], S. Tisserant[83], J. Tobias[48], B. Toczek[37], T. Todorov[4], S. Todorova-Nova[161], B. Toggerson[163], J. Tojo[66], S. Tokár[144a], K. Tokunaga[67], K. Tokushuku[66], K. Tollefson[88], M. Tomoto[101], L. Tompkins[14], K. Toms[103], G. Tong[32a], A. Tonoyan[13], C. Topfel[16], N.D. Topilin[65], I. Torchiani[29], E. Torrence[114], H. Torres[78], E. Torró Pastor[167], J. Toth[83,w], F. Touchard[83], D.R. Tovey[139], D. Traynor[75], T. Trefzger[173], L. Tremblet[29], A. Tricoli[29], I.M. Trigger[159a], S. Trincaz-Duvoid[78], T.N. Trinh[78], M.F. Tripiana[70], W. Trischuk[158], A. Trivedi[24,v], B. Trocmé[55], C. Troncon[89a], M. Trottier-McDonald[142], A. Trzupek[38], C. Tsarouchas[29], J.C.-L. Tseng[118], M. Tsiakiris[105], P.V. Tsiareshka[90], D. Tsionou[4], G. Tsipolitis[9], V. Tsiskaridze[48], E.G. Tskhadadze[51], I.I. Tsukerman[95], V. Tsulaia[14], J.-W. Tsung[20], S. Tsuno[66], D. Tsybychev[148], A. Tua[139], J.M. Tuggle[30], M. Turala[38], D. Turecek[127], I. Turk Cakir[3e], E. Turlay[105], R. Turra[89a,89b], P.M. Tuts[34], A. Tykhonov[74], M. Tylmad[146a,146b], M. Tyndel[129], H. Tyrvainen[29], G. Tzanakos[8], K. Uchida[20], I. Ueda[155], R. Ueno[28], M. Ugland[13], M. Uhlenbrock[20], M. Uhrmacher[54], F. Ukegawa[160], G. Unal[29], D.G. Underwood[5], A. Undrus[24], G. Unel[163], Y. Unno[66], D. Urbaniec[34], E. Urkovsky[153], P. Urrejola[31a], G. Usai[7], M. Uslenghi[119a,119b], L. Vacavant[83], V. Vacek[127], B. Vachon[85], S. Vahsen[14], J. Valenta[125], P. Valente[132a], S. Valentinetti[19a,19b], S. Valkar[126], E. Valladolid Gallego[167], S. Vallecorsa[152], J.A. Valls Ferrer[167], H. van der Graaf[105], E. van der Kraaij[105], R. Van Der Leeuw[105], E. van der Poel[105], D. van der Ster[29], B. Van Eijk[105], N. van Eldik[84], P. van Gemmeren[5], Z. van Kesteren[105], I. van Vulpen[105], W. Vandelli[29], G. Vandoni[29], A. Vaniachine[5], P. Vankov[41], F. Vannucci[78], F. Varela Rodriguez[29], R. Vari[132a], E.W. Varnes[6], D. Varouchas[14], A. Vartapetian[7], K.E. Varvell[150], V.I. Vassilakopoulos[56], F. Vazeille[33], G. Vegni[89a,89b], J.J. Veillet[115], C. Vellidis[8], F. Veloso[124a], R. Veness[29], S. Veneziano[132a], A. Ventura[72a,72b], D. Ventura[138], M. Venturi[48], N. Venturi[16], V. Vercesi[119a], M. Verducci[138], W. Verkerke[105], J.C. Vermeulen[105], A. Vest[43], M.C. Vetterli[142,e], I. Vichou[165], T. Vickey[145b,z], G.H.A. Viehhauser[118], S. Viel[168], M. Villa[19a,19b], M. Villaplana Perez[167], E. Vilucchi[47], M.G. Vincter[28], E. Vinek[29], V.B. Vinogradov[65], M. Virchaux[136,*], J. Virzi[14], O. Vitells[171], M. Viti[41], I. Vivarelli[48], F. Vives Vaque[11], S. Vlachos[9], M. Vlasak[127], N. Vlasov[20], A. Vogel[20], P. Vokac[127], G. Volpi[47], M. Volpi[86], G. Volpini[89a], H. von der Schmitt[99], J. von Loeben[99], H. von Radziewski[48], E. von Toerne[20], V. Vorobel[126], A.P. Vorobiev[128], V. Vorwerk[11], M. Vos[167], R. Voss[29], T.T. Voss[174], J.H. Vossebeld[73], N. Vranjes[12a], M. Vranjes Milosavljevic[105], V. Vrba[125], M. Vreeswijk[105], T. Vu Anh[81], R. Vuillermet[29], I. Vukotic[115], W. Wagner[174], P. Wagner[120], H. Wahlen[174], J. Wakabayashi[101], J. Walbersloh[42], S. Walch[87], J. Walder[71], R. Walker[98], W. Walkowiak[141], R. Wall[175], P. Waller[73], C. Wang[44], H. Wang[172], H. Wang[32b,aa], J. Wang[151], J. Wang[32d], J.C. Wang[138], R. Wang[103], S.M. Wang[151], A. Warburton[85], C.P. Ward[27], M. Warsinsky[48], P.M. Watkins[17], A.T. Watson[17], M.F. Watson[17], G. Watts[138], S. Watts[82], A.T. Waugh[150], B.M. Waugh[77], J. Weber[42], M. Weber[129], M.S. Weber[16], P. Weber[54], A.R. Weidberg[118], P. Weigell[99], J. Weingarten[54], C. Weiser[48], H. Wellenstein[22], P.S. Wells[29], M. Wen[47], T. Wenaus[24], S. Wendler[123], Z. Weng[151,q], T. Wengler[29], S. Wenig[29], N. Wermes[20], M. Werner[48], P. Werner[29], M. Werth[163], M. Wessels[58a], C. Weydert[55], K. Whalen[28], S.J. Wheeler-Ellis[163], S.P. Whitaker[21], A. White[7], M.J. White[86], S.R. Whitehead[118], D. Whiteson[163], D. Whittington[61], F. Wicek[115], D. Wicke[174], F.J. Wickens[129], W. Wiedenmann[172], M. Wielers[129], P. Wienemann[20], C. Wiglesworth[75], L.A.M. Wiik[48], P.A. Wijeratne[77], A. Wildauer[167], M.A. Wildt[41,o], I. Wilhelm[126], H.G. Wilkens[29], J.Z. Will[98], E. Williams[34], H.H. Williams[120], W. Willis[34], S. Willocq[84], J.A. Wilson[17], M.G. Wilson[143], A. Wilson[87], I. Wingerter-Seez[4], S. Winkelmann[48], F. Winklmeier[29], M. Wittgen[143], M.W. Wolter[38], H. Wolters[124a,h], W.C. Wong[40], G. Wooden[118], B.K. Wosiek[38], J. Wotschack[29], M.J. Woudstra[84], K. Wraight[53], C. Wright[53], B. Wrona[73], S.L. Wu[172], X. Wu[49], Y. Wu[32b,ab], E. Wulf[34], R. Wunstorf[42], B.M. Wynne[45], L. Xaplanteris[9], S. Xella[35], S. Xie[48], Y. Xie[32a], C. Xu[32b,ac], D. Xu[139], G. Xu[32a], B. Yabsley[150], S. Yacoob[145b], M. Yamada[66], H. Yamaguchi[155], A. Yamamoto[66], K. Yamamoto[64], S. Yamamoto[155], T. Yamamura[155], T. Yamanaka[155], J. Yamaoka[44], T. Yamazaki[155], Y. Yamazaki[67], Z. Yan[21], H. Yang[87], U.K. Yang[82], Y. Yang[61], Y. Yang[32a], Z. Yang[146a,146b], S. Yanush[91], W-M. Yao[14], Y. Yao[14], Y. Yasu[66], G.V. Ybeles Smit[130], J. Ye[39], S. Ye[24], M. Yilmaz[3c], R. Yoosoofmiya[123], K. Yorita[170], R. Yoshida[5], C. Young[143], S. Youssef[21], D. Yu[24], J. Yu[7], J. Yu[32c,ac], L. Yuan[32a,ad], A. Yurkewicz[148], V.G. Zaets[128], R. Zaidan[63], A.M. Zaitsev[128], Z. Zajacova[29], Yo.K. Zalite[121], L. Zanello[132a,132b], P. Zarzhitsky[39], A. Zaytsev[107], C. Zeitnitz[174], M. Zeller[175], M. Zeman[125], A. Zemla[38], C. Zendler[20], O. Zenin[128], T. Ženiš[144a], Z. Zenonos[122a,122b], S. Zenz[14], D. Zerwas[115], G. Zevi della Porta[57], Z. Zhan[32d], D. Zhang[32b,aa], H. Zhang[88], J. Zhang[5], X. Zhang[32d], Z. Zhang[115], L. Zhao[108], T. Zhao[138], Z. Zhao[32b], A. Zhemchugov[65], S. Zheng[32a], J. Zhong[151,ae], B. Zhou[87], N. Zhou[163], Y. Zhou[151], C.G. Zhu[32d], H. Zhu[41], J. Zhu[87], Y. Zhu[172], X. Zhuang[98], V. Zhuravlov[99], D. Zieminska[61], R. Zimmermann[20], S. Zimmermann[20], S. Zimmermann[48], M. Ziolkowski[141], R. Zitoun[4], L. Živković[34], V.V. Zmouchko[128,*], G. Zobernig[172], A. Zoccoli[19a,19b], Y. Zolnierowski[4], A. Zsenei[29], M. zur Nedden[15], V. Zutshi[106], L. Zwalinski[29]

[1]University at Albany, Albany NY, United States of America
[2]Department of Physics, University of Alberta, Edmonton AB, Canada
[3(a)]Department of Physics, Ankara University, Ankara; [(b)]Department of Physics, Dumlupinar University, Kutahya; [(c)]Department of Physics, Gazi University, Ankara; [(d)]Division of Physics, TOBB University of Economics and Technology, Ankara; [(e)]Turkish Atomic Energy Authority, Ankara, Turkey
[4]LAPP, CNRS/IN2P3 and Université de Savoie, Annecy-le-Vieux, France
[5]High Energy Physics Division, Argonne National Laboratory, Argonne IL, United States of America
[6]Department of Physics, University of Arizona, Tucson AZ, United States of America
[7]Department of Physics, The University of Texas at Arlington, Arlington TX, United States of America
[8]Physics Department, University of Athens, Athens, Greece
[9]Physics Department, National Technical University of Athens, Zografou, Greece
[10]Institute of Physics, Azerbaijan Academy of Sciences, Baku, Azerbaijan
[11]Institut de Física d'Altes Energies and Universitat Autònoma de Barcelona and ICREA, Barcelona, Spain
[12(a)]Institute of Physics, University of Belgrade, Belgrade; [(b)]Vinca Institute of Nuclear Sciences, Belgrade, Serbia
[13]Department for Physics and Technology, University of Bergen, Bergen, Norway
[14]Physics Division, Lawrence Berkeley National Laboratory and University of California, Berkeley CA, United States of America
[15]Department of Physics, Humboldt University, Berlin, Germany
[16]Albert Einstein Center for Fundamental Physics and Laboratory for High Energy Physics, University of Bern, Bern, Switzerland
[17]School of Physics and Astronomy, University of Birmingham, Birmingham, United Kingdom
[18(a)]Department of Physics, Bogazici University, Istanbul; [(b)]Division of Physics, Dogus University, Istanbul; [(c)]Department of Physics Engineering, Gaziantep University, Gaziantep; [(d)]Department of Physics, Istanbul Technical University, Istanbul, Turkey
[19(a)]INFN Sezione di Bologna; [(b)]Dipartimento di Fisica, Università di Bologna, Bologna, Italy
[20]Physikalisches Institut, University of Bonn, Bonn, Germany
[21]Department of Physics, Boston University, Boston MA, United States of America
[22]Department of Physics, Brandeis University, Waltham MA, United States of America
[23(a)]Universidade Federal do Rio De Janeiro COPPE/EE/IF, Rio de Janeiro; [(b)]Federal University of Juiz de Fora (UFJF), Juiz de Fora; [(c)]Federal University of Sao Joao del Rei (UFSJ), Sao Joao del Rei; [(d)]Instituto de Fisica, Universidade de Sao Paulo, Sao Paulo, Brazil
[24]Physics Department, Brookhaven National Laboratory, Upton NY, United States of America
[25(a)]National Institute of Physics and Nuclear Engineering, Bucharest; [(b)]University Politehnica Bucharest, Bucharest; [(c)]West University in Timisoara, Timisoara, Romania
[26]Departamento de Física, Universidad de Buenos Aires, Buenos Aires, Argentina
[27]Cavendish Laboratory, University of Cambridge, Cambridge, United Kingdom
[28]Department of Physics, Carleton University, Ottawa ON, Canada
[29]CERN, Geneva, Switzerland
[30]Enrico Fermi Institute, University of Chicago, Chicago IL, United States of America
[31(a)]Departamento de Fisica, Pontificia Universidad Católica de Chile, Santiago; [(b)]Departamento de Física, Universidad Técnica Federico Santa María, Valparaíso, Chile
[32(a)]Institute of High Energy Physics, Chinese Academy of Sciences, Beijing; [(b)]Department of Modern Physics, University of Science and Technology of China, Anhui; [(c)]Department of Physics, Nanjing University, Jiangsu; [(d)]High Energy Physics Group, Shandong University, Shandong, China
[33]Laboratoire de Physique Corpusculaire, Clermont Université and Université Blaise Pascal and CNRS/IN2P3, Aubiere Cedex, France
[34]Nevis Laboratory, Columbia University, Irvington NY, United States of America
[35]Niels Bohr Institute, University of Copenhagen, Kobenhavn, Denmark
[36(a)]INFN Gruppo Collegato di Cosenza; [(b)]Dipartimento di Fisica, Università della Calabria, Arcavata di Rende, Italy
[37]Faculty of Physics and Applied Computer Science, AGH-University of Science and Technology, Krakow, Poland
[38]The Henryk Niewodniczanski Institute of Nuclear Physics, Polish Academy of Sciences, Krakow, Poland
[39]Physics Department, Southern Methodist University, Dallas TX, United States of America
[40]Physics Department, University of Texas at Dallas, Richardson TX, United States of America

[41]DESY, Hamburg and Zeuthen, Germany
[42]Institut für Experimentelle Physik IV, Technische Universität Dortmund, Dortmund, Germany
[43]Institut für Kern- und Teilchenphysik, Technical University Dresden, Dresden, Germany
[44]Department of Physics, Duke University, Durham NC, United States of America
[45]SUPA - School of Physics and Astronomy, University of Edinburgh, Edinburgh, United Kingdom
[46]Fachhochschule Wiener Neustadt, Johannes Gutenbergstrasse 3, 2700 Wiener Neustadt, Austria
[47]INFN Laboratori Nazionali di Frascati, Frascati, Italy
[48]Fakultät für Mathematik und Physik, Albert-Ludwigs-Universität, Freiburg i.Br., Germany
[49]Section de Physique, Université de Genève, Geneva, Switzerland
[50(a)]INFN Sezione di Genova; [(b)]Dipartimento di Fisica, Università di Genova, Genova, Italy
[51]Institute of Physics and HEP Institute, Georgian Academy of Sciences and Tbilisi State University, Tbilisi, Georgia
[52]II Physikalisches Institut, Justus-Liebig-Universität Giessen, Giessen, Germany
[53]SUPA - School of Physics and Astronomy, University of Glasgow, Glasgow, United Kingdom
[54]II Physikalisches Institut, Georg-August-Universität, Göttingen, Germany
[55]Laboratoire de Physique Subatomique et de Cosmologie, Université Joseph Fourier and CNRS/IN2P3 and Institut National Polytechnique de Grenoble, Grenoble, France
[56]Department of Physics, Hampton University, Hampton VA, United States of America
[57]Laboratory for Particle Physics and Cosmology, Harvard University, Cambridge MA, United States of America
[58(a)]Kirchhoff-Institut für Physik, Ruprecht-Karls-Universität Heidelberg, Heidelberg; [(b)]Physikalisches Institut, Ruprecht-Karls-Universität Heidelberg, Heidelberg; [(c)]ZITI Institut für technische Informatik, Ruprecht-Karls-Universität Heidelberg, Mannheim, Germany
[59]Faculty of Science, Hiroshima University, Hiroshima, Japan
[60]Faculty of Applied Information Science, Hiroshima Institute of Technology, Hiroshima, Japan
[61]Department of Physics, Indiana University, Bloomington IN, United States of America
[62]Institut für Astro- und Teilchenphysik, Leopold-Franzens-Universität, Innsbruck, Austria
[63]University of Iowa, Iowa City IA, United States of America
[64]Department of Physics and Astronomy, Iowa State University, Ames IA, United States of America
[65]Joint Institute for Nuclear Research, JINR Dubna, Dubna, Russia
[66]KEK, High Energy Accelerator Research Organization, Tsukuba, Japan
[67]Graduate School of Science, Kobe University, Kobe, Japan
[68]Faculty of Science, Kyoto University, Kyoto, Japan
[69]Kyoto University of Education, Kyoto, Japan
[70]Instituto de Física La Plata, Universidad Nacional de La Plata and CONICET, La Plata, Argentina
[71]Physics Department, Lancaster University, Lancaster, United Kingdom
[72(a)]INFN Sezione di Lecce; [(b)]Dipartimento di Fisica, Università del Salento, Lecce, Italy
[73]Oliver Lodge Laboratory, University of Liverpool, Liverpool, United Kingdom
[74]Department of Physics, Jožef Stefan Institute and University of Ljubljana, Ljubljana, Slovenia
[75]Department of Physics, Queen Mary University of London, London, United Kingdom
[76]Department of Physics, Royal Holloway University of London, Surrey, United Kingdom
[77]Department of Physics and Astronomy, University College London, London, United Kingdom
[78]Laboratoire de Physique Nucléaire et de Hautes Energies, UPMC and Université Paris-Diderot and CNRS/IN2P3, Paris, France
[79]Fysiska institutionen, Lunds universitet, Lund, Sweden
[80]Departamento de Fisica Teorica C-15, Universidad Autonoma de Madrid, Madrid, Spain
[81]Institut für Physik, Universität Mainz, Mainz, Germany
[82]School of Physics and Astronomy, University of Manchester, Manchester, United Kingdom
[83]CPPM, Aix-Marseille Université and CNRS/IN2P3, Marseille, France
[84]Department of Physics, University of Massachusetts, Amherst MA, United States of America
[85]Department of Physics, McGill University, Montreal QC, Canada
[86]School of Physics, University of Melbourne, Victoria, Australia
[87]Department of Physics, The University of Michigan, Ann Arbor MI, United States of America
[88]Department of Physics and Astronomy, Michigan State University, East Lansing MI, United States of America
[89(a)]INFN Sezione di Milano; [(b)]Dipartimento di Fisica, Università di Milano, Milano, Italy

[90]B.I. Stepanov Institute of Physics, National Academy of Sciences of Belarus, Minsk, Republic of Belarus
[91]National Scientific and Educational Centre for Particle and High Energy Physics, Minsk, Republic of Belarus
[92]Department of Physics, Massachusetts Institute of Technology, Cambridge MA, United States of America
[93]Group of Particle Physics, University of Montreal, Montreal QC, Canada
[94]P.N. Lebedev Institute of Physics, Academy of Sciences, Moscow, Russia
[95]Institute for Theoretical and Experimental Physics (ITEP), Moscow, Russia
[96]Moscow Engineering and Physics Institute (MEPhI), Moscow, Russia
[97]Skobeltsyn Institute of Nuclear Physics, Lomonosov Moscow State University, Moscow, Russia
[98]Fakultät für Physik, Ludwig-Maximilians-Universität München, München, Germany
[99]Max-Planck-Institut für Physik (Werner-Heisenberg-Institut), München, Germany
[100]Nagasaki Institute of Applied Science, Nagasaki, Japan
[101]Graduate School of Science, Nagoya University, Nagoya, Japan
[102(a)]INFN Sezione di Napoli; [(b)]Dipartimento di Scienze Fisiche, Università di Napoli, Napoli, Italy
[103]Department of Physics and Astronomy, University of New Mexico, Albuquerque NM, United States of America
[104]Institute for Mathematics, Astrophysics and Particle Physics, Radboud University Nijmegen/Nikhef, Nijmegen, Netherlands
[105]Nikhef National Institute for Subatomic Physics and University of Amsterdam, Amsterdam, Netherlands
[106]Department of Physics, Northern Illinois University, DeKalb IL, United States of America
[107]Budker Institute of Nuclear Physics (BINP), Novosibirsk, Russia
[108]Department of Physics, New York University, New York NY, United States of America
[109]Ohio State University, Columbus OH, United States of America
[110]Faculty of Science, Okayama University, Okayama, Japan
[111]Homer L. Dodge Department of Physics and Astronomy, University of Oklahoma, Norman OK, United States of America
[112]Department of Physics, Oklahoma State University, Stillwater OK, United States of America
[113]Palacký University, RCPTM, Olomouc, Czech Republic
[114]Center for High Energy Physics, University of Oregon, Eugene OR, United States of America
[115]LAL, Univ. Paris-Sud and CNRS/IN2P3, Orsay, France
[116]Graduate School of Science, Osaka University, Osaka, Japan
[117]Department of Physics, University of Oslo, Oslo, Norway
[118]Department of Physics, Oxford University, Oxford, United Kingdom
[119(a)]INFN Sezione di Pavia; [(b)]Dipartimento di Fisica Nucleare e Teorica, Università di Pavia, Pavia, Italy
[120]Department of Physics, University of Pennsylvania, Philadelphia PA, United States of America
[121]Petersburg Nuclear Physics Institute, Gatchina, Russia
[122(a)]INFN Sezione di Pisa; [(b)]Dipartimento di Fisica E. Fermi, Università di Pisa, Pisa, Italy
[123]Department of Physics and Astronomy, University of Pittsburgh, Pittsburgh PA, United States of America
[124(a)]Laboratorio de Instrumentacao e Fisica Experimental de Particulas - LIP, Lisboa, Portugal; [(b)]Departamento de Fisica Teorica y del Cosmos and CAFPE, Universidad de Granada, Granada, Spain
[125]Institute of Physics, Academy of Sciences of the Czech Republic, Praha, Czech Republic
[126]Faculty of Mathematics and Physics, Charles University in Prague, Praha, Czech Republic
[127]Czech Technical University in Prague, Praha, Czech Republic
[128]State Research Center Institute for High Energy Physics, Protvino, Russia
[129]Particle Physics Department, Rutherford Appleton Laboratory, Didcot, United Kingdom
[130]Physics Department, University of Regina, Regina SK, Canada
[131]Ritsumeikan University, Kusatsu, Shiga, Japan
[132(a)]INFN Sezione di Roma I; [(b)]Dipartimento di Fisica, Università La Sapienza, Roma, Italy
[133(a)]INFN Sezione di Roma Tor Vergata; [(b)]Dipartimento di Fisica, Università di Roma Tor Vergata, Roma, Italy
[134(a)]INFN Sezione di Roma Tre; [(b)]Dipartimento di Fisica, Università Roma Tre, Roma, Italy
[135(a)]Faculté des Sciences Ain Chock, Réseau Universitaire de Physique des Hautes Energies - Université Hassan II, Casablanca; [(b)]Centre National de l'Energie des Sciences Techniques Nucleaires, Rabat; [(c)]Université Cadi Ayyad, Faculté des sciences Semlalia Département de Physique, B.P. 2390 Marrakech 40000; [(d)]Faculté des Sciences, Université Mohamed Premier and LPTPM, Oujda; [(e)]Faculté des Sciences, Université Mohammed V, Rabat, Morocco
[136]DSM/IRFU (Institut de Recherches sur les Lois Fondamentales de l'Univers), CEA Saclay (Commissariat a l'Energie Atomique), Gif-sur-Yvette, France

[137]Santa Cruz Institute for Particle Physics, University of California Santa Cruz, Santa Cruz CA, United States of America
[138]Department of Physics, University of Washington, Seattle WA, United States of America
[139]Department of Physics and Astronomy, University of Sheffield, Sheffield, United Kingdom
[140]Department of Physics, Shinshu University, Nagano, Japan
[141]Fachbereich Physik, Universität Siegen, Siegen, Germany
[142]Department of Physics, Simon Fraser University, Burnaby BC, Canada
[143]SLAC National Accelerator Laboratory, Stanford CA, United States of America
[144(a)]Faculty of Mathematics, Physics & Informatics, Comenius University, Bratislava; [(b)]Department of Subnuclear Physics, Institute of Experimental Physics of the Slovak Academy of Sciences, Kosice, Slovak Republic
[145(a)]Department of Physics, University of Johannesburg, Johannesburg; [(b)]School of Physics, University of the Witwatersrand, Johannesburg, South Africa
[146(a)]Department of Physics, Stockholm University; [(b)]The Oskar Klein Centre, Stockholm, Sweden
[147]Physics Department, Royal Institute of Technology, Stockholm, Sweden
[148]Department of Physics and Astronomy, Stony Brook University, Stony Brook NY, United States of America
[149]Department of Physics and Astronomy, University of Sussex, Brighton, United Kingdom
[150]School of Physics, University of Sydney, Sydney, Australia
[151]Institute of Physics, Academia Sinica, Taipei, Taiwan
[152]Department of Physics, Technion: Israel Inst. of Technology, Haifa, Israel
[153]Raymond and Beverly Sackler School of Physics and Astronomy, Tel Aviv University, Tel Aviv, Israel
[154]Department of Physics, Aristotle University of Thessaloniki, Thessaloniki, Greece
[155]International Center for Elementary Particle Physics and Department of Physics, The University of Tokyo, Tokyo, Japan
[156]Graduate School of Science and Technology, Tokyo Metropolitan University, Tokyo, Japan
[157]Department of Physics, Tokyo Institute of Technology, Tokyo, Japan
[158]Department of Physics, University of Toronto, Toronto ON, Canada
[159(a)]TRIUMF, Vancouver BC; [(b)]Department of Physics and Astronomy, York University, Toronto ON, Canada
[160]Institute of Pure and Applied Sciences, University of Tsukuba, Ibaraki, Japan
[161]Science and Technology Center, Tufts University, Medford MA, United States of America
[162]Centro de Investigaciones, Universidad Antonio Narino, Bogota, Colombia
[163]Department of Physics and Astronomy, University of California Irvine, Irvine CA, United States of America
[164(a)]INFN Gruppo Collegato di Udine; [(b)]ICTP, Trieste; [(c)]Dipartimento di Fisica, Università di Udine, Udine, Italy
[165]Department of Physics, University of Illinois, Urbana IL, United States of America
[166]Department of Physics and Astronomy, University of Uppsala, Uppsala, Sweden
[167]Instituto de Física Corpuscular (IFIC) and Departamento de Física Atómica, Molecular y Nuclear and Departamento de Ingenierá Electrónica and Instituto de Microelectrónica de Barcelona (IMB-CNM), University of Valencia and CSIC, Valencia, Spain
[168]Department of Physics, University of British Columbia, Vancouver BC, Canada
[169]Department of Physics and Astronomy, University of Victoria, Victoria BC, Canada
[170]Waseda University, Tokyo, Japan
[171]Department of Particle Physics, The Weizmann Institute of Science, Rehovot, Israel
[172]Department of Physics, University of Wisconsin, Madison WI, United States of America
[173]Fakultät für Physik und Astronomie, Julius-Maximilians-Universität, Würzburg, Germany
[174]Fachbereich C Physik, Bergische Universität Wuppertal, Wuppertal, Germany
[175]Department of Physics, Yale University, New Haven CT, United States of America
[176]Yerevan Physics Institute, Yerevan, Armenia
[177]Domaine scientifique de la Doua, Centre de Calcul CNRS/IN2P3, Villeurbanne Cedex, France
[a]Also at Laboratorio de Instrumentacao e Fisica Experimental de Particulas - LIP, Lisboa, Portugal
[b]Also at Faculdade de Ciencias and CFNUL, Universidade de Lisboa, Lisboa, Portugal
[c]Also at Particle Physics Department, Rutherford Appleton Laboratory, Didcot, United Kingdom
[d]Also at CPPM, Aix-Marseille Université and CNRS/IN2P3, Marseille, France
[e]Also at TRIUMF, Vancouver BC, Canada
[f]Also at Department of Physics, California State University, Fresno CA, United States of America
[g]Also at Faculty of Physics and Applied Computer Science, AGH-University of Science and Technology, Krakow, Poland
[h]Also at Department of Physics, University of Coimbra, Coimbra, Portugal

[i]Also at Università di Napoli Parthenope, Napoli, Italy
[j]Also at Institute of Particle Physics (IPP), Canada
[k]Also at Department of Physics, Middle East Technical University, Ankara, Turkey
[l]Also at Louisiana Tech University, Ruston LA, United States of America
[m]Also at Group of Particle Physics, University of Montreal, Montreal QC, Canada
[n]Also at Institute of Physics, Azerbaijan Academy of Sciences, Baku, Azerbaijan
[o]Also at Institut für Experimentalphysik, Universität Hamburg, Hamburg, Germany
[p]Also at Manhattan College, New York NY, United States of America
[q]Also at School of Physics and Engineering, Sun Yat-sen University, Guanzhou, China
[r]Also at Academia Sinica Grid Computing, Institute of Physics, Academia Sinica, Taipei, Taiwan
[s]Also at High Energy Physics Group, Shandong University, Shandong, China
[t]Also at Section de Physique, Université de Genève, Geneva, Switzerland
[u]Also at Departamento de Fisica, Universidade de Minho, Braga, Portugal
[v]Also at Department of Physics and Astronomy, University of South Carolina, Columbia SC, United States of America
[w]Also at KFKI Research Institute for Particle and Nuclear Physics, Budapest, Hungary
[x]Also at California Institute of Technology, Pasadena CA, United States of America
[y]Also at Institute of Physics, Jagiellonian University, Krakow, Poland
[z]Also at Department of Physics, Oxford University, Oxford, United Kingdom
[aa]Also at Institute of Physics, Academia Sinica, Taipei, Taiwan
[ab]Also at Department of Physics, The University of Michigan, Ann Arbor MI, United States of America
[ac]Also at DSM/IRFU (Institut de Recherches sur les Lois Fondamentales de l'Univers), CEA Saclay (Commissariat a l'Energie Atomique), Gif-sur-Yvette, France
[ad]Also at Laboratoire de Physique Nucléaire et de Hautes Energies, UPMC and Université Paris-Diderot and CNRS/IN2P3, Paris, France
[ae]Also at Department of Physics, Nanjing University, Jiangsu, China
[*]Deceased